Mechanical Properties of a Sustainable Composite Made of Mineral Fibers and a Recyclable Resin

by

Shahriar Ahmed Chowdhury

Submitted in partial fulfilment of the requirements for
the degree of Master of Applied Science

at

Dalhousie University
Halifax, Nova Scotia
August 2024

Dalhousie University is located in Mi'kma'ki, the
ancestral and unceded territory of the Mi'kmaq.

TABLE OF CONTENTS

LIST OF TABLES

LIST OF FIGURES

ABSTRACT

Fiber-reinforced polymer composites (FRPs) are used in various applications in several industries (e.g., aerospace, marine, transportation, construction and sporting goods). They are the primary choice because of their lightweight, corrosion resistivity, lower life-cycle cost, and tailorability. However, a significant volume of today's FRPs consists of fibers like carbon, aramid, glass and thermoset resins (e.g., epoxy, polyester vinyl ester and phenolics) that are non-recyclable or non-biodegradable. Consequently, their disposal in landfills has created critical environmental issues. To combat the problem, researchers have been promoting the application of natural fiber-reinforced plastics (NFRPs) in various engineering applications in recent years. However, a significant and persisting concern about the current NFRPs is susceptibility to environmental elements (e.g., immersion in liquids and hot and humid environments) and their full recyclability issue, as most reinforcing natural fibres are embedded in thermoset resins.

Therefore, this research aims to establish a cost-effective, fully sustainable, and recyclable composite made of mineral-based fiber (basalt) and a recyclable resin (Recyclamine). A comprehensive experimental investigation is conducted to characterize the composite's basic mechanical properties (i.e., tensile, compressive, shear and flexural strengths and stiffnesses) and its impact characteristics. Microscopic analysis is conducted to assess the failure modes. Additionally, various micromechanical analytical approaches' predictive capabilities are evaluated and specifically applied to these new composites. The evaluated properties are compared against the properties of comparable basalt epoxy composite to establish the feasibility and effectiveness of the developed fully sustainable and recyclable composite.

The results demonstrate the viability of basalt-Recyclamine as a cost-effective contender to basalt-epoxy. The theoretical models are also validated, endorsing their utility as a preliminary predictive tool for establishing the basic mechanical properties of the new composite. Finally, Microscopic and SEM analyses highlight the microstructural differences that explain the observed variations in mechanical properties.

LIST OF ABBREVIATIONS USED

BoF	Back-out factor
CFRP	Carbon fiber-reinforced plastic
CLC	Combined loading compression
CAGR	Compound annual growth rate
FML	Fiber-metal laminate
FRP	Fiber-reinforced plastic
GFRP	Glass fiber-reinforced plastic
ILSS	Interlaminar shear strength
NFRP	Natural fiber-reinforced plastic
PU	Polyurethane
RTM	Resin transfer molding
SEM	Scanning electron microscopy
VIP	Vacuum infusion process
E^f	Flexural modulus
F^{cu}	Ultimate compressive strength
G_{xz}	Through-thickness shear modulus
ε^{ult}	Ultimate strain
σ_c	Compressive strength
σ_t	Tensile strength
τ_{12}	Shear strength
h	Thickness of the specimen
A	The cross-section area of the specimen
E	Young's modulus
G	Shear modulus
L	Span length
P	Load
b	Width

m	Mass
t	Time
t	Thickness
ε	Strain
ν	Poisson's Ratio
ρ	Density

ACKNOWLEDGEMENTS

First and foremost, I would like to express my deepest gratitude to my supervisor for mentoring me and guiding me to excel both academically and in life. His wisdom and advice on balancing personal and professional life have been invaluable and will always guide my future endeavours.

I would also like to sincerely thank the Department of Mechanical Engineering and Dalhousie University for providing me with the resources, support, and a conducive environment for my studies and research. Moreover, I would like to thank my thesis committee members, Dr. Noubar Yemenidjian, Dr. Hany El Naggar, and Dr. Nouman Ali for their invaluable feedback, patience, time, and effort. Their constructive recommendations have greatly enriched the quality of my research.

I extend my heartfelt thanks to my closest friends, Abu Bakkar Chowdhury, Faisal Alam, and Kulsum Zahid, for being there through thick and thin. Your unwavering support and friendship have been crucial throughout this journey. I am also immensely grateful to my colleagues, Taha Anwar and Ke Wang for their guidance and advice on coping with education and living in Canada, which have significantly helped me during my time here.

Most importantly, I sincerely appreciate my parents, Jamal Ahmed Chowdhury and Morium Akhter Chowdhury. Their endless support, including financial assistance, encouragement, and unwavering belief in my abilities, has been the bedrock of my success. Their sacrifices and dedication have allowed me to reach this milestone.

I also want to acknowledge all my other friends and family members who, directly and indirectly, contributed their inspiration to my life. The support from friends, community leaders, members, and well-wishers has enabled me to focus on science and contribute to a more significant cause. Thank you all for your unwavering support.

CHAPTER 1 INTRODUCTION

1.1 BACKGROUND AND MOTIVATION

In recent years, there has been a growing interest in making any mode of transport lightweight. For instance, the application of lightweight materials in aircraft has directly impacted factors such as fuel consumption, agility, and navigation dynamics. Similarly, it is estimated that a decrease of approximately 25% in vehicle weight, which is possible using fiber-reinforced plastics (FRPs), can save 250 million barrels of crude oil yearly [1]. The use of lightweight materials in the aviation industry is also predicted to increase in recent years. Furthermore, the incorporation of lightweight materials in windmill construction, the leading renewable energy source, is also becoming apparent. The worldwide lightweight materials market volume was projected to be around USD 113.78 billion in 2016 and is estimated to record a compound annual growth rate (CAGR) of 8.9% over the predicted period. These recent data, acquisition and merger agreements show lightweight materials' potential growth [1].

To meet these demands, lightweight composite materials like FRPs have become quite popular amongst industries and researchers. Fiber-reinforced polymers (FRPs) are composite materials consisting of two or more materials with unique characteristics when combined. They are different than traditional materials like aluminum or steel, which are isotropic, meaning their properties are uniform in all directions regardless of the applied load. As FRPs are anisotropic, their mechanical properties are prevalent in the direction of fiber and applied load [2]. As a result, fibers are placed in various directions to sustain the common multiaxial loading states.

Traditional FRPs typically contain glass, carbon, or aramid fibres embedded in resins like epoxy, polyester, or vinyl ester. The first FRPs were introduced after World War II by the petrochemical industry. Their lightweight and high-performing characteristics were commercialized in the late 1960s and early 1970 in the aerospace and aeronautical industries. Funding provided by various industries and governments promoted the interest in composite research in the late 1980s and throughout the 1990s. As a result, besides

their applications in sporting goods, marine and aerospace, composites gained acceptance for use in the construction industry [3].

Despite several attempts to recycle and reform FRPs in recent years in certain applications like cabins and gatehouses [4], a great majority of FRPs still go to waste and landfills since they are made from materials that are not easily deformable and recyclable and for specific applications. Consequently, their environmental impact has become a growing concern. The primary problem lies in their end-of-life disposal; these materials are often non-biodegradable and pose challenges in recycling, leading to environmental pollution [5].

To combat these environmental challenges, researchers have focused their resources on biofilters or natural fiber-reinforced polymers (NFRPs), which are biodegradable and environmentally friendly. These consist of bast fibers (flax. hemp, jute, etc.), leaf fibers (like sisal and banana) and mineral and synthetic fibers (like basalt and aramid). Some of these materials are more advantageous in terms of availability, affordability and machinability than some traditional FRPs, like glass fibers, making them very competitive in specific applications in the automotive and aerospace industries. For example, Ford started using the NFRPs in their cars as early as the 1930s and flax-reinforced polymers were first used in planes in 1940s [6,8].

Despite the advancement, the polymer matrix used for resins like thermoplastic and thermoset polymer matrices is generally used to manufacture components. These still pose an environmental threat since they can be toxic and dependent on petroleum resources. Improper disposal of polymer composites can be carcinogenic and potentially pollute waters [9].

Few studies have been conducted to find a suitable alternative, such as the recyclability of the matrix resin. Most research focused on fibers has aimed to address their recyclability/biodegradability. This research is particularly relevant as it addresses the pressing need for sustainable materials in industries heavily reliant on traditional FRPs. By investigating the viability of basalt fibers with eco-friendly resins, this study

contributes to advancing the field of sustainable materials science, potentially impacting a range of applications from construction to consumer goods.

1.2 Problem Statement and Objectives

In response to the environmental and health challenges posed by traditional FRPs and matrix resins, this study focuses on developing sustainable composite materials using biodegradable and sustainable basalt fibers combined with an eco-friendly and recyclable resin, specifically Recyclamine. Basalt fibers, derived from natural basalt rock, offer an environmentally friendly alternative to synthetic fibers. Moreover, Recyclamine presents an innovative approach to resin formulation, a recyclable option with the potential to significantly reduce the environmental footprint of composite materials.

The main objective of this study is to investigate the mechanical performance of Basalt fiber composites using Recyclamine under various loading states and compare the performance to that of equivalent basalt-epoxy and the more commonly used E-glass epoxy. This research aims to determine the effectiveness of these materials in creating a more sustainable composite without compromising on mechanical performance. In brief, the study aims to reach the following goals:

a. To establish the void content of the composites used in this study.
b. To establish the basic mechanical properties (i.e., tensile, compressive, shear, flexural) and impact response of the basalt-Recyclamine and basalt-epoxy composites in accordance with the ASTM Standards.
c. To understand the failure mechanism and modes of the composites using digital and scanning electron microscopy.
d. To assess the feasibility and potential of basalt-Recyclamine as a recyclable alternative to E-glass epoxy for use in industrial applications.

1.3 Scope and Limitations

As stated, this thesis will focus on characterizing the mechanical properties of basalt fiber composites formulated with Recyclamine and epoxy resins. The study includes the items noted above. While the research primarily concentrates on mechanical performance, it

will also touch lightly upon the environmental aspects of using basalt fibres and Recyclamine in the literature review section.

However, the study will not cover other important aspects like the environmental impact assessment, such as life cycle analysis or long-term biodegradability and other important influences, such as the effect of moisture absorption/wettability and the resin's recyclability.

1.4 THESIS OVERVIEW

CHAPTER 1 of the thesis presents the motivation and justification for the research and the current trends in the industry regarding sustainability.

CHAPTER 2 presents a literature review of the use of traditional and natural fibres in different polymer matrices. This review includes tables comparing different types of NFRPs and matrices generally used in laminated composites as well as the mechanical properties of several different natural fibers and natural fiber-reinforced polymer composites.

CHAPTER 3 discusses the fabrication techniques and materials used in the development of the composites presented in this research. It provides a detailed overview of the materials selected, including the fibers and resins, and the method used to fabricate the composite samples.

CHAPTER 4 discusses the experimental setup and procedures used in the fabrication and study of the mechanical properties of the mentioned composites. The appropriate American Society for Testing and Materials (ASTM) test standards are also presented in this research.

CHAPTER 5 presents the experimental results and theoretical analysis, which provide a discussion of these results. The relationship between the proposed composite's mechanical properties and other findings from research on fibers.

CHAPTER 6 presents the conclusion and recommendations for additional investigations. As the material used in this work is relatively new, more research is required to establish a complete and reliable mechanical database for the fully recyclable composite. Hence, a brief section about additional studies on basalt-Recyclamine is included.

The appendix contains the list of references and detailed results from the experiment.

CHAPTER 2 LITERATURE REVIEW

2.1 OVERVIEW OF FIBER-REINFORCED POLYMER (FRP) COMPOSITE

Composite Materials, as the name implies, consist of two or more constituent materials with different physical or chemical properties, which offer unique characteristics distinct from their constituents. In the context of this research, Fiber-reinforced polymers (FRPs) refer to composite materials consisting of fibers embedded in a polymer matrix. There has been a significant surge in applications of FRPs in various engineering fields such as construction, automotive, aerospace, biomedical, and marine [4]. Consequently, numerous research works and articles have been published on this topic.

FRPs offer benefits such as weight reduction, high specific stiffness and strength, resistance against corrosion, low manufacturing costs, and improved integration. They are used in non-structural, semi-structural, and structural applications, with the latter being particularly important for crashworthy automobile structures [10]. Figure 2-1 shows the exterior body parts of a Volkswagen x11 car made of carbon fiber.

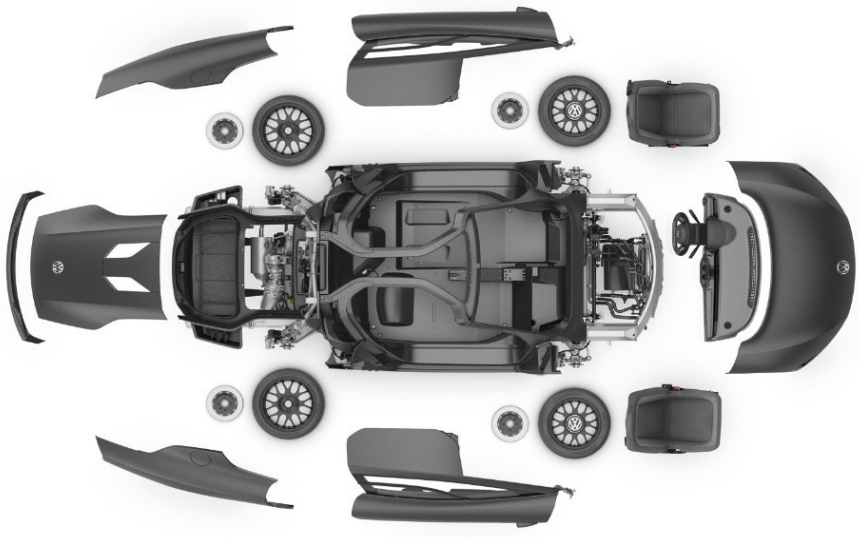

Figure 2-1: Volkswagen xl1 carbon fiber body parts, reproduced from [11].

The advent of advanced composites (those composites made of stiff fibers such as carbon) has been a focus and attracted a significant volume of research into their potential for structural lightweight structural design with improved stiffness and strength increases [12,13]. Fibers like carbon, aramid, and glass, along with thermosetting resins like epoxy, polyester, vinyl ester, and phenolics, have been the common choices for FRP fabrication due to their mechanical, corrosion-resistant, and weight advantages over traditional materials. Table 2-1 illustrates the broad classification of fibers based on organic, inorganic, and other fibers.

Table 2-1: Classification of fibers based on organic, inorganic, and other fibers [14,15].

Organic	Polyamides	
	Nylon, Aramids	
	Polyesters	PET, PBT, PCDT
	Polyvenyl Derivatives	Polyacrilonitrile
		PVC
		PVA
	Polyurethane	Elastane
		Spandex
	Polyolefins	Polyehtyline
		Polypropylene
Inorganic	Glass	
	Carbon	
	Boron	
	Silicone carbide	
Others	Bio-component	
	Multicomponent	

2.2 ENVIRONMENTAL CONCERNS OF NON-RECYCLABLE FRPS

Despite several benefits of FRPs, the non-recyclable nature of conventional FRPs has raised critical environmental concerns. The increased awareness of the environment and its legislation have compelled scientists and industries to focus on the environmental impact of such materials in all stages of their life cycle, from manufacturing to ultimate recycling and disposal. The process is determined by a "life cycle assessment" (LCA) approach. It also considers the environmental impact of a given material/product during its service and its recycling, incineration, or dumping in a landfill site [16].

For instance, various researches [10] have pointed out the air quality issue related to the manufacturing of FRPs using the typical processes such as grille, sheet, twining, twining, moulding, pultrusion and others, which emit volatile organic compounds (VOC) into the atmosphere. The VOC emission studied by Hao [18] related to the manufacturing of FRPs showed that the most significant emission is of the benzene series, with a considerable ozone formation potential (OFP).

Furthermore, the production of plastics from fossil resources and burning plastic waste emit roughly 400 million tonnes of CO_2 each year globally [19]. These points to the considerable environmental challenge posed by the current practices surrounding plastic use and disposal, highlighting the urgency for adopting sustainable measures and enhancing recycling efforts to reduce the ecological footprint. Figure 2-2 shows the results for typical grille, sheet, twining, moulding, and pultrusion processes; the ozone formation potential (OFP) of the benzene series produced by styrene, which mainly comes from the use of unsaturated resin contributed far more to OFP than other VOC species. Benzene is also highly carcinogenic, which can affect the air quality and human health, especially children, the elderly, pregnant women and people with existing health conditions [20].

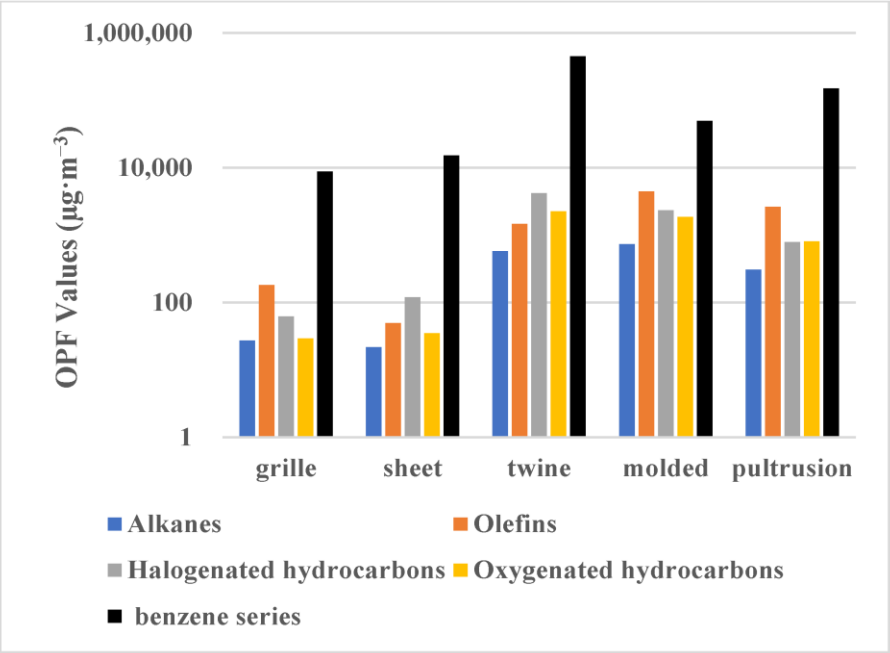

Figure 2-2: Ozone formation contributes to VOC emissions from different processes [18].

The epoxy resin market is also expected to grow significantly, driven by rising demand in various sectors such as automotive, aviation, construction, and electronics. the epoxy resin market is projected to produce around 5,000 thousand tonnes, with a Compound Annual Growth Rate (CAGR) of approximately 4.16% from 2022 to 2030. The forecast indicates continued expansion due to advancements in resin technology and increasing applications in renewable energy sectors [21].

Environmental problems arise from the release of elementary flows during different phases of a product's life cycle. The carbon footprint (CFP) measures the total greenhouse gas emissions, primarily from LER (Low Emission Resin) production, which accounts for 84.5% of the product's overall carbon footprint. Additionally, the removal of LER during End-of-Life Vehicle (ELV) waste management contributes 7.8% to the total CFP [22].

If effective recycling techniques are not implemented, the total waste of composite, especially carbon fiber-reinforced polymer composites utilized by wind turbines and the aviation industry, is expected to reach approximately 840,300 tons by 2050. This amount is comparable to the volume occupied by 34 large football stadiums [23]. By 2016, the

most recent year for which extensive economic data was available, the global car population had reached 1.32 billion vehicles, following an annual growth rate of 4.48%. Industry analyses predict car ownership will increase to 2.4 billion by 2050 [24]. The estimated number of vehicles and the projected generation of end-life vehicles (ELVs) for several countries are detailed in Table 2-2.

Table 2-2: Global and country estimates of car ownership and ELVs [24].

Country	Automobile ownership (units)	Deregistered vehicles (units/year)	ELVs (units/year)
USA	*239,811,984*	*20,419,898*	*12,000,000*
Japan	*75,361,876*	*4,080,000*	*2,960,000*
EU	*271,319,000*	*14,077,000*	*7,823,211*
Germany	*45,261,188*	*2,570,137*	*500,193*
Italy	*41,649,877*	*1,835,293*	*1,610,137*
France	*37,744,000*	*2,002,669*	*1,583,283*
UK	*35,478,652*	*1,810,571*	*1,157,438*
Spain	*27,750,000*	*996,718*	*839,637*
Global total	*1,016,763,420*	*115,805,275*	*40,176,051*

Due to raising concerns about landfill waste and landfill sites producing greenhouse gases like methane and carbon dioxide [25], several countries and regions have addressed the critical need to meet sustainability goals. These countries have enforced measures to reduce the volume of products ending up in landfills and have encouraged companies to develop effective waste management strategies, especially for end-of-life (EoL) products.

Several legislations have been adopted and applied by various countries like Germany [26], the Netherlands [27], France [27], China [28], Japan [29], and Korea [29] to address the challenge. One prominent instance is the EU directives End of Life Vehicles (ELV,

2000/53/EC), legislation that requires 85% of the ELV to be reused or recycled by 1st January 2015, with 10% incinerated for energy recovery and only 5% landfill waste [30]. Moreover, Germany has wholly banned composite landfill waste, and the other EU countries are forecasted to follow [31]. Table 2-3 shows the legislation adopted by different regions and their recyclable goal.

Table 2-3: A comparison of the ELV management methods in various countries and regions (adopted from [32]*).*

	EU	**Japan**	**Korea**	**China**	**US**
ELV management system	*Law:* *Directive 2000/53/EC of the European Parliament.* *The Council of 18 September 2000 on end-of-life vehicles (enforced in 2000)*	*Law:* *Law for the Recycling of End-of-Life Vehicles (enforced in 2005)*	*Law:* *Act for Resource Recycling of Electrical/Electronic Equipment and Vehicles (enforced in 2008)*	*Law:* *End-of-Life Vehicle Recycling Regulation (enforced in 2001)* *Automotive Products Recycling Technology Policy (declared in February 2006)*	*Related law:* *Resource Conservation Recovery Act* *Clean Air Act, etc.*
Recycle target	*Until 2006:* *Reuse +Recovery: 85 %* *Reuse + Recycle: 80 %* *Until 2015:* *Reuse +Recovery: 95 %* *Reuse + Recycle: 85 %*	*Airbag: 85 %* *ASR: 70 % (from 2015 onwards)* *50 % (2010 - 2014)* *30 % (2005–2009)*	*Until 2014:* *Material + energy recovery: 85 % (of which energy recovery rate is within 5 %)* *After 2015:* *Material + energy recovery: 95 % (of which energy recovery rate is within 10 %)*	*Possibility of recycling:* *2010: about 85 % (material recycling of 80 % or more)* *2012: about 90 % (material recycling of 80 % or more)* *2017: about 95 % (material recycling of 85 % or more)*	*No specific goals (95 % of ELVs enter the recycling route, of which 80 % of the materials are recycled)*

2.3 Overview of the Research of Natural Fiber Reinforced Composites

Natural fiber-reinforced composites have gained significant attention due to their environmental friendliness, cost-effectiveness, and potential for improved mechanical properties [23,24]. These composites (or biocomposites) are suitable for various automotive, aerospace, marine, and construction applications [35]. However, their mechanical properties are not at par with most FRPs, but they can be further enhanced through proper synthesis and treatment of natural fibers [36]. With chemically treated fibers showing improved interfacial adhesion, better impact toughness and fatigue strength [24,26], the use of Natural Fiber-Reinforced Polymers (NFRPs) has been deemed particularly promising. The potential of applying these composites in the construction industry has also been undertaken since NFRPs can offer satisfactory mechanical properties and are renewable and biodegradable [37]. Abuthakeer [38] also highlights the importance of developing NFRPs, which, in return, also contribute to replacing heavy structures with lightweight materials without compromising the required strength.

Moreover, NFRPs have been widely utilized in the automotive industry to enhance vehicle design and functionality. For instance, Ford uses NFRPs in models like the Mondeo CD 162 and Focus in components such as floor trays, door inserts, door panels, B-pillars, and boot liners. Similarly, Mercedes Benz incorporates a mix of flax, sisal, and wood fibers combined with epoxy resin or unsaturated polyester (UP) matrix in various classes (C, S, E, and A) of its vehicles. Additionally, Mercedez trucks are adopting NFRPs for fabricating engine covers, engine insulation, sun visors, interior insulation, bumpers, wheel boxes, and roof covers. These showcase these components' versatility and environmental benefits in modern automotive manufacturing [39]. Table 2-4 shows the most used types of NFRPs in well-known manufacturers of automobiles.

Table 2-4: Automotive models, manufacturers, and components using natural fiber composites (adapted from [40]*).*

Model	Manufacturer	Components
A2, A3, A4, A4 Avant, A6, A8, Roadster, Coupe	*Audi*	*Seat back, side and back door panel, boot lining, hat rack, spare tire lining*
3, 5, 7 series	*BMW*	*Door panels, headliner panel, boot-lining, seat back, noise insulation panels, moulded foot well linings*
Raum, Brevis, Harrier, Celsior	*Toyota*	*Door panels, seat backs, floor mats, spare tire cover*
Golf A4, Passat Variant, Bora	*Volkswagen*	*Door panel, seat back, boot-lid finish panel, boot-liner*
Space star, Colt	*Mitsubishi*	*Cargo area floor, door panels, instrumental panels*
Clio, Twingo	*Renault*	*Rear parcel shelf*
Mercedes A, C, E, S class, Trucks, Evo Bus (exterior)	*Daimler-Benz*	*Door panels, windshield/dashboard, business table, pillar cover panel, glove box, instrumental panel support, insulation, molding rod/apertures, seat backrest panel, trunk panel, seat surface/backrest, internal engine cover, engine insulation, sun visor, bumper, wheel box, roof cover*
Pilot	*Honda*	*Cargo area*
C70, V70	*Volvo*	*Seat padding, natural foams, cargo floor tray*

Model	Manufacturer	Components
Cadillac Deville, Chevrolet Trail Blazer	*General Motors*	*Seat backs, cargo area floor*
Mondeo CD 162, Focus, Free Star	*Ford*	*Floor trays, door panels, B-pillar, boot liner*

In the aerospace sector, NFRPs are also progressively utilized in aircraft construction due to their effectiveness in reducing weight and cost. Specifically, an aircraft's front top skin and floor stand are made of NFRPs, by integrating NFRPs, the overall aircraft weight can be decreased by up to 35%, which will significantly enhance fuel efficiency of the aircraft, hence, reducing environmental impact [41]. Figure 2-3 below shows typical applications of NFRPs in an aircraft.

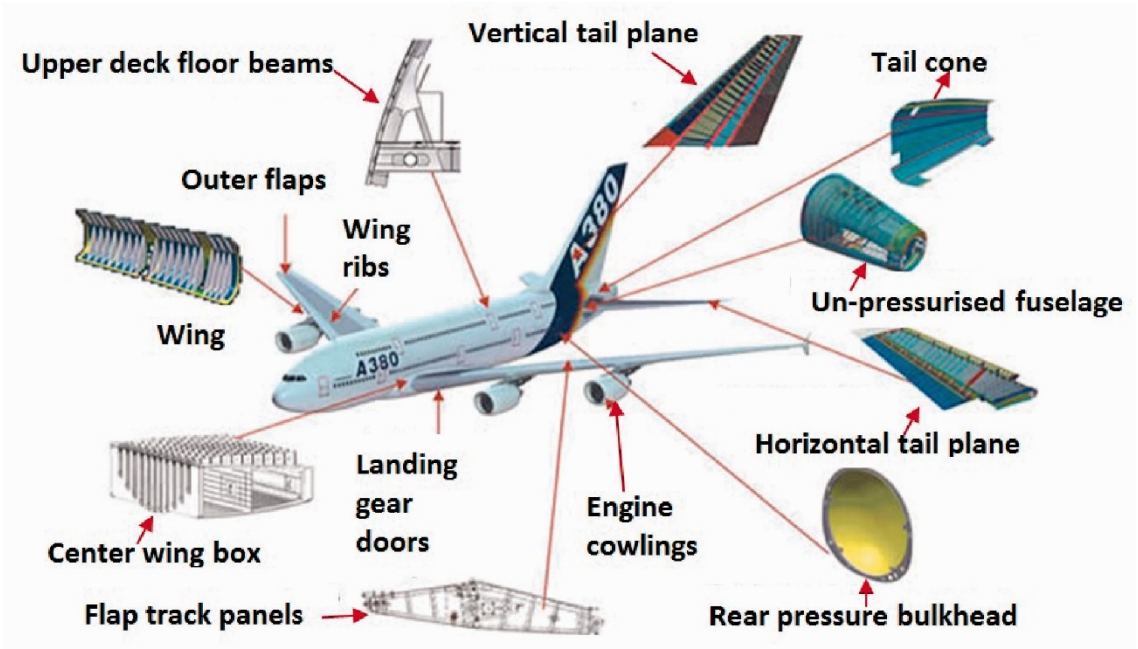

Figure 2-3:Natural fiber-reinforced polymer applications for a typical aircraft [41].

The global plastics and composites market is projected to grow from USD 624.8 billion in 2023 to USD 645.1 billion by 2030 at a Compound Annual Growth Rate (CAGR) of 4.2% [42]. This growth is driven by the increasing substitution of traditional materials like glass, metals, and wood with plastics across various industries, including automotive

and construction. The U.S. leads the North American market, with increasing demand in the automotive and construction sectors. Innovations and sustainability efforts will likely shape the market landscape.

2.3.1 Types of Natural Fiber

As briefly stated earlier, FRPs are highly desirable for their lower densities and higher specific mechanical characteristics compared to the traditional materials used in the industry [43]. As also stated, FRPs constitute two or more materials, such as reinforcement, matrix, and additives, aiming to merge the ideal properties of each constituent to form an optimal desired application-specific material [43]. Fibers exhibit greater strength and stiffness than matrix materials, serving as the principal load-bearing component within composite structures [15].

Fibers can be divided into synthetic, non-synthetic, and natural fibers. Non-synthetic fibers, such as carbon and glass fibers, form most of the fibers used in the industry [43]. Synthetic fibers are human-made fibers created through chemical synthesis, classified as organic or inorganic. However, the raising environmental concerns like toxicity, recyclability, renewability, and biodegradability that have been highlighted in recent years have led scientists to look for alternatives fibers like natural fibers since they possess several advantages that address some of the issues faced by the composite industry [44].

Natural fibers, also known as bio-based fibers are good alternatives to traditional synthetic fibers like fiberglass, carbon, Kevlar, boron, etc., due to their biodegradability, recyclability, and lower carbon footprint. Pervaiz and Sain [45] claimed that substituting 50% of glass fiber composites with natural fiber composites in North American automotive applications could cut CO_2 emissions by approximately 3.07 million tonnes and conserve around 1.19 million cubic meters of crude oil. The statistic shows the importance of natural fiber as a greener substitute for conventional fibers like glass and carbon fibers widely used in the industry today.

Natural fibers are classified into three main categories based on their derivation (i.e., plant-based, animal-based, and mineral-based). Plant fibers, also called botanical or

cellulose-based fibers, are the oldest known fibers cultivated and produced by humans ey. They are critical components in NFRPs and are predominantly used in engineering due to their availability and low cost. Animal fibers, rich in proteins like silk and wool, are valued in eco-friendly composites for their surface toughness and flexibility. Despite their higher cost and lesser availability, attributed to their unique properties, they are found in specialized applications in fields like biomedicine and electronics. Mineral fibers are the least used in the industry since some of their earliest types (e.g., asbestos) pose health risks, particularly to the lungs, which has limited their application [35,38,1]. Table 2-5 tabulates the three classifications of natural fibers based on the categories mentioned earlier.

Table 2-5: Classification of natural fibers extracted from [15,43,47–49].

Natural Fibers	**Animal**	**Silk**
		Animal Hair (Wool, Feather)
	Mineral	**Basalt**
		Wollastonite
		Fibrous Brucite
		Asbestos (Amosite, Tremolite, Actinolite, etc)
	Plant	**Grass** (Bamboo, Corn, Canary, Sabai, etc)
		Leaf (Sisal, Banana, Pineapple, Abaca, Date Palm, etc)
		Wood (Soft Wood, Hard Wood)
		Fruit (Coir, Oil Palm)
		Stalk (Rice, Wheat, Oat, Maize, etc)
		Bast (Hemp, Jute, Kanaf, Flax, Ramie, etc)
		Seed (Cotton, Milk wood, etc)

2.3.1.1 Properties and Applications of Natural Fibers

Natural fibers, such as jute, hemp, sisal, and coir, are increasingly used in various industries due to their biodegradability, lightweight, cost-effectiveness, and eco-friendliness [50]. These fibers are used in the automotive industry for applications like thermoforming and in the textile industry for clothing and technical applications. The use

of natural fibers in the automotive sector is particularly significant due to their potential to reduce the environmental impact of vehicles and lighter weight than traditional materials used in the industry [51], [52]. Table 2-6 below summarises the typical applications and properties of some known natural fibers used in the industry.

Table 2-6: List of common natural fibers, their application, and mechanical properties.

		Properties			
Fibers	**Application**	***Elongation (%)***	***Tensile strength (MPa)***	***Young's modulus (GPa)***	**Ref**
Abaca	*Automobile, paper, pulp, textile and furnishing industry, also used in making ropes, twines, fishing lines and nets*	*1—12*	*400—980*	*6-45*	[53–55]
Bamboo	*Reinforcement agent in polymeric materials, also used for making houses, bridges, and traditional boats.*	*3-4*	*140—800*	*10—40*	[53,56]
Banana	*First used in textile industry, now used in food and paper*	*1-4*	*52-910*	*3—34*	[53,57]
Coir	*Building panels, door shutters, storage tanks, packing materials, helmets, bags, mats, etc.*	*3-40*	*106-770*	*2-55*	[39,53, 58]
Cotton	*Furniture, textiles and yarn, and goods*	*2-16*	*250-800*	*5-13*	[39,53, 58]

Fibers	Application	Properties			Ref
		Elongation (%)	*Tensile strength (MPa)*	*Young's modulus (GPa)*	
Flax	*Window frame, railing systems, fencing, tennis racket, bicycle frame, fork, snowboarding, and laptop cases*	*1-4*	*345-1500*	*28-90*	[53,58, 59]
Hemp	*Construction products, textiles, paper & packaging, furniture, electrical, and manufacture of pipes*	*1.5-4*	*530-1100*	*30-70*	*[52,53, 57]*
Jute	*Building panels, roofing sheets, door frames, transport, packaging and geotextiles*	*1.1—3 2*	*200-860*	*3-60*	*[56]*
Kenaf	*Packing material, mobile cases, bags and insulations*	*1-7*	*295-1191*	*22-66*	*[52,53, 57]*
Ramie	*Used in products such as packing materials, fishing nets, and filter cloths. It is also made into fabrics for household furnishings, clothing, and paper manufacturing.*	*2-4*	*220-938*	*9-128*	*[57]*

Fibers	Application	Properties			Ref
		Elongation (%)	*Tensile strength (MPa)*	*Young's modulus (GPa)*	
Sisal	*In the construction industry, such as panels, doors, shutting plates, etc., also for the manufacturing of paper and pulp.*	*2-14*	*80-855*	*9-38*	*[53, 56]*
Oil Palm	*Building materials, including windows, door frames, roofing, decking, and fencing*	*2.50*	*248*	*3.20*	*[53,58]*
Date Palm	*Used in applications such as textile, sporting goods, baggage, automobiles, cabinets, mats*	*2-5*	*97-196*	*3-5*	*[,59]*
Sugarcane	*Paper and textile industry*	*6-8*	*257-291*	*15-18*	*[60]*
Wood	*Window frame, panels, decking, railing systems, and fencing*	*4*	*1000*	*40*	*[37,52]*
Feather	*impact absorption like helmets, car fenders, etc. Also, construction of building*	*7*	*100-203*	*3-11*	*[52,56, 61]*

Fibers	Application	Properties			Ref
		Elongation (%)	*Tensile strength (MPa)*	*Young's modulus (GPa)*	
	structures and light automobile parts.				
Spider Silk	*Biomedical sutures, manufacturing of implants and tissue engineering*	*27*	*1100*	*10*	*[52,56, 62]*

2.3.1.2 Some Notable Advantages of Natural Fibers

Natural fibers possess many environmental and practical benefits, making them highly desirable for various uses. Their biodegradability and renewability align them with global sustainability efforts by significantly reducing waste. Natural fibers are non-toxic, which minimizes health risks such as skin irritation and respiratory issues [65].

Natural fibers are abundant worldwide, making them accessible with lower production costs. Additionally, growing these fibers consumes relatively low energy and complements this with a zero-carbon footprint, as the plants absorb carbon dioxide from the atmosphere [66].

Moreover, natural fibers are known for their excellent thermal and acoustic insulating properties. They also boast high specific strength and stiffness relative to their low density and specific weight, which is advantageous in creating lightweight yet strong materials. The mentioned and non-abrasive properties make them suitable for various industrial applications [49].

2.3.2 **Resins as Matrices**

As stated above, resin is the polymer matrix constituent of an FRP. Polymers are created through a process where small molecular units, known as monomers, are linked together to form larger, more complex chain-like molecules [67]. These chains are linear, branched, and cross-linked polymer chains. Resins bind the reinforcing fibers, giving the

composite component its shape, facilitating load transfer among reinforcing fibers, and providing surface quality. The matrix properties determine the composite's resistance to most degradative processes, such as delamination, crack propagation, water absorption, impact damage, thermal creep, and chemical attack. These degenerative properties eventually lead to the failure of the structure. Additionally, the matrix ensures that the fibers are correctly positioned and oriented within the composite to carry the intended loads; this arrangement helps distribute the loads almost evenly across the fibers, providing resistance to crack propagation due to the plastic flow at the cracked tips [68].

One of the two categories of resins is thermoplastic resins, which are classified as linear or slightly branched polymers synthesized through the addition polymerization process. These polymers exhibit unique thermal properties; they soften upon heating and solidify when cooled. This behaviour is attributed to the weak intermolecular forces that link the polymer chains, allowing them to move relative to one another under heat. Crucially, this characteristic enables thermoplastics to be repeatedly recycled or reshaped. They can withstand numerous heating and cooling cycles without undergoing any chemical degradation. This capability makes thermoplastics versatile in various applications and environmentally beneficial due to their reusability [69].

Another category of resin is the thermosetting resin. Thermosets are polymers characterized by a highly cross-linkable with an extensive three-dimensional (3D) molecular structure. The 3D structure results from a cross-linking reaction between resins and curing agents under specific exposure conditions such as heat, UV light, microwave radiation, or moisture. Once cross-linked, thermosets display distinctive properties that set them apart from thermoplastics. In other words, thermoset polymers become primarily unaffected by heat exposure after their initial heat curing further.

Consequently, they exhibit exceptional corrosion resistance, heat, and mechanical creep compared to thermoplastics. These characteristics render them especially valuable in applications requiring precise tolerances and excellent strength-to-weight ratios at high temperatures. Additionally, the irreversible bonds formed during the curing process

prevent thermosets from softening under heat (up to a specific limit), making them ideal for high-voltage applications [62,63].

The following Table 2-7 shows the classification of the resins commonly used in industrial applications.

Table 2-7: Classification of commonly used resins used in industrial applications [62,64,65].

Thermoplastic Resin	Thermosetting Resins
• Polycarbonate • Acetal Copolymer • Acrylic (PMMA) • Nylon • Polyethylene • Polypropylene (PP) • Polystyrene • Polyvinyl chloride (PVC) • Teflon • ABS • Polylactic Acid (PLA) • Elium	• Vulcanized rubber • Phenolic resin (bakelite) • Polyurethane • Epoxy resin • Vinyl ester resin • Polyester • Polyimides • pDCPD (polydicyclopentadiene) • Polyurea • Structural Foams • Melamine • Silicone • Urea Formaldehyde • Recyclamine

In recent years, interest has risen significantly in developing polymers from renewable resources for industrial applications. The interest has mainly stemmed from the increasing use of epoxy resins, which account for about 70% of the thermosetting market. Additionally, almost 90% of the epoxy resins are made using Bisphenol A (BPA) [74]. Bisphenol A (BPA), an industrial chemical that has been used to create certain plastics and resins since the 1950s [75], is among the highest volume chemicals produced globally, with current estimates showing that over 4 million tons are produced annually, and about 100 tons are released into the atmosphere each year. The adverse effects of BPA on human health include disruptions in the immune and reproductive systems, as well as changes in brain chemistry. BPA is also known for its estrogenic properties,

prompting ongoing efforts to replace the traditional Di-glycidyl Ether of Bisphenol A (DGEBA) epoxy with bio-based alternatives that match conventional materials' performance [73].

Therefore, the need to develop harmless alternative biopolymers is particularly appealing due to their low production costs and potential biodegradability [76]. One promising area of development is in bio-based epoxy resins. These resins have been used in various applications, including paints, coatings, adhesives, and biomedicine. The use of biocomposites in critical applications, such as aircraft fabrication, has also been explored by various researchers [77]. For instance, hyperbranched epoxy resins (HERs), a complex 3D polymer, have attracted attention for their ability to surpass traditional BPA-based resins' limitations [74]. These resins are derived from natural sources like natural oils, polyphenols, saccharides, natural rubber, and rosin and offer properties comparable to those of petroleum-based resins[78]. Despite their potential, hyperbranched epoxy resins still require enhancements in terms of their thermomechanical and mechanical properties as well as thermal stability to fully meet industrial standards and applications [79].

2.3.2.1 Application and Properties of Resins

A range of polymer resin applications have been explored in various fields. For instance, Chowdhury [80] emphasizes the significant role that resin composites play in dentistry, aerospace, and automotive industries, noting their critical contribution to advancements in these fields. The table below summarises the applications and mechanical properties of a few resins. Another instance is investigating the utilization of specific polyester and epoxy resins. The author highlights these resins' vital applications in producing cosmetic products and protective coatings [81]. Table 2-8 below summarises a few of the available commercial applications of various resins and their properties.

Table 2-8: Commonly used commercial resins, their properties, and applications (adapted from [80,4]).

Matrix Material	Properties	Applications
Polyethylene (PE)	*Resistance to corrosion*	*Piping*
Polypropylene (PP)	*Resistance to chemicals*	*Packaging, automotive, construction*
Polylactic acid (PLA)	*Biodegradable, non-toxic*	*Food handling, bio-medical*
Polyurethane (PU)	*Wear resistance, low cost, sound and waterproof*	*Structural, acoustic*
Poly-vinyl alcohol (PVA)	*High tensile strength*	*Bio-medical*
Natural rubber	*Low density, low cost, biodegradable*	*Structural, automobile*
Epoxy based resin	*High strength*	*Automotive, aerospace, marine, construction, sporting goods and several other applications*
Polyester	*Durable, resistance to water, chemicals*	*Structural*
Phenolic Resin	*Corrosion, chemical and heat resistance, low density*	*Electronics, ballistics, mine ventilation, aerospace, rail and mass transit*

2.3.2.2 Advantages and Disadvantages of Resins

As mentioned previously, various sectors such as defence, aerospace, marine, construction, and automobile manufacturing utilize FRPs in large quantities due to their distinctive advantages over metals. Polymer composites offer improved thermal insulation and fatigue resistance, which is crucial for applications exposed to extreme environmental conditions [83]. As a result, the integration of polymer composites continues to grow, driving innovations in materials engineering and manufacturing processes.

Thermoplastic polymer resins are frequently used to produce various profiles and are materials we interact with daily. The market for thermoplastic composites was projected to expand at a compound annual growth rate (CAGR) of 5.2% between 2019 and 2024. The market value is expected to reach US $36 billion by the end of 2024 [84]. This growth demonstrates the increasing reliance on these materials across various industries, mainly driven by their recyclability and robust performance attributes.

On the other hand, traditional FRPs typically employ a thermosetting resin, which effectively secures the structural fiber in position. The thermoset composites market was projected to grow to US$ 57.98 billion between 2016 and 2021, with a CAGR of 6.67%. The Thermoset composites market is notably larger compared to its thermoplastic counterparts. Typical applications of thermoset composites are found in aerospace, civil engineering, appliances and electrical components,, where their robustness and durability are particularly valued [84].

The classified polymer resins have merits and demerits that make them suitable for application-specific industries. Table 2-9 below illustrates the general advantages and drawbacks of thermoplastic resin and thermoset resins.

Table 2-9: Comparison of thermoplastic and thermoset matrices [82,83].

Thermoplastic Resin	Advantage	Unlimited shelf life
		Easy to handle (no tackiness)
		Recyclable
		Easy to repair by welding and solvent bonding
		Post Formable
		Tough
	Disadvantage	Prone to creep
		Poor melt flow characteristics
		Thermoplastics need to be heated above the melting point to sufficiently wet the fibres
		Majority of the thermoplastic comes in solid state
Thermosetting Resin	Advantage	Low resin viscosity
		Good fibre wetting
		Excellent thermal stability once
		polymerized
		Chemically resistant
		Creep resistant
	Disadvantage	Brittle
		Non-recyclable via standard techniques
		Not post-formable

2.4 MANUFACTURING TECHNIQUES OF POLYMER COMPOSITES

Manufacturing of FRPs involves the manufacturing of fiber preforms and then reinforcing these fibers with the matrix material by various techniques. Researchers have explored various effective manufacturing techniques for composite fabrication over the last few decades. For instance, Nishida [86] emphasized the importance of understanding fabrication processes' technical and economic features, explicitly highlighting the need for good bonding between matrix metal and reinforcements. Cherouat [87] considered composite fabrics and automated technologies to optimize properties and reduce costs. These studies underscore the importance of systematically understanding fabrication processes and the potential for cost-effective, high-performance structures. A range of

fabrication techniques have also been considered in [88–95], with a summary reported in Table 2-10.

Table 2-10: Fabrication techniques of fiber-reinforced composites [88–95].

Technique	Process Details	Advantages	Typical Applications
Hand Lay-Up Technique	*Manual placement of fiber preforms into an open mould followed by the application of resin either by pouring or brushing. A roller is used to consolidate the resin into the fabrics, ensuring proper impregnation and interaction between the layers of reinforcement and matrix materials.*	*Simple, cost-effective, highly flexible operator skills crucial for quality. Allows for customizations in size and shape.*	*Custom, large-scale components like boat hulls and aerospace parts.*
Prepreg Hand Lay-Up Technique	*Fibers are pre-impregnated with resin, then laid, consolidated, and cured using heat and pressure.*	*High-quality and consistent properties, reduced processing time, lower risk of voids, and improved health and safety.*	*Aerospace, automotive, sports goods, and high-performance applications require precision.*
Spray-Up Technique	*A chopper gun is used to spray a mix of resin and chopped fibers directly onto the mould surface. The sprayed layers are rolled to ensure thorough integration and reduce air pockets.*	*Faster than hand lay-up, suitable for complex contours, allows moderate control over fiber orientation.*	*Parts with complex shapes, such as automotive body panels and boat hulls.*
Vacuum Bag Molding	*Starts with a hand lay-up to place the laminate, which is then covered with a vacuum bag. Air is evacuated using a vacuum pump, compressing the laminate against the mould under atmospheric pressure.*	*Uniform pressure distribution enhances the fiber-to-resin ratio, reduces voids, and improves mechanical properties. Excellent surface finish.*	*High-quality structural components in aerospace and automotive industries.*

Technique	Process Details	Advantages	Typical Applications
Resin Transfer Molding (RTM)	*Fiber preforms are placed into a closed mould; the resin is then injected under controlled pressure and temperature, permeating uniformly through the fibers.*	*Produces parts with two good surfaces and consistent thickness, excellent structural integrity, and surface finish. Can incorporate complex fiber orientations.*	*High-performance components in aerospace, automotive, and sports equipment.*
Compression Molding	*Fiber preforms or prepregs are placed in a heated mold, which is then closed under high pressure. The heat and pressure cure the resin, moulding the material into the desired shape.*	*High volume production capability, excellent dimensional stability, and mechanical properties. Efficient for medium to high-volume parts.*	*Structural automotive components, electrical insulators, and household items.*
Vacuum Assisted Resin Transfer Molding (VARTM)	*An advanced RTM that uses a vacuum to draw resin into the mould over the fiber lay-up, ensuring complete saturation and reducing air entrapment.*	*Ideal for large and complex structures, it reduces void content and enhances mechanical properties and durability.*	*Large structures like wind turbine blades, boat hulls, and architectural components.*
Filament Winding	*Continuous fibers are soaked in resin, then wound around a rotating mandrel and cured. Allows precise control of fiber placement and orientation.*	*High production efficiency, suitable for large and complex shapes, consistent properties.*	*Manufacturing of pipes, tanks, and pressure vessels.*
Pultrusion	*Pultrusion involves pulling continuous fiber rovings or tapes through a resin bath, typically of*	*Efficient for producing consistent, long*	*Used to manufacture structural*

Technique	Process Details	Advantages	Typical Applications
	thermosetting polymers like epoxy or unsaturated polyester. The fibers, impregnated with resin, are then pulled through, forming dies that shape the final product. The composite material is then cut to the required lengths.	*sections with complex profiles, low labour intensity, and continuous production process.*	*profiles, rods, and bars, often employed in construction, electrical utility, and infrastructure projects.*
Extrusion	*Pushes or pulls material through a die to produce profiles with uniform cross-sectional shapes. Effective for continuous production.*	*High production rate, continuous production of long sections like rods, tubes, and channels.*	*Profiles and parts with uniform cross-sectional shapes.*
Automated Fiber Placement (AFP)	*Robotic systems lay down fibers and resin layer by layer with precise control over fiber orientation and placement.*	*High precision, reduced material waste, and ability to create complex geometries and large structures.*	*Aerospace components require high-performance and precision.*
Electrospinning	*A relatively new technique which uses an electrostatic process to create ultrafine fibers from solutions or melts.*	*It produces fibers with high fineness and control over composition and morphology, as well as a high surface area-to-volume ratio.*	*Biomedical applications like tissue engineering scaffolds.*

When fabricating FRPs, choosing the proper manufacturing process is essential to ensure the final product meets the desired specifications and is free of defects. This choice starts with a careful review of several essential factors. These include the shape and size of the composite, which can affect which manufacturing methods are possible, and the specific properties the composite needs to have, like strength or resistance to heat.

The cost of manufacturing is also a key consideration. The cost includes how much the raw materials cost, the required labour hours, and the process efficiency. Additionally, production speed is important, especially when large quantities are needed quickly. How the fibers behave and handle during the manufacturing process and their compatibility with each other also play a crucial role in deciding which process to use. All these factors need to be balanced to choose the best manufacturing method for producing NFRCs that are effective and economical.

Figure 2-4 below illustrates several main manufacturing techniques used in the industry.

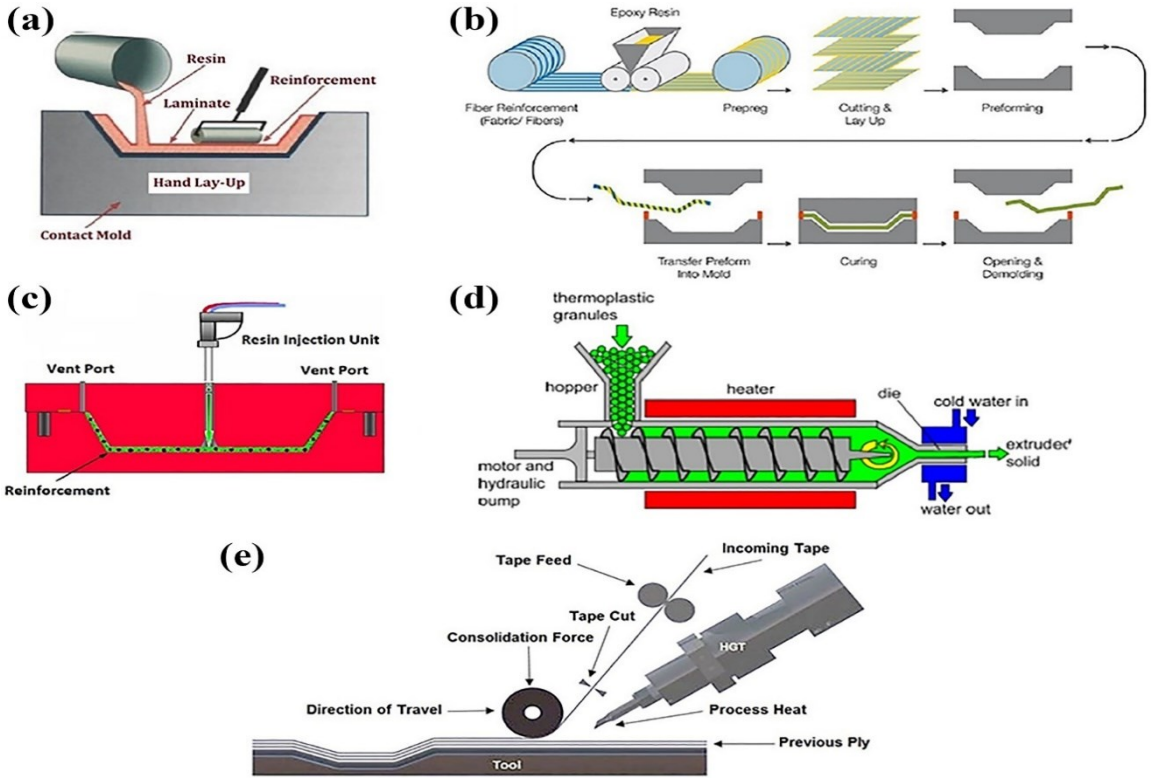

Figure 2-4: Schematics of various manufacturing techniques. (a) Hand layup process, (b) compression molding, (c) resin transfer moulding, (d) extrusion process, and (e) automated fiber placement [93].

2.5 Sustainable Fibers and Recyclable Resins

Flax and basalt fibers are emerging as promising sustainable alternatives to traditional fibers. Flax is biodegradable and offers adequate mechanical properties. Basalt, derived from volcanic rock, boasts high-temperature stability and low environmental impact.

Recyclamine and Elium resins offer biodegradability and recyclability, respectively, contributing to the goal of creating a sustainable composite.

2.5.1 **Flax**

Though not a type of fiber considered in this work, a brief introduction to flax fibers is deemed appropriate. Flax fibers have been used since ancient times, and it is assumed that this type of fibers has been used since the beginning of civilization. Flax fiber reinforcements are the dominant type of natural fibers used in the composite industry because of their relatively higher mechanical properties than the other natural fibers. Its composites are vastly used in the automotive sector, and other researchers have explored the option of using them in marine, sports and entertainment, household, and other engineering applications. In addition, research is ongoing on utilizing flax fiber reinforcement for aerospace, satellite and wind turbine components. The flax fiber reinforcement can be comparable to E-glass in specific criteria like cost per weight (0.5-1.5 vs 1.6–3.25 USD/kg) [58]. A comprehensive physio-mechanical property of flax and a few commonly used fibers for comparison is given in Table 2-11. However, the variability of flax fibers reduces the confidence in usage over its counterpart E-glass. Additionally, like all natural fibers, flax fibers are moisture-sensitive, affecting the quality of the final product.

2.5.2 **Basalt**

Basalt is made from solidified volcanic lava with a melting temperature between 1500°C and 1700°C. Its properties are highly affected by the rate of temperature change during the quenching (cooling) process, which leads to complete crystallization. Moscow Research Institute of Glass and Plastic developed it in the early 1950s.

Basalt fiber production varies in cost, depending on the quality of raw materials, production techniques, and final product characteristics. The manufacturing process of basalt fiber closely resembles that of glass fiber, but it is more energy-efficient, making it a cost-effective alternative. Basalt fibers are processed using conventional equipment and techniques without the need for additional additives, thus significantly lowering their production cost. In brief, natural volcanic basalt rock is melted at 1450°C to 1500°C and

extruded to produce both chopped and continuous fibers, which are then used in textile manufacturing and fabrication of composites.

Though basalt has a similar composition to asbestos, basalt fibers are considered safe due to their different surface properties, without any risk of being carcinogenic or toxic, as confirmed by research confirms; therefore, they are being increasingly used in industrial applications. Moreover, basalt fibers offer numerous advantages over glass fibers (as discussed below) as a reinforcing material for fabricating composites. These advantages have rendered them an effective alternative to glass. and hence used across marine, automotive, sporting equipment, and civil applications.

Basalt fibers have good mechanical properties similar to glass fibres and show even better features such as non-combustibility, high chemical stability, and resistance to weather, alkaline, and acids. Basalt can withstand subfreezing temperatures (as low as around 200°C) and comparatively very high temperatures (600°C to 800°C). Table 2-11 compares a few mechanical properties of basalt fiber, flax, and other fibers. Lastly, their thermal stability, facilitated by numerous micro-pores, makes basalt fibers ideal for thermal insulation and passive fire protection applications [96].

Table 2-11: Physio-mechanical properties of basalt and flax fibers [58,96].

Fiber	Density (g/cm^3)	Tensile Strength (MPa)	Tensile Modulus (GPa)	Elongation (%)
Flax	*1.4 - 1.5*	*343 - 2000*	*27.6 - 103*	*1.2 - 3.3*
Hemp	*1.4 - 1.5*	*270 - 900*	*23.5 - 90*	*1 - 3.5*
Ramie	*1.0 - 1.55*	*400 - 1000*	*24.5 - 128*	*1.2 - 4.0*
Basalt	*2.8*	*2,800*	*89*	*3.15*

Fiber	Density (g/cm^3)	Tensile Strength (MPa)	Tensile Modulus (GPa)	Elongation (%)
E-glass	*2.5 - 2.59*	*2000 - 3500*	*70 - 76*	*1.8 - 4.8*

2.5.3 **Elium®**

Elium® was developed in 2009 by Arkema S.A. of France as a novel resin and the world's first liquid thermoplastic resin. This resin is chemically crosslinked by radical polymerization, where its monomer, methyl methacrylate (MMA), transitions to its polymer form methyl methacrylate (PMMA). The transition is facilitated using a peroxide catalyst. This novel resin is cured at room temperature and exhibits low viscosity, and hence, is used as an alternative to the widely used thermoset epoxy resins in the fabrication of FRPs. Another attractive feature of Elium® is that it is fully recyclable, which addresses the environmental concerns associated with thermosetting plastics by potentially reducing waste.

The resin's ductility and toughness improve the impact resistance and increase the durability of its composites. These attributes have rendered Elium® an excellent sustainable alternative resin in the FRP industry [97–99].

2.5.4 **Recyclamine®**

Recyclamine® is an amine-based epoxy curing agent, another novel resin developed in 2012 by Connora Technologies (CA, USA) to address the significant environmental and sustainability challenges posed by traditional epoxy thermosets, which are inherently non-recyclable. Unlike conventional thermoset resins that cannot be reformed or reused once cured, Recyclamine® is formulated to have cleavable bonds within the epoxy matrix that can be broken by exposure to acetic acid at high temperatures (100^oC). This feature allows the thermosetting epoxies to convert into thermoplastics, allowing the matrix to disintegrate and enabling the recovery and recycling of reinforcing the fibers forming its FRPs.

Recyclamine® can be used with any epoxy resin and is compatible with regular manufacturing processes like wet lay-up, resin infusion, and resin transfer moulding (RTM). Moreover, the environmental benefits of Recyclamine® are quite significant, as it offers a solution to the end-of-life recyclability issue of thermosetting composites, typically disposed off through incineration or landfilling, contributing to pollution and global warming. The development of Recyclamine® enables the recycling and reuse of composite materials and aligns with the goals of reducing the carbon footprint and advancing towards a more sustainable, circular economy [100,101]. This is very different than commercially available epoxy resins, which can't be recycled due to their unbreakable monomeric structure, causing the composite to be totally disposed of at landfill sites or incineration, emitting greenhouse gas as mentioned in 2.2.

Table 2-12 shows the properties of Elium, Recyclamine and epoxy for comparison.

Table 2-12: Mechanical properties of Elium, Recyclamine and epoxy for comparison [97–99,102].

Matrix	Glass Transition Temperature (T_g) (°C)	Tensile Strength (MPa)	Tensile Modulus (GPa)	Flexural Strength (MPa)	Flexural Modulus (GPa)
Elium® 150	*~105*	*66*	*3.17*	*111*	*2.91*
Recyclamine®	*~90*	*73.49*	*3.28*	*131.11*	*3.388*
Recovered Recyclamine	*~78*	*51.2*	*2.90*	*100*	*2.7*
Epoxy	*~100*	*50.33*	*3.17*	*81.36*	*3.1*

The recycling process of Recyclamine®-based epoxy composites involves several steps, mainly focusing on the disintegration of the thermoset matrix into a recyclable form and the recovery of the reinforcement materials. Here is a step-by-step process [102]:

Manufacturing of Composite: Initially, the composite is manufactured using Recyclamine® as the curing agent for the epoxy resin. Depending on the application

requirements, this is done through wet lay-up, resin transfer moulding (RTM), or infusion processes.

End-of-Life Composite Treatment: Once the composite reaches its end of life, it is subjected to a specific recycling condition. This involves immersing the composite in an acid solution, typically acetic acid, at a controlled temperature (e.g., 80°C) for a set duration (e.g., 4 hours)

Separation and Recovery: The solution containing the dissolved epoxy matrix is then filtered. The reinforcement materials such as glass fibers, carbon fibers, or Kevlar® are recovered and separated from the dissolved matrix. These materials can be neutralized, rinsed, dried, and prepared for reuse.

Reprocessing of Recycled Epoxy Matrix: The dissolved epoxy matrix in the solution can be neutralized and coagulated to recover it as a thermoplastic polymer. This recovered material can then be compounded with other polymers (e.g., polyethylene) and repurposed into new products, such as foot strap inserts for surfboards. Figure 2-5 shows the reprocessing method of Recyclamine resin.

Reuse of Recovered Materials: Both the recovered reinforcement materials and the reprocessed epoxy-based thermoplastic can be used to manufacture new composite materials or other products, thereby closing the loop in the material's lifecycle and contributing to a circular economy.

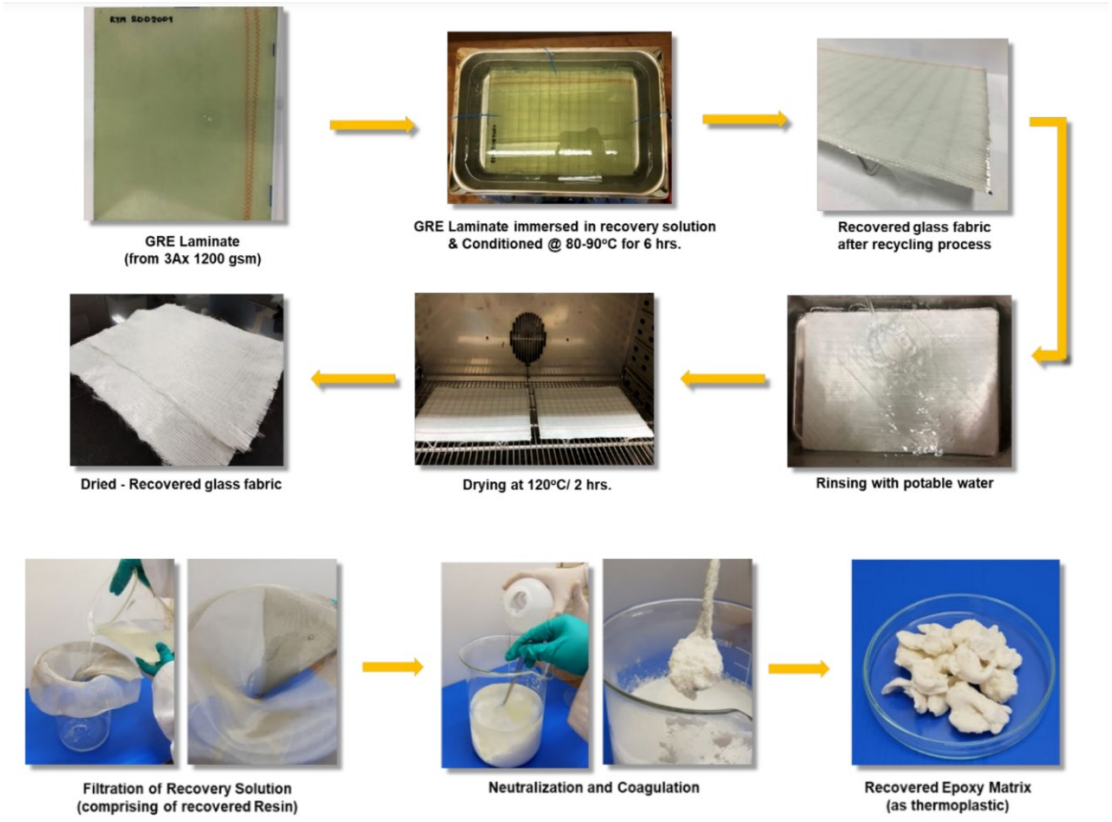

Figure 2-5: Recycling of glass-reinforced epoxy (GRE) and recovery of the matrix and reinforcement [102].

2.5.4.1 Industrial Applications of Recyclamine

Recyclamine® technology was used to develop recyclable epoxy resin systems specifically designed for manufacturing wind rotor blades. Two main fabrication techniques were utilized: the wet lay-up process and the infusion process. In the wet lay-up process, layers of fiber reinforcement are manually placed and saturated with resin. In the infusion process, the resin is drawn through the fibers under vacuum pressure, ensuring even distribution [102]. Siemens Gamesa, in collaboration with Aditya Birla Advanced Materials, has achieved significant accomplishments in producing durable and fully recyclable blades. These blades maintain high performance and can be easily dissolved at the end of their life cycle, allowing for the recovery and reuse of materials, significantly reducing environmental impact and costs, earning recognition in the 2022 JEC Composites Innovation Awards. [103,104].

Recyclamine® technology was also utilised for manufacturing snowboards using injection molding fabrication technique [105]. Niche Snowboards integrated

Recyclamine to develop durable and fully recyclable snowboards. This innovation earned them recognition in the 2020 JEC Innovation Awards. They said in an interview that they are also open to collaboration with other industry leaders to further extended Recyclamine's application to skis, surfboards, and kayaks [106].

2.6 Related Studies on Similar Composite Systems

Previous studies have explored the combination of sustainable fibers and recyclable resins to address environmental concerns. A few researchers have evaluated and compared the mechanical properties of the resin. For instance, Rangappa et al. [58] examined flax fibers in great detail and claimed continuous flax fiber composites to have superior mechanical properties than glass/epoxy composites. However, the performance was revered when considering the short fiber-reinforced composites.

The authors also discussed biodegradable composites produced by biobased polymer matrices and natural fibers. Examples of reported bio-based matrices for bio-composites are bio-epoxy resin, PLA (polylactic acid) and bio-phenolic (tannin) resin. Moreover, they stated that surface modification of fibers also plays a vital role in ensuring good fiber/resin adhesion; one of the cited examples is the Alkali (NaOH) treatment. This treatment has been reported as a powerful tool for the surface treatment of flax and other natural fiber composites, which has led to up to ~21% enhancement in tensile, bending and shear properties compared to the untreated composites.

Yaghoobi and Taheri [97] presented a detailed survey of prior studies conducted on Elium. They also evaluated the tensile, flexural and buckling response of basalt-Elium and basalt-epoxy composites. The tensile strength of the basalt-Elium composite was found to be 23.9% higher than the epoxy counterpart. Also, the fracture response of basalt-Elium was observed to be slightly more ductile than its counterpart. Moreover, the Flexural strength and buckling strength of their basalt-Elium were marginally lower than their basalt-epoxy composite. The authors then compared the performance of thermoplastic fiber metal laminates (TP-FML) fabricated with thin sheets of magnesium sandwiching basalt-Elium laminate. They demonstrated the significantly superior performance of the TP-FML compared to an equivalent basalt-Elium composite.

Moreover, other researchers have studied the moisture absorption characteristics of these materials. For instance, Muñoz and García-Manrique [107] investigated the effect of water absorption on the mechanical properties of Flax and SuperSap epoxy resin composite. The authors confirmed the Fickian absorption of the composite. The results showed that water absorption increased with increasing fiber content. Their tensile and flexural specimens with 40% fiber volume had weight gains of 6.23% and 6.56%, respectively.

In contrast, the weight gains were 8.71% and 9.76% for the composites with 50% fiber content for tensile and flexural. These %weight gains were taken after composites were exposed to water for 768 hours at room temp. Moreover, the tensile strength and strain of the composites increased after the immersion, and the author deduces that it is due to plasticization. However, the tensile modulus of both composites and the flexural modulus of 0.55 fiber content composite decreased by about 20% after immersion.

Chilali et al. [98] evaluated the moisture absorption rate of flax-epoxy and flax-Elium 150. They observed degradation of the elastic modulus and tensile strength in both composites and attributed to them the degradation of the flax and the weakening of fiber matrix interface. It was also stated that water could directly affect the hydrophilic constituents of the flax fiber, which weakens the interface between the layers. However, plasticization of the resin caused by water absorption resulted in a 27% increase in the strain of both composites. Moreover, both the composites exhibited comparable properties after immersion in tap water for 2,7,15 and 30 days at 20°C. However, after 30 days, the tensile modulus and strength decreased by 42% and 58%, respectively.

A detailed literature review on flax fiber and its composite, along with moisture absorption, was presented by Moudood et al. [108]. A notable mention in the article was the nonlinear moisture absorption of flax fibers behaviour of water intake after RH% 90, where the flax does not follow a linear intake (does not follow Fickian's law of diffusion) but instead has a very steep jump of water intake. He also noted that moisture-absorbed raw flax fibers presented higher tensile strength than those subjected to drying stages. They concluded that the cohesion between the matrix and the microfibrils is lost after

drying, potentially decreasing tensile strength. Moreover, he mentioned that few researchers studied the effect of moisture in flax fibers on the properties of flax fiber-reinforced epoxy (FFRE) composites. They found that composite panels with fibres from high-humidity environments showed severe warping, which was attributed to the moisture in the fibers, which caused fiber shrinkage during the vacuum infusion process, resulting in residual compressive stresses that led to part warping after demolding. High moisture content in the fibers weakened the fiber-matrix interface and increased porosity in the microstructure of the composites.

The researchers found that the optimum tensile strength was obtained at 50% RH-conditioned fabrics; anything else decreased the properties. Water molecules increased the strain at break and decreased Young's modulus, while the flexural strength and modulus decreased with increasing humidity. Composites fabricated with fibers conditioned at 95% RH showed a sharp drop in mechanical properties. Furthermore, Esleman [109] examined the moisture effect on basalt along with glass and carbon plus hybrid models. As expected, the water intake was highest for basalt, and the trend relating to tensile, flexural strength, and modulus followed a similar pattern to that of flax. However, the water intake was much less (0.55% after 6 months) than that of flax fibers.

Comparative studies considering the response of composites made with Recyclamine® are very scarce. In a study by Dattilo et al. [110], the authors used biocomponent resins using Polar Bear and Recyclamine 101 from R*Concept Biocomposites Solutions (Barcelona, Spain), with 28% biocarbon. Nearly a third of the resin's carbon is derived from renewable biological sources, making the resin eco-friendlier than the usual epoxies. The research focused extensively on the chemical component of the resin at different curing conditions. The notable thermomechanical finding was the glass transition temperature (T_g), which was found to be 60^{o}C when the resin was cured for 24 h at 25^{o}C. An additional three h curing at 100^{o}C increased the T_g to around 103 ^{o}C. A mixing ratio of 100:22 of Polar Bear Recyclamine was used in this study.

In another study [111], composite panels were prepared with recyclable epoxy using high-pressure RTM (Resin Transfer Moulding) technology. The panels were fabricated using eight layers of cross-ply carbon fabrics with $[0/90]_8$ layup sequence. Then, a mixture of epoxy monomer SUPERSAP 300 and amine-based Recyclamine® was injected into a preheated mould subjected to 160 bar pressure. Each panel was cured at 120°C for 5 minutes, followed by 1 hour 120 °C. The recycling process involved breaking the cross-links of the cured epoxy in a hot acidic acid (vinegar) bath, dissolving the resin away from the fibers and collecting the resulting thermoplastic material while keeping the original fiber architecture intact.

Testing of panels made with virgin and recycled fiber preforms showed that the mechanical properties were nominally the same. Scanning electron microscope analysis showed that the chemical treatment produced clean fibers with no damage, similar to virgin fibers. Additionally, the composites exhibited higher tensile strength than magnesium and Aluminum alloys. A similar study conducted by Ferrari et al. [112] assessed the life cycle of composites consisting of Recyclamine, Super Sap® epoxies, and hybrid (flax and carbon) fibers. The authors claimed that the Recyclamine-enabled chemical recycling method provides a 60% reduction in global warming potential. The author concluded that the recoverable and recyclable hybrid composite offered good tensile strength and life cycle.

As you can see, to the best of the author's knowledge, the properties of composites made of basalt fiber and Recyclamine matrix have not been explored yet. This composite type is believed to have great potential for use in various industrial applications and is eco-friendly and fully recyclable. In an experimental investigation [113], the tensile, compressive and shear properties of unidirectional basalt-epoxy were compared with those of E-glass-epoxy, S-glass-epoxy and carbon-epoxy from the literature search, all with fiber volume content to 60%. The specimens were cured in an autoclave, and C-scanning was used to confirm that porosities were nonexistent. Table 2-13 shows the unidirectional properties of the basalt-epoxy composite.

Moreover, the authors observed that their basalt composite showed similar tensile properties to their E-glass composite; however, the compressive strength of the E-glass composite was superior to the basalt composite. Basalt-epoxy also shows better compressive strength compared to S-Glass. However, both glass composites fell short in shear strength.

Table 2-13: Uniaxial properties of basalt-epoxy composite [113].

Basalt Fiber Orientation	Tensile Young's Modulus (GPa)	Tensile Strength (MPa)	Compressive Young's Modulus (GPa)	Compressive Strength (MPa)
0 Degree	*44.3*	*1310*	*46.2*	*776*
90 Degree	*11.9*	*49.8*	*15.2*	*135*

In another research by Kulpa et al. [114], the authors attempted a three-stage properties comparison to select the best material for constructing an FRP deck panel. The author used Araldite LY1564 SP epoxy resin and Aradur 3489 hardener. In the first testing stage, bi-directional (0/90) basalt-epoxy produced an elastic modulus of 23.72 GPa compared to 24.65 GPa for bi-directional E-glass epoxy. In contrast, the other properties of the composites were similar. Nonetheless, the authors decided to continue the rest of their investigation of E-glass based on their previous "positive" experience and limited resources. An interesting finding of the study was that the compressive strength of basalt and glass composites was as much as two and three times higher than that of aramid composites. The difference in the values of the longitudinal and transverse moduli estimated using micromechanics and the experimental value for the basalt composite was 11%, whereas the difference in the compressive strength was very large, with the analytical value being 175% higher than the experimental value. Table 2-14 shows the experimental results obtained in the research.

Yasmeem et al. [115] evaluated the Izod impact Brinell hardness for basalt continuous fiber and fiberglass chop-strand mat epoxy composites fabricated by hand lay-up procedure. Eight layers of basalt only, eight layers of fiberglass chops strand mat (CSM)

only, and alternating layers of chops strand mat fibreglass and basalt were used. The author observed that the basalt composite exhibited higher impact strength than the CSM composite (5.7 MPa vs. 2.81 MPa, respectively).

Table 2-14: Properties of some common laminates with 0/90 fiber direction [114].

Laminate	Tensile Strengths (MPa)	Tensile Modulus (GPa)	Compressive Strengths (MPa)
Basalt	*399.13 ± 31.61*	*23.72 ± 1.09*	*217.24 ± 29.32*
E-Glass	*454.39 ± 23.11*	*24.65 ± 3.03*	*290.09 ± 36.88*
Aramid	*458.80 ± 37.85*	*26.80 ± 4.07*	*93.79 ±13.10*
Carbon	*806.68 ± 62.01*	*66.31± 4.31*	*323.90 ± 43.39*

Additionally, other research related to surface modification and hybridization (stacking sequence of basalt fibers Laminates) was carried out. The research paper by Li et al. [116] investigates the effects of La^{3+} modification (rare earth modification) on the mechanical properties of basalt fiber/epoxy resin composites. The author also conducted tensile tests to measure the mechanical properties of the composites. Li et al. found that La^{3+} modification improved the interfacial adhesion between the BFs and the epoxy resin matrix. The tensile tests showed that La^{3+} modification significantly improved the composites' tensile and bending strengths. The tensile strength of the modified composites was highest with the concentration of Lanthanum ions of 0.5 wt%, which increased to 458.7 MPa from 250 MPa, and the bending strength increased to 556.7 MPa from around 275 MPa. The authors concluded that La^{3+} modification effectively improves the mechanical properties of basalt fiber/epoxy resin composites.

Another research study by Manikandan et al. [117] attempted to prove that surface modification of basalt increases its strength compared to E-glass. The author soaked the fibers in a base solution (NaOH) and an acidic solution H_2SO_4 and analyzed the mechanical properties. It was found that the acid-treated basalt had the highest tensile and

impact strengths with 246 MP (24% increase compared to untreated basalt) and 2.9 J/mm (11.94% more), respectively. However, the base-treated basalt had the highest ILSS with 23.06 MPa.

The author compared the fracture mechanism using SEM, which showed a precise crack formation on the surface of the acid-treated fiber glass leading to its lower strength. The writer speculates that the lower bond strength may have caused large fiber-to-matrix (interfacial) debonding for glass fiber compared to the basalt fiber. Manikandan also notes the SEM image showed that the glass fiber was highly affected by the base and affected on the surface when treated with acid, contributing to its lower overall properties. In contrast, the base did not affect the basalt and was very little affected by acidic treatment.

In another study conducted by Karthik et al. [118], composites made with six layers of bidirectional woven carbon fabric only (C_6), similarly six layers of basalt fabrics only (B_6), and a hybrid combination of six layers of carbon and basalt (CBCBCB), and Araldite hot cured epoxy resin was used. Different wt% (5%, 10% and 15%) of SiC Nanoparticles were used for filler materials with the hybrid stacking sequence. The authors found a considerable increase in the tensile and flexural strengths and Izod impact energy. The maximum tensile and flexural strengths of 346 MPa and 388 MPa, respectively, were exhibited by the composite prepared using CBCBCB sequencing with 15 wt% SiC. In another study [119], the hybrid composites of basalt and jute were analyzed with varying combinations of fiber percentages of basalt from 10% to 90% and vice-versa for Jute and the mechanical properties were discussed. The matrix used was polyester resin and MEKP (methyl ethyl ketone peroxide) was used as the catalyst. The basalt and jute fibers were mixed thoroughly and the composite was prepared using a compression molding machine. The basalt composite had the highest tensile strength of around 131 MPa. However, the maximum elongation 10.6 mm was observed with the composite of 30% basalt and 70% jute.

Moreover, the highest flexural strength of 140 MPa was exhibited by the 50-50 basalt-jute composite, whereas the basalt composite had the highest flexural modulus of around

5.2 GPa. Lastly, the unnotched Izod impact test was carried out, and the basalt composite was found to have the highest impact strength at around 57.5 J/cm^2. The author stated that the impact strength of the hybrid composite was improved by adding high-energy-absorbing basalt fibres.

2.7 RESEARCH GAP AND MOTIVATION

As shown by several investigators, basalt fibers are known for their strong mechanical properties, cost-effectiveness, and other positive attributes, as mentioned above, making them a rational alternative to E-glass in fabricating cost-effective composites. Unlike most natural fiber-reinforced polymers, basalt fibers absorb virtually no water, which makes them particularly useful in applications and environments with essential moisture resistance (e.g., in the marine, automotive and aerospace industries).

Additionally, Recyclamine resin technology has introduced a significant advancement in thermosetting resins. With its superior mechanical properties and fully recyclable nature, Recyclamine will enable one to reuse both the reinforcing fibers and the resin. Such an outcome would be significant for meeting the eco-friendly and sustainable development goals (SDGs), as it encourages more environmentally friendly production of various structural components, notably critical and pressing matters for major industries.

However, while promising studies have demonstrated the viability of Recyclamine and basalt fibers separately, the volume of comprehensive studies investigating the mechanical performance of basalt-reinforced Recyclamine composites is quite scarce. This gap presents a valuable opportunity to conduct a systematic experimental investigation to enrich the required database and encourage using eco-friendly and recyclable high-performance composites for industrial applications. Therefore, the motivation for this study stemmed from the noted gap, which inspired us to investigate the feasibility of basalt-Recyclamine composite creation as an effective alternative to the most widely used FRP, E-glass-epoxy composite. The expected favourable results will also address the environmental concerns associated with using composite materials without compromising mechanical performance, contributing to a greener and safer world for future generations.

CHAPTER 3 MATERIALS AND FABRICATION

This chapter focuses on the detailed exploration of the materials and methods used as part of this experimental investigation. The chapter begins by introducing the material used in this study, namely basalt fiber, Recyclamine®, and epoxy. Each of the materials is discussed in terms of their source, properties, reasons for selection, optimization of fiber volume and fraction, and how they contribute to a better and more sustainable composite system.

The chapter then describes the rationale behind the manufacturing technique used to fabricate the composite materials, how the composite is cured, and post-processed. The optimization of the fiber orientation and how it impacts manufacturing properties for industrial applications are also described.

3.1 SELECTED MATERIALS

The reinforcing materials chosen for this investigation are basalt fiber, and two matrix materials, namely Recyclamine® resin and epoxy resin.

3.1.1 Reinforcing Fiber

As mentioned previously, fibers are the primary load-bearing components of a composite; they are derived from various sources like plants, minerals or animals and can be synthetically made fibers or hybrid fibers. One significant aspect to consider when selecting a reinforcing fiber for making a composite is the fiber composition, which directly impacts the composite properties. There are two methods to describe how much fiber is in a composite. One method measures the fibres weight compared to the composite's total weight, called the fiber weight fraction (FWF). The other method measures the fibre volume relative to the composite's total volume, known as the fiber volume fraction (FVF) [41].

The fiber volume in a composite influences the type of failure, such as matrix-based or fiber-based failure modes. These happen depending on whether the fibre volume fraction (V_f) is above or below a certain minimum value ($V_{f,\,min}$). When the composite has a fiber

volume fraction lower than this minimum ($V_f < V_{f,\,min}$) and it's put under stress, the failure of the fibers does not necessarily lead to the failure of the entire composite. In this case, the polymer matrix can still handle the load. However, the broken fibers become like a series of aligned voids within the matrix. The voids make the composite weaker rather than strengthening it, making it weaker than the matrix material itself [120].

A fiber reinforced thermoset composite consists of brittle fibers embedded in a relatively more ductile thermoset polymer matrix, where the fibers fail at a lower strain than the matrix. Therefore, it is important to know both the minimum and critical fiber volume fractions when using plant fibres as reinforcements since the composite should be designed with a fiber volume fraction (V_f) greater than the critical value ($V_{f,crit}$). Figure 3-1 shows a graphical representation of the strength–fiber content relationship [113,114].

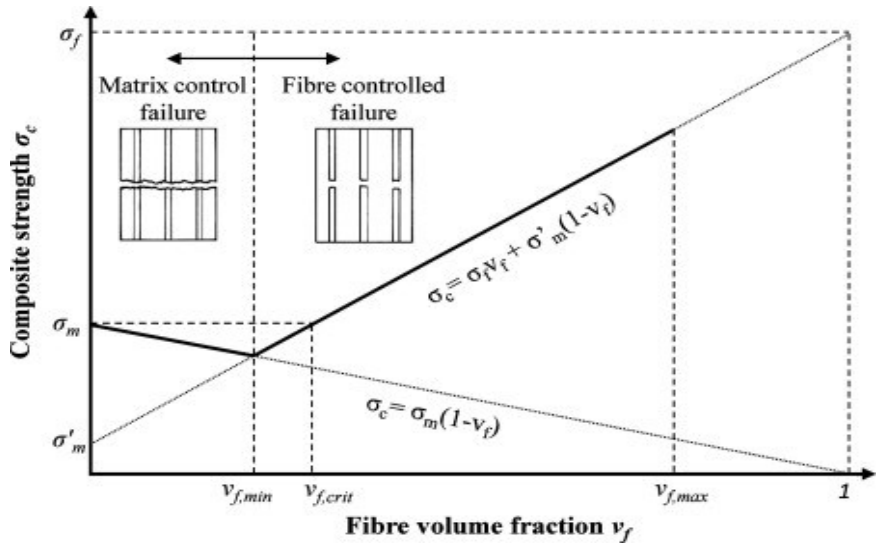

Figure 3-1: Relationships between composite tensile strength and fiber volume fraction [121].

3.1.1.1 Basalt Fibers

Basalt fibers are derived from the natural volcanic rock known as basalt. They have emerged as a cost-effective material in various industrial applications, especially as an alternate to glass fibers in construction and manufacturing fields. Basalt is formed from the rapid cooling of the lava and has a chemical composition mainly of Silica, aluminum oxide, copper oxide, and calcium oxide, among other compositions. These compositions give the fibres good heat and chemical resistance [122].

Basalt fibers is created by melting crushed basalt rock at around 1400°C to 1600°C, followed by extrusion through small nozzles to produce continuous filaments of basalt fiber. This technique is similar to glass fibers processing but done at higher temperatures, exhibiting better thermal stability, higher tensile strength, better chemical resistance (both acidic and alkaline), and biological resistance compared to glass fibers. These properties make basalt fibers an excellent alternative to traditional building materials in structural applications and a viable substitute for asbestos in high-temperature insulation applications [123].

Since basalt is abundant naturally, manufacturing basalt fibers requires much less processing than traditional fibers like asbestos. Because of this, the waste from basalt fiber production has a minimal impact on the environment, primarily if these fibers are used with a recyclable matrix, making the resulting composite completely eco-friendly in terms of sustainability and reusability.

The basalt fabric used in this research is manufactured by Zhejiang GBF Basalt Fibre Co., Ltd (Dongyang City, China), and supplied by Advanced Filament Technologies LLC (Houston, USA). The 0/90° fabric consists of two continuous fiber stitched mats with a total fiber weight of 669 g/m^2. The fiber is made with 13-micron roving [117,118]. The sizing is a surface treatment which is done while extruding fibers during the production of fiber filaments, commonly by acid-alkali etching, coupling agent modification, plasma modification, or surface coating modification to improve the characteristics of the fibers like adhesion with polymer matrices and resistance properties [126,127].

It should be noted that biaxial fabrics made by stitching two orthogonal layers of unidirectional (0°/90°) fabric together differ significantly from their woven counterparts. Stitched biaxial fabrics are classified as non-crimp fabrics, meaning that the rovings are not interlaced as they are in woven fabrics. This structural difference is advantageous because woven fabric composites often fail under high fatigue conditions due to the crimps in the fibers. In contrast, stitched bidirectional fabrics do not have these issues and offer better fatigue resistance. Another advantage of biaxial fabric is the very few or absence of bumps or high points that naturally form due to the weaving process.

Moreover, the likelihood of creation of resin-rich regions in woven fabrics is much greater in comparison [128].

Adding to it, the straight, flat format of the fiber bundles in biaxial fabrics leads to better strength and stiffness. By making these straight and flat fibers align directly with the loading-imposed forces, the fibers are better aligned to resist stretching and/or breaking during loading. Additionally, biaxial fabrics generally have a higher fiber count than woven fabrics. The increase in fibers results in greater overall strength, and a higher concentration of fibers means there is less matrix (resin) needed and hence, a less brittle composite. Consequently, having less matrix (resin) also reduces the overall weight of the material [128].

Figure 3-2 and Figure 3-3 show a picture of the biaxial fiber stitched and a visual image of the stitches in the fibers, respectively.

Figure 3-2: Stitched biaxial fabric [128].

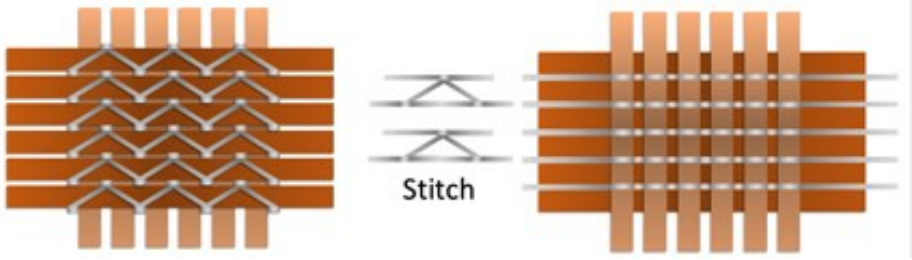

Figure 3-3: Schematics of the stitches used to make bidirectional fabrics [128].

Table 3-1 reports the physio-mechanical properties of basalt fiber given by the manufacturer.

Table 3-1: Physio-mechanical properties of the basalt fiber [126].

Material	Density (g/cm^3)	Tensile Strength (MPa)	Tensile Modulus (GPa)	Elongation at Break (%)
Basalt	2.75	4,840	89	3.15

3.1.2 **Matrix (Resin)**

As briefly stated in the previous chapter, the matrix is the constituent that holds the fibers together fiber-reinforced composites (FRC), ensuring they remain in their place and are distributed uniformly. Otherwise, any misalignment of fibers could compromise the strength and performance of the composite. The matrix also transfers the load from one fiber to another. Matrix enables the fibers to carry mechanical loads effectively, which makes the composite gain more impact resistance and transverse strength than is achievable with fibers alone. Lastly, the matrix determines the final product's surface quality, affecting its appearance and functionality in various applications [129]. Additionally, the matrix acts as a shield for the fibers, protecting the fibers from moisture, chemicals, UV radiation, and abrasion between the fibers, extending the composite's lifespan by minimizing wear and tear [122,92].

3.1.2.1 Recyclamine® Technology Based Resin

As noted in 2.5.4, Recyclamine® (THR9357) is an amine-based recyclable thermoset epoxy curing agent (hardener) with low viscosity and moderate curing temperature. The cross-linked thermosetting matrix derived from Recyclamine® can be cleaved through low-energy solvolysis under specific conditions. This process converts the recovered epoxy matrix into a thermoplastic resin. This phenomenon renders a recovered resin that can be reused or repurposed, closing the sustainability loop in the manufacturing process [131]. Figure 3-4 shows the difference between a conventional epoxy (thermoset) and the Recyclamine amine link cleavage points changing Recyclamine® from thermoset to thermoplastic.

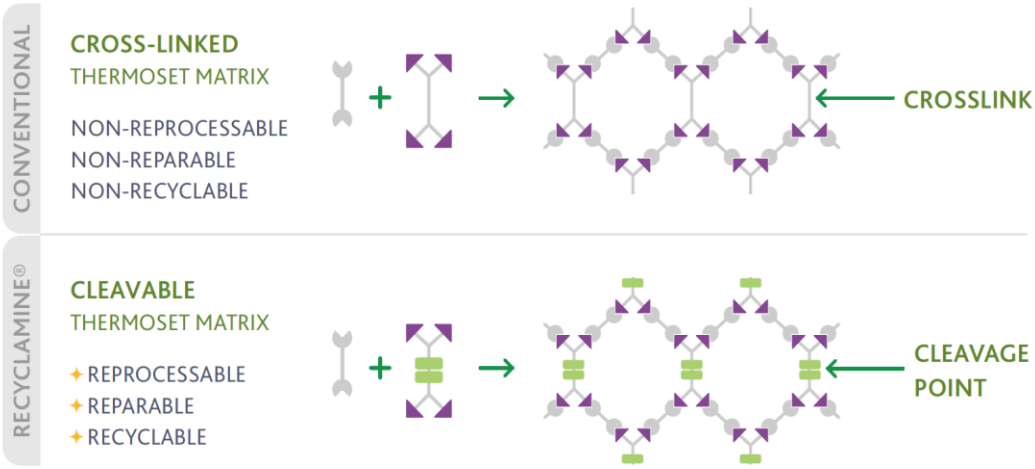

Figure 3-4: Polymer links in the conventional epoxy and Recyclamine® [132].

The amine-based curing agent (hardener) THR9357 is based on Recyclamine® Technology. The two-component recyclable epoxy laminating system consists of one epoxy resin from Briozen recyclable series Epotec YDL5557 and the hardener Epotec THR9357. The use of this resin facilitates the recycling and recovery of the reinforcement and matrix in a fiber-reinforced composite by a low-energy solvolysis process. The system is designed to suit various fabrication techniques under different environmental conditions due to its low reactivity and lower exothermic reaction than traditional epoxy. The lower viscosity of the system also allows fast and complete impregnation of different fibers [133]. Figure 3-5 below shows the two parts of Recyclamine-based epoxy resin.

Figure 3-5: Two-part Recyclamine-based Epotec YDL_5557/THR 9357.

The system, Briozen Recyclable Series Based on Recyclamine® Technology, Epotec YDL5557-THR9357 was generously sampled from Aditya Birla Chemicals (Thailand) Ltd (Advanced Materials) and supplied by Aditya Birla Chemicals-Epoxy Business Americas. Table 3-2 shows the two-part system's physio-mechanical properties and mixing ratio according to the manufacturer and the curing condition used for this research.

Table 3-2: Physio-mechanical properties of neat cured Epotec system.

Materials	**Briozen YDL5557-THR9357**
Mixing Ratio (Resin: Hardener) (Parts by Weight)	100: 27
Viscosity (mPa.s)	180-250
Pot Life (Minutes)	200-300
Curing Temperature	Room Temp + 80°C / 8 hrs
Tensile Strength (MPa)	75 - 85
Tensile Elongation (%)	4.0 - 6.0
Tensile Modulus (GPa)	3.0 - 3.5
Flexural strength (MPa)	120 - 140

3.1.2.2 West System® Epoxy Resin

West System® epoxy system is another resin used in this research. The resin system is a two-part system, 105 Resin and 206 Hardener. The resin system is cured at room temperature and has very low chemical volatility. This resin is compatible with various fabrication techniques like vacuum-assisted resin transfer moulding and other manufacturing processes. This choice of fabrication technique reduces the creation of voids during the process and, hence, improves the quality of the composite [134,135]. Table 3-3 shows the system's physio-mechanical properties. Figure 3-6 shows the two-part West System epoxy resin and hardener.

Table 3-3: Manufacture's material properties of cured 105 epoxy resin [128].

Materials	**105 Resin and 206 Hardener**
Mixing Ratio (Resin: Hardener) (Parts by Weight)	5:1
Viscosity (mPa.s)	725
Pot Life (Minutes)	20-25
Working Time	90-110
Curing Temperature	Room temp./10-15 hrs, full strength/1-4 days
Tensile Strength (MPa)	50
Tensile Elongation (%)	4.5
Tensile Modulus (GPa)	3.172

Figure 3-6: Two-part West System 105 Epoxy Resin and 206 Hardener.

3.2 COMPOSITE FABRICATION: VACUUM ASSISTED RESIN INFUSION MOULDING

This study used the vacuum-assisted resin transfer moulding (VARIM) method to fabricate the composite panels. As stated in the literature review, this method helps in uniform resin distribution, minimizing voids within the composite in a controlled fiber/resin ratio. This technique involves several essential steps, which are outlined as follows [129,130]:

Mold Preparation: The process starts with a rigid, one-sided mould (a flat aluminum plate in our case) to create the panels. This mould is essential as it defines the shape and dimensions of the composite. Acetone was applied to the mould as a cleaning agent, followed by wax coating to remove the composite laminates easily.

Preparing the Fiber Preform: Fiber preforms are reinforcement materials made from fibers (basalt in this study). They are carefully cut to the desired dimensions and orientation. The orientation and placement of these fibers are the critical parameters used in controlling mechanical properties. The correct arrangement of fibers in laminate composites is also crucial for improving their performance.

For example, aligning the fibers parallel to the load's direction improves the strength and stiffness of the composite. However, if the load is applied transverse to the fibers, the composite is generally much weaker but has stronger bending stiffness and torsion [94]. Hence, to achieve the best of both, cross-ply orthotropic $[0/90]_{ns}$ was used in this research, with “n” being determined by the thickness required for the experiment.

Stacking sequence in VART: The next step is to place a nylon-based, porous, non-stick peel ply (also known as release fabric) to the mould to better control the fiber volume fraction, for a distinctive surface finish, and for easy removal of the composite once cured. This step is followed by laying the fiber preforms with the correct fiber orientation and stacking after measuring the fiber laminate weight using a mass balance. Table 3-4 reports the specifications of the various panels made for the different experiments conducted in this study.

Once all the fabrics layers are laid, another sheet of peel-ply is placed on the stack followed by a distribution media such as an infusion mesh to ensure the uniform channelling of the resin flow. Moreover, breather clothes are placed around the fabric stacks. The cloth's function is to allow air and other volatiles to be efficiently removed from the vacuum bagging and across the edges of the laminate.

A spiral tube is placed across the inflow edge of the layup to facilitate a uniform resin distribution from the resin inlet to the outlet. A similar spiral tube is also placed on the opposite outlet edge of the layup. Lastly, the resin inflow and outlet tubes are placed in the middle of the spiral tubes.

Table 3-4: Specifications of the test panels.

Test Type	Panel Dimension (mm^3)		No. of Layers of 0/90 Basalt fabric
	Basalt-Epoxy	Basalt-Recyclamine	
Tensile	280 × 230 × 3	280 × 230 × 2.5	8 Layers of Biaxial Fibers
Compression	140 × 150 × 3.7	140 × 150 × 3.7	10 Layers of Biaxial Fibers
Flexural	160 × 65 × 4.5	160 × 100 × 4.25	12 Layers of Biaxial Fibers
Shear	150 × 130 × 4	150 × 130 × 4	10 Layers of Biaxial Fibers
Impact	100 × 120 × 6.35	100 × 120 × 6.35	18 Layers of Biaxial Fibers

Sealing the Mould: After placing the fiber preform and other necessary layers, sealant tapes are used to seal the resin inlet and outlet tubes and around the entire layup. The mould is then covered with a vacuum bag; the vacuum bagging is essential for creating an airtight seal around the mould and preform. A proper seal is necessary to prevent resin from leaking and to maintain a controlled vacuum environment inside the bag during resin infusion to minimize air-pockets and enforce consolidation of the composite panels.

Applying Vacuum: A vacuum pump is connected to the sealed mould through the resin outlet tube; the vacuum is induced at -1 bar to remove air and volatiles from within the

mould cavity and the fiber preform. The vacuum removes trapped air and helps achieve the desired resin-to-fiber ratio, and facilitates consolidating the fibers. Moreover, once this is done, the vacuum bag is kept in a similar state by clamping the tubes for 15-30 minutes to ensure proper assembly sealant.

Resin Preparation: During this time, the resin is prepared with a fiber-to-resin ratio of 1:1.2 to compensate for the resin lost in the process, like the resin sticking in the tubes' wall and resins absorbed by the peel-ply. The two-part system resins (both the West System Epoxy and Recyclamine® Epotec), on separate fabrications, are mixed thoroughly according to their ratio for at least 1 minute and then placed in a vacuum chamber to remove any air bubbles (entrapped air) in the resin. Figure 3-7 shows the vacuum pump and chamber used.

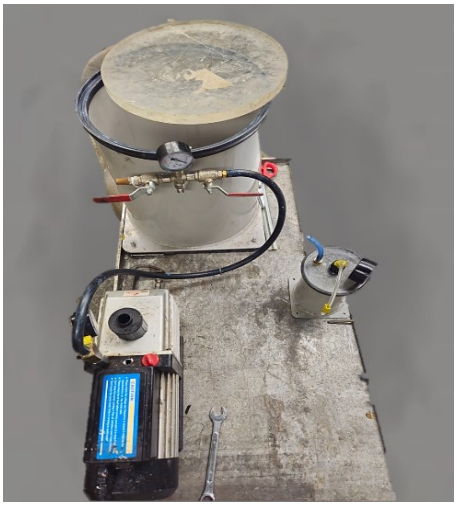

Figure 3-7: The vacuum pump and chamber.

Resin Infusion: With the vacuum applied, the resin is introduced at one end of the mould through the resin inlet tube after removing the clamps. The vacuum pulls the resin through the inlet tube, and the fiber preforms with the help of the infusion mesh to the outlet tube through the spirals, ensuring the structure soaks completely. The tubes are clamped once the resin and the entrapped airs have passed through the resin outlet tube.

Resin Flow: The flow of resin needs to be carefully controlled to prevent the formation of dry spots (areas not wetted by resin) and to ensure a uniform distribution of resin throughout the preform. It is suggested by Chen [138] that the best method to have the

least void content is by reducing non-uniform resin flow and reducing continuous resin evaporation. The best method found was to have the full vacuum at the start of resin infusion, and once the fibers are impregnated with the resin, close the resin inlet and let the vent on with higher increased pressure.

Curing Process: The curing process begins once the mold is fully infused with resin. The resin is polymerized and hardened, which can be accelerated by applying additional heat. The curing cycle, like the temperature and duration, enables the composite to attain its optimal performance, depends on the specific resin system used, and significantly influences the performance characteristics of the final composite part. The West System Epoxy system is cured at room temperature in 24 hrs. In contrast, according to manufacturer instructions, the Recyclamine ® Epotec was kept at room temperature for 24 hours and then cured at 80°C for 8 hours in a temperature-controlled oven, as shown in Figure 3-8.

Figure 3-8: Temperature-controlled oven.

Demolding: After completion of the curing cycle, the vacuum is released, and the composite part is recovered from the bag and removed from the mould. This step must be handled carefully to prevent damage to the newly formed composite. Figure 3-9 and

Figure 3-10 show the schematic diagram of the assembly and the actual assembly during this research fabrication process, respectively.

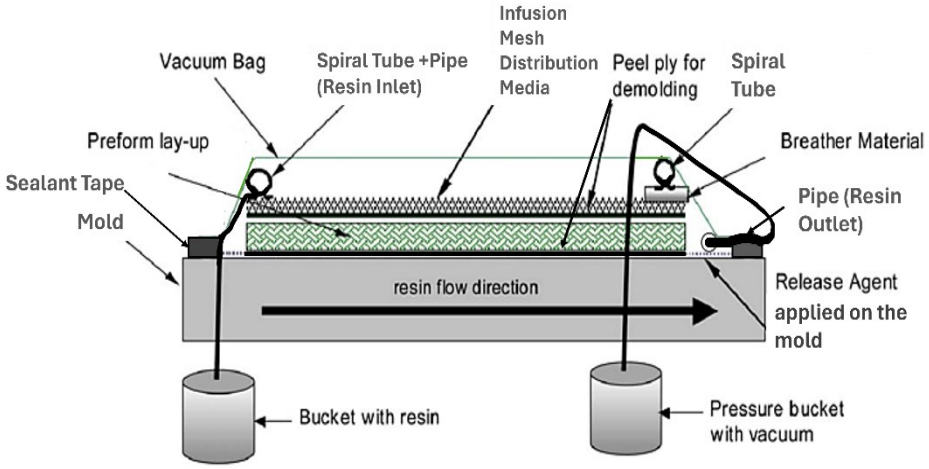

Figure 3-9: Schematic diagram of VARTM process [139].

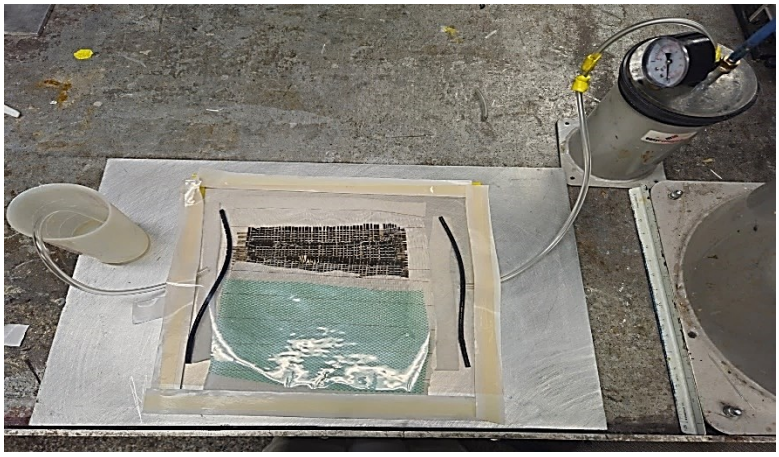

Figure 3-10: The actual VARTM process.

CHAPTER 4 METHODOLOGY AND EXPERIMENTAL SETUP

The methods used to evaluate the mechanical properties of the composites, including tensile, compressive, flexural, shear, and impact strengths, are outlined in this chapter. The chapter provides specifics on the testing equipment and their validation, as well as the fixtures, procedures, and standards, to ensure the results are reliable and replicable.

4.1 TESTING EQUIPMENT

An electronically controlled MTS servo-hydraulic universal testing machine was used to evaluate the tensile, compression, flexural, and shear properties. The impact test was conducted using an Izod Impact Tester. The other experiments conducted in this research required various test equipment, as outlined below.

4.1.1 Muffle Furnace

One of the key pieces of equipment used was the muffle box furnace, the Lindberg Model 51748, for determining the fiber volume content and void content, which followed the burn-off test following ASTM D3171-22 [140]. The box furnace is designed for high-temperature applications and can maintain stable temperatures up to 1100°C. The furnace ensures effective control over the heating process and has an inner chamber volume of around 100 x 100 x 200 mm^3.

4.1.2 Universal Material Testing System, MTS

This digitally controlled system features a hydraulically actuated testing mechanism that provides precise control over the application of loads during testing. Tensile tests followed ASTM standards D638-22 and D3039M-17 for basalt-Recyclamine and basalt-epoxy composites. Compression tests followed ASTM D6641M-1E2, flexural tests were conducted according to ASTM D7264M-07, and shear tests were performed according to ASTM D5379M-19 [141–144].

The MTS system's digital control unit incorporated a user-friendly LabView application for controlling the loading rate and capturing the desired data for storage on a personal computer.

4.1.3 **Waterjet Cutter**

The Flow Paser 3 with Abrasive System Waterjet Cutter was utilized to extract the impact test specimens for Izod impact testing (ASTM D256-23) and tensile testing of basalt composites (ASTM D638-22) [145–147]. This advanced water jet cutting machine features a 0.010" orifice diameter and is powered by a pump capable of reaching a maximum pressure of 440 MPa (60 ksi). This system's precise cutter diameter and power allow for the accurate and clean cutting of composite materials, ensuring the samples are prepared to the specifications required for their respective mechanical testing.

The water jet system is integrated with a retrofitted CNC gantry, enhancing its operational precision and control. The KMotion CNC control system controls the system. The water jet cutter can produce high-quality test specimens consistently. The pressure used for cutting the specimen was around 275 MPa (40 ksi).

4.1.4 **Izod Equipment**

The Tinius Olsen Model 66 Plastic Impact Tester was used to conduct the Izod impact tests on the composite samples following ASTM D256-23 standard. The Tinius Olsen Impact Tester has a capacity of 22.6 Joules (200 in-lbs.), with weights available for testing ranges of 25, 50, 100, and 200 in-lbs. The device is equipped with an Izod striker, a 25 in-lb. hammer, a weight set for 50 in-lb. testing, and an Izod devise.

Figure 4-1 shows various test equipment used in this research.

Figure 4-1: (a) Muffle Furnace, (b) MTS Universal Testing Machine, (c) Izod Impact Tester, and (d) Waterjet Cutter.

4.2 DATA ACQUISITION

This section covers the methods and tools used for collecting data during the experiments. Accurate data collection is essential for analyzing the mechanical properties of the composites. Various instruments were used to gather precise measurements, including a mass balance, NIDAQ system, strain gauges, laser extensometer, etc. The following subsections will describe each important equipment and fixture, how they were calibrated, and the protocols followed to collect the data needed for subsequent analysis.

4.2.1 **Analytical Balance**

The standard test method D792-20 for Density and Specific Gravity (Relative Density) of Plastics by Displacement was used for the density measurement of the burnt-off fibers [148]. The precision balance used in this procedure was the Sartorius Analytical Balance. It is very well known for its high accuracy and precision in mass measurements. It has a

maximum capacity of 220 grams, suitable for measuring small samples with high precision, and a readability of 0.1 milligrams (0.0001 grams). The digital display provides real-time updates during the measurement process, and the balance sensitivity helped determine the presence and removal of bubbles during measurements.

4.2.2 **Strain Gauge and National Instrument Data Acquisition (NIDAQ)**

Various strain gauges and a National Instrument Data Acquisition (NIDAQ) system were used to measure strain during the composites' tensile, compressive, and shear testing. The strain gauges used were from Micro Measurement (Toronto, Canada), with a 350 ohm resistance and a gauge factor of 2.1. These gauges were configured in a quarter-bridge format using NI 9945 quarter-bridge completion module(s).

Moreover, the NIDAQ system used in this study included the Compact DAQ chassis 9172, Which was paired with the NI 9237 module, a 4-channel full/half-bridge analog input module designed for dynamic strain measurements. The setup also incorporated RJ 50 cables for reliable and accurate signal transmission from the strain gauges to the NIDAQ system through NI 9945.

During testing, the strain gauges were carefully bonded to specimens at specified locations using super glue, which yields the largest modulus (110% increase both numerically and experimentally), according to Komurlu et al [149]. The NI 9237 module captures the analog signals from the strain gauges and converts them into digital data for analysis. The collected data were processed and analyzed using NI software known as Signal Express 2015 (the latest software compatible with this lab's NIDAQ 9327 module), which facilitates the real-time visualization and recording of strain.

4.2.3 **Laser Extensometer**

Another strain-measuring device used in this study was a laser extensometer (Model LE-05) manufactured by Electronic Instrument Research (Irwin, PA). This advanced extensometer is designed to provide precise, non-contact strain measurement during mechanical testing. The laser measures the slightest change in a given distance by the reflective rays emitting back from two retroreflective pieces of tape attached to the specimens during testing events. The laser extensometer is placed on a levelling surface

before the test, and the reflective tapes are typically placed at a specific gauge distance where the strain is desired to be captured.

4.2.3.1 Strain Gauges and Laser Extensometer Calibration and Validation

The strain gauges and laser extensometer were calibrated by testing them against one another on a material with a known modulus (aluminum alloy 3003). The two devices captured the aluminum specimen's deformation at a gauge length subjected to tensile loading, and the resulting strain was calculated. The tests were repeated three times, and data were collected to calculate the modulus of elasticity. The calculated modulus from the strain gauge data was an average of 65.2 GPa, while the laser extensometer yielded a modulus 65.2±5 GPa, displaying some inconsistencies and discrepancies. These results were then compared to the standard modulus of aluminum (modulus of 68.9 GPa) to assess the accuracy of both measurement devices.

Other devices, such as two Instron clip-on extensometers, were also tried but exhibited more significant inconsistencies compared to the strain gauge and the laser extensometer readings. Due to these findings, the strain gauges and the laser extensometer were selected as the primary devices for measuring strain in this study despite the minor inconsistencies observed with the laser extensometer.

4.2.4 **Other Measurement devices**

In addition to the analytical balance, strain gauges, laser extensometers, and other measurement devices were also used. For example, a digital micrometer was required to measure all the test specimens' dimensions. This device provides high precision and accuracy in measuring thickness, width, and length up to 0.01 mm or 0.000001 m. Moreover, using the Archimedes principle, a graduated cylinder was used to determine the density of the specimens. This method involves immersing the specimen in water and measuring the volume of water displaced to calculate the specimen's volume.

Figure 4-2 shows the data collection devices used in this research.

Figure 4-2: (a) and (b) the laser extensometer, (c) NIDAQ data acquisition system, (d) the balance, e) the graduated cylinder.

4.3 PROCEDURE

This section outlines the procedures for conducting various tests on the composite materials. The processes include description and significance of each test, test setup and specimen preparation. It covers the specific testing parameters for each type of test, including machine settings and environmental conditions. Data collection methods are described as well. Finally, the formulas used to analyze the collected data and derive the key material properties are presented.

4.3.1 Fiber Volume Content and Void Content Determination

The burn-off test is conducted as per Test Method I, Procedure G of ASTM 3171-22 [140]. This test method focuses on the combustion and annihilation of the matrices in a

furnace, leaving the high-temperature resistant reinforcement like basalt unaffected. Additionally, the void volume of a composite material significantly impacts its mechanical properties; higher void volumes often lead to lower fatigue resistance, greater susceptibility to moisture penetration and weathering, and increased variation in strength properties.

The procedure began with preparing and weighing the composite specimens of approximately 40 mm × 20 mm, with each test repeated three times to ensure accuracy. The fabricated panels were cut to the required shape using a water-cooled table saw equipped with a diamond-coated saw blade to extract the test specimens. The specimens were then dried in a drying oven for 30 minutes at 25 °C to ensure moisture removal. Each specimen's density was then determined per Test Method D792 [148]. The specimen's length (l), width (w), and thickness (t) were measured using a digital micrometer. The mass of each specimen was measured in air ($m_{comp,\,air}$) and subsequently in distilled water at 21°C ($m_{comp,w}$), with the analytical balance. The composites' density ($\rho_{comp\,1}$) were then calculated using the following equation.

$$\rho = \frac{m}{V} \qquad \textit{Equation 4-1}$$

where, m and V are the mass and volume of the specimen.

The density of the composites was also evaluated in accordance with ASTM D792-20. First, the specimen's specific gravity (γ) was assessed at room temperature using Equation 4-2:

$$\gamma = a(a - b) \qquad \textit{Equation 4-2}$$

where a and b are the apparent masses of the specimen in air and when immersed in liquid, respectively.

Following the specific gravity calculation, the density of the composite, $\rho_{comp\,2}$ can be determined using Equation 4-3:

$$\rho = \gamma \times 0.99773$$ *Equation 4-3*

Each specimen was then placed in a desiccated, reweighed crucible. The crucible itself was cleaned by heating it to 500-600 °C in the muffle furnace and then cooled in a desiccator before weighing. The crucible containing the specimen was then placed into the preheated muffle furnace set at 500 °C to avoid spontaneous ignition of the samples. The temperature was gradually increased to around 600 °C, to burn off the matrix and leave only the reinforcement. The burn-off process was conducted for 1 hour, and by that time, the matrix was considered fully combusted, leaving only ash and reinforcement visible.

After the combustion, the specimen and crucible were placed in a desiccator (dry oven) to cool to room temperature. Finally, the specimen was transferred to the analytical balance to measure the mass of the fiber in air and the mass of the fiber in water. The fibre density, ρ_f was then calculated using equations Equation 4-2 and Equation 4-3

The weight percent of the fiber was calculated using Equation 4-4:

$$W_f = M_f/M_i \times 100$$ *Equation 4-4*

where, M_i and M_f are the initial mass of the composite before and after combustion (in grams), respectively.

The volume percent of the fiber, V_f in percent, can be calculated using Equation 4-5

$$V_f = M_f/M_i \times 100 \times \rho_c/\rho_f$$ *Equation 4-5*

where ρ_c and ρ_f are the densities of the composite and the fibers, in g/cm^3.

The weight percent of the matrix, W_m can be calculated using the following equation

$$W_m = (M_f - M_i)/M_i \times 100$$ *Equation 4-6*

where M_i and M_f are the initial and final mass of the composite specimen in grams before and after combustion, respectively.

Similarly, the volume percent of the matrix, V_m is calculated by

$$V_m = M_i - M_f / M_i \times \rho_c / \rho_m \times 100$$ *Equation 4-7*

where ρ_m is the density of the matrix in g/cm^3.

Finally, the void volume, V_v in percent, was calculated according to Equation 4-8.

$$V_v = 100 - (V_f + V_m)$$ *Equation 4-8*

Henceforth, the specimens' void content and fiber volume will be determined. Figure 4-3 shows images of the equipment used for calculating the density and the burn-off test.

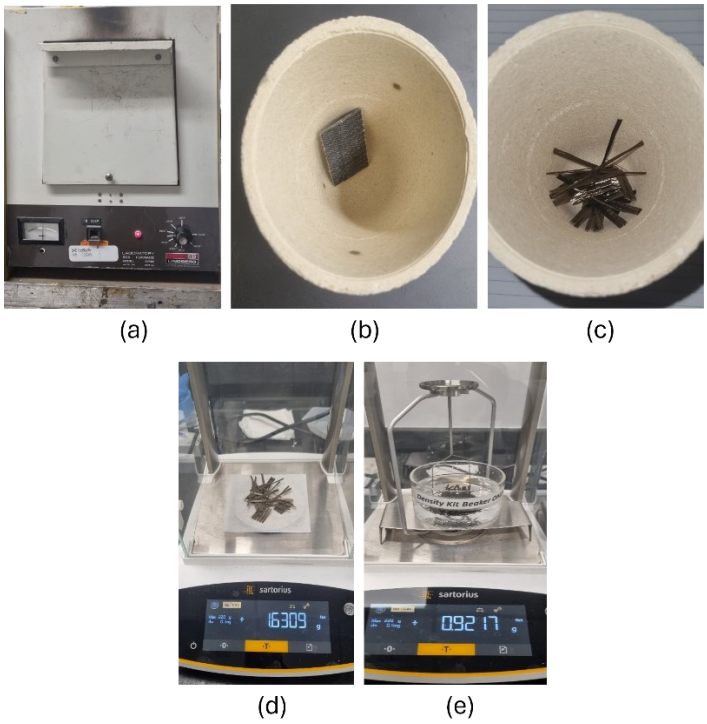

Figure 4-3: Equipment used to conduct the burn-off test and density measurement, (a) muffle Furnace, (b) composite specimen before combustion, (c) fibers after matrix combustion, (d) analytical balance, measuring the mass of fibers in the air, and (e) when submerged in water.

4.3.2 **Tensile Test**

The tensile test measures the force required to break a sample and the extent to which it elongates or stretches the specimen to fracture. The results of tensile tests are typically represented as a stress-strain diagram, which is used to determine the tensile modulus of the material. This data is essential for material selection and designing parts. Even when the material is primarily loaded in shear or compression, the tensile modulus and strength

are still measured to provide a general indication of the material's quality and performance.

4.3.2.1 Testing Fixture and Specimen Preparation

The tensile test is carried out per the ASTM D638 [146] for both basalt-epoxy and basalt-Recyclamine. The specimen is placed and secured in the test machine using the mechanical grips attached to the MTS machine, as shown in Figure 4-4.

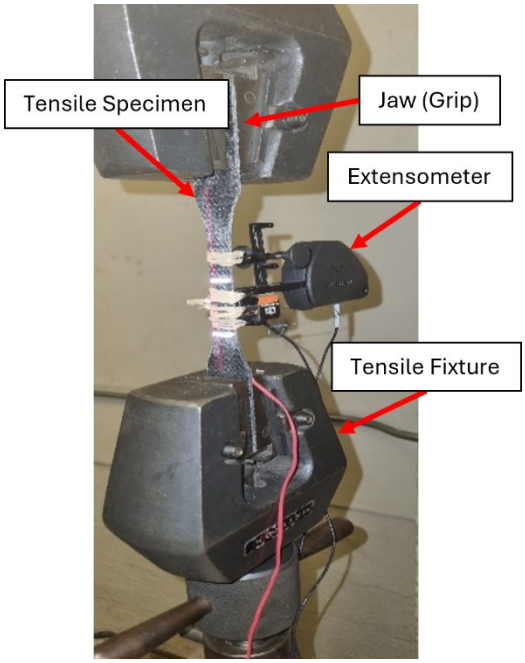

Figure 4-4: Tensile test setup basalt-epoxy specimens.

The specimen was equipped with a strain gauge or extensometer in its gauge length and was subjected to tensile load until failure. The specimen tested according to ASTM D638 requires a 2D dog-bone shape-like specimen. The specimen was drawn in SolidWorks and predefined in Adobe Fusion 360, the CAM software that controls the waterjet cutter for dimensional accuracy and precision without affecting the specimens. The basalt-epoxy and basalt-Recyclamine specimens had a rectangular shape with dimensions of $250 \times 25 \times 2.5$ mm^{3,} with a neck in the middle, as shown in Figure 4-5.

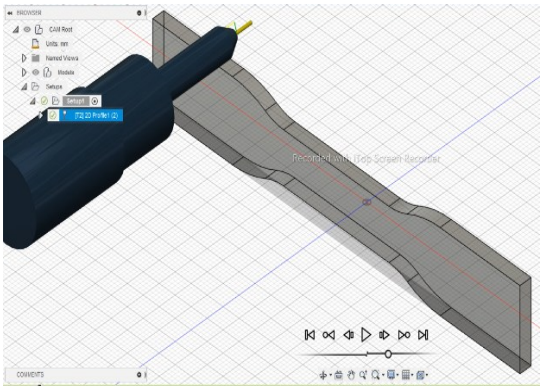

(a)

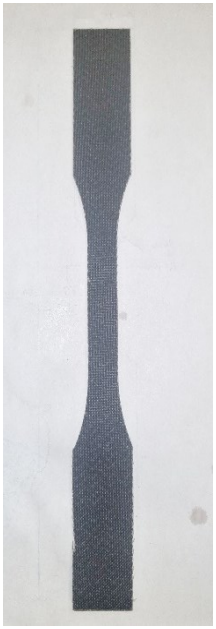

(b)

Figure 4-5: a) CAM design of basalt-Recyclamine (dog-bone) specimen, (b) prepared dog-bone specimen.

4.3.2.2 Testing Parameters

ASTM D638 suggests a nominal loading rate of 5 mm/min. The rate provides a completion test time of less than 5 minutes.

4.3.2.3 Data Collection

Each specimen's width, thickness and gage length were measured using a digital micrometer in different places. Each dimension was measured at least three times, and the average values were taken. The MTS software was used to collect the real-time in seconds from the start of the experiment till the end. The force in 'kN' and the laser extensometer reading in 'mm' were also recorded by the MTS software. The frequency of data collection was set to 2048 Hz to be consistent with NIDAQ data collection from the strain gauges.

The collected data from the experiment is then processed to calculate the tensile stress, strain and modulus of elasticity using the following equations.

$$\sigma_n = \frac{F_n}{A} \times 1000$$ *Equation 4-9*

$$\varepsilon_n = \frac{l_{n+1} - l_0}{l_0}$$ *Equation 4-10*

$$E = \frac{\Delta\sigma}{\Delta\varepsilon}$$ *Equation 4-11*

In the above equations, σ_n is the tensile stress in MPa at the n^{th} data point, F_n is the applied load at the n^{th} data point, A is the cross-section area of the specimen measured during sample preparation, in mm^2, E is the tensile modulus of elasticity, in MPa Additionally, the strain, ε, was captured by strain gauges, in mm/mm. To verify and as a precautionary measure, in the likely event the strain gauge fails the laser strain, ε_L, was also obtained from the data captured through the laser displacement reading using Equation 4-10, where l_0 and l_n are the initial length and length at n_{th} point of the laser reading, respectively.

The curve of stress-strain ($\sigma_n - \varepsilon_n$) was plotted for each specimen to see the correlation, better visualize, and compare the ultimate strength and modulus among the specimens. Lastly, the increments of stress ($\Delta\sigma$) and strain($\Delta\varepsilon$) in the linear part of the curves were used to establish elastic modulus, E.

4.3.3 **Compression Test**

The compression test traces the material's behaviour under compressive loading and establishes the force required to break a specimen. Like the test tensile, the behaviour of the compressive tests is typically represented as a stress-strain diagram, which is used to determine the material's compressive strength, strain, and modulus.

4.3.3.1 Testing Fixture and Specimen Preparation

The compressive test is carried out following the ASTM D6641M-16e2 – "Compressive Properties of Polymer Matrix Composite Materials" using a Combined Loading Compression (CLC) test fixture [142]. As shown in Figure 4-6, the CLC test fixture consists of two halves (blocks), with the upper block sliding up and down in relation to

the lower block on a roller bearing over two cylindrical rods. The specimen is gripped by the two blocks and secured using the bolts on the blocks, torqued to around 2.5 Nm. The specimen's ends are in contact with the lower and upper platens. Then, the fixture itself is loaded in compression between the flat platens, as shown in Figure 4-6.

Both the basalt-epoxy and basalt-Recyclamine test specimens are rectangular in shape (see Figure 4-6), with dimensions of 140 x 25 x 4 mm^3 as per ASTM D6641M-16e2 were cut. The specimen thickness is based on Equation 4-12 given in the standard to ensure Euler buckling is prevented in the gage section during the loading:

$$h \geq \frac{l_g}{0.9069\sqrt{\left(1-\frac{1.2F^{cu}}{G_{xz}}\right)\left(\frac{E^c}{F^{cu}}\right)}} \qquad \textit{Equation 4-12}$$

In the above equation, h is specimen thickness in mm, l_g is gauge length in mm, F^{cu} is the expected ultimate compressive strength in MPa, E^c is the expected flexural modulus in MPa, and G_{xz} is the expected through-the-thickness (interlaminar) shear modulus in MPa.

As can be seen, several values should be speculated when using Equation 4-12. This becomes difficult when testing a new material for which data is scarce. In such a case, the standard suggests the use of ASTM D3410/D3410M – 16, "Standard Test Method for Compressive Properties of Polymer Matrix Composite Materials with Unsupported Gage Section by Shear" [150]. In this method, the calculation of specimen dimensions requires the value of the expected compressive strength. Accordingly, the thickness of the specimen was determined to be at least 3.17 mm to prevent Euler buckling; hence, the thickness of the coupons used in this experiment is close to 4 mm. The thickness and other dimensions satisfy the standards requirement for preventing Euler buckling. The exact dimensions and the actual coupon are illustrated in Figure 4-6.

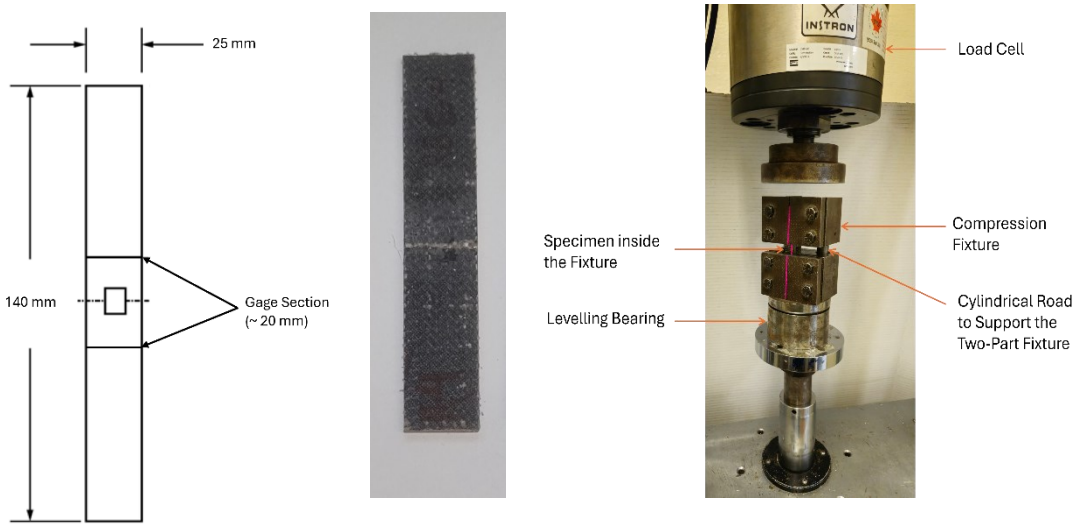

(a) (b) (c)

Figure 4-6: (a) Schematics of the of compression test coupon, (b) a basalt Recyclamine coupon, (c) the compression test setup.

4.3.3.2 Testing Parameters

Like tensile, the strain rate as per ASTM D6641M is also determined by the material specification. This study uses a loading rate of 1.3 mm/min. The laser extensometer was used to collect the change in gauge length displacement. Two stripes of retroreflective tape were placed across the specimen's width in parallel within a specified gauge distance. Additionally, a strain gauge was glued to the reverse surface of the specimen. Finally, the test was started and stopped when an apparent visible failure occurred either visually or through observation made on the real-time load-displacement graph produced by LabVIEW Software.

Further data processing was carried out using basic mechanics of material analyses similar to tensile tests (see section 4.3.2.3).

4.3.4 **Flexural Test**

The flexural test determines polymer matrix composite materials' strength, stiffness, and load/deflection behaviour under a bending state. The flexural properties are helpful for quality control and specification purposes and are even preferred over uniaxial properties in cases when the material is predominantly subjected to flexural loading.

4.3.4.1 Test Fixture and Specimen Preparation

The flexural tests were carried out in accordance with the D7264/D7264M – 07, "Standard Test Method for Flexural Properties of Polymer Matrix Composite Materials" [143]. Procedure B's standard flexural test fixture subjects the specimen to a four-point loading. This configuration uses two symmetrically distanced load points (with respect to the mid-span), equally spaced from their adjacent support points, with the distance between load points set to one-half of the support span. This setup ensures that the maximum bending moment and flexural stress are uniformly distributed between the central load points with no shear forces between the load as opposed to the three-point bending test.

The fixture includes free-rotating cylindrical loading noses and supports, each with a radius of 3.00 mm. The system is carefully aligned to ensure that the axes of the cylindrical surfaces are parallel, maintaining consistency in the load applied. The fixture was designed in SolidWorks and fabricated by a machine shop technician at Dalhousie University. Figure 4-7a and Figure 4-7b show the fixture design and the test setup.

The specimen is rectangular with dimensions of 160 × 13 × 4 mm^3, and the span length was 97 mm, adopting a thickness-to-length ratio of 1:20 to eliminate the shear deformation. The test fixture schematic and actual test setup are illustrated in Figure 4-7.

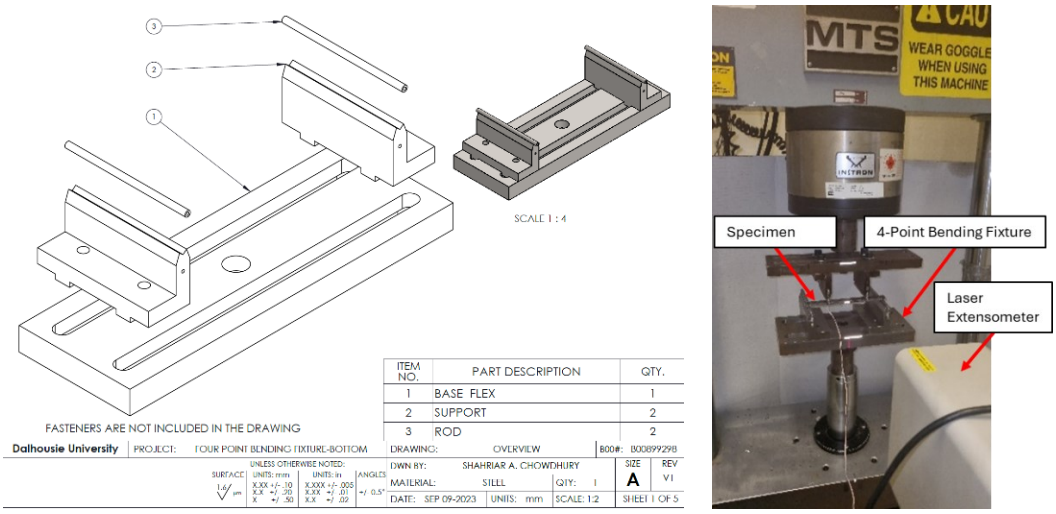

(a) (b)

Figure 4-7: (a) Schematics of the Four-point bending test fixture and (b) test setup.

4.3.4.2 Testing Parameters

The loading rate was set to 5 mm/min according to the standard. The laser extensometer was used to record the exact mid-span deflection, as seen in Figure 4-7. Additionally, a strain gauge was used to acquire the tensile strain at the specimen mid-span. Finally, the test was initiated, observed, and stopped when a clear, visible failure occurred either visually or through the live load-displacement graph produced by MTS Software.

4.3.4.3 Data Collection and Processing

During specimen preparation, each specimen's width, thickness, and gage length were measured by a digital micrometer in different places in three different locations, and the averages were taken. The LabVIEW software collected the time and load increments during each test. Each test was continued till failure of the specimen was observed.

The collected data from the experiment was then processed using Equation 4-13 *and* Equation 4-14 to establish the flexural stress and strain, and the modulus of elasticity was calculated using the equation provided earlier. To calculate the stress and strain, the following equations were used:

$$\sigma = \frac{3PL}{4bh^2} \qquad \textit{Equation 4-13}$$

where σ is the maximum stress across the cross in MPa, P is the applied force in *N,* and L, b and h are the support span specimen's span length, width and thickness in mm, respectively,

and

$$\varepsilon = \frac{4.36\delta h}{L^2} \qquad \textit{Equation 4-14}$$

In the above equation, ε is the maximum tensile strain in mm/mm, and δ is the mid-span deflection in mm.

4.3.5 **Shear Test**

Shear testing is used to evaluate materials' shear strength and modulus, crucial parameters indicating the material's ability to withstand shear stresses. This type of test measures how a material responds to shear forces, that is, (i) the forces that cause one layer of the

material to slide past an adjacent layer (interlaminar shear) or (ii) forces that cause fibers and matrix to slide within the same layer (in-plane shear).

4.3.5.1 Testing Fixture and Specimen Preparation

The shear properties of the composite materials were evaluated by following ASTM D5379 Standard, "Test Method for Shear Properties of Composite Materials by the V-Notched Beam Method (Iosipescu test)" [144]. The test fixture in this method consists of two primary blocks: the upper block and lower block, as can be seen in Figure 4-8 and an actual notches specimen is also shown in An actual specimen is shown in Figure 4-8c. The specimen is secured in the wedge clamp in each block. The lower grip is mounted on a base plate, which also supports a linear bearing shaft, while the upper grip contains a linear bearing that slides over this shaft. An aligner rod is in place to ensure the specimen is aligned with the fixture at the v-notch and to ensure maximum shear stress distribution in the centre region between the v-notches.

The v-notches in each specimen is cut using a similar-looking guiding fixture that sandwiches each specimen (see Figure 4-8b). A reciprocating air saw was used to cut the v-notches following the guiding fixture.

The standard specimen dimensions include two notches at an angle of 90 degrees, a notch depth of 20% of the specimen width from each side, and a notch radius of 1.3 mm. These notches are designed to create a uniform shear stress in a region between the notches. The specimens have dimensions of 76 mm in length, 19 mm in width, a notch width of 11.4 mm, and 3 to 4 mm in thickness. The notch width and the thickness of the specimen were measured using a digital micrometer in different places (at least three readings), and the average was taken. A pair of 350 ohms orthogonal stacked rosette strain gauges (Kyowa Model KFGS-2-350-D16-11 L1M2S) was used to measure the strains. The gauges have a 10 mm diameter base size with a gauge length of 2 mm. The gauges were glued to the specimens at a 45°angle with respect to the loading axis between the notches.

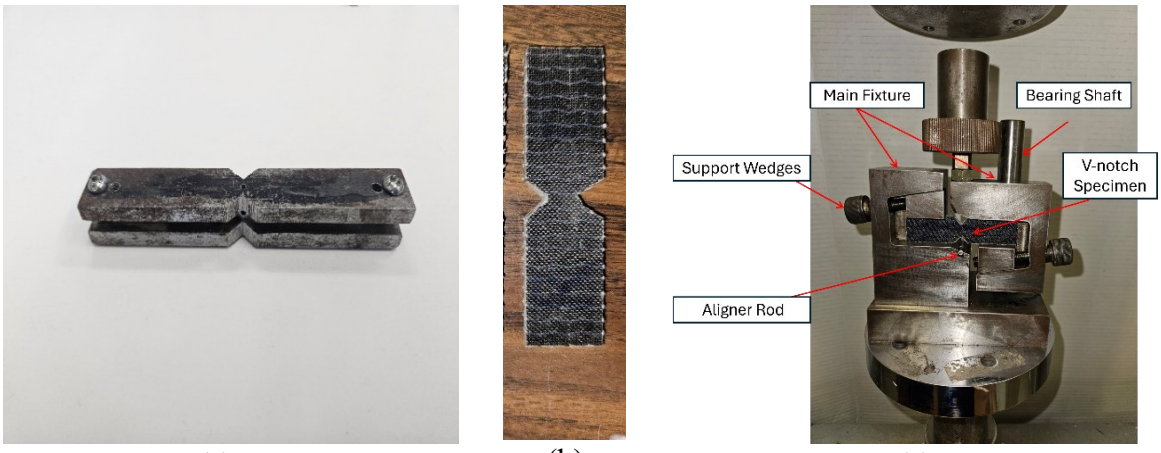

(a) (b) (c)

Figure 4-8: a) Fixture for coupon cutting, b) Shear test Coupon, c) Shear test assembly.

4.3.5.2 Test Parameters

The specimen is inserted into the fixture using an alignment tool to ensure the notches are correctly positioned relative to the loading axis. The testing speed was set to 2 mm/min according to the standard.

Moreover, the relative displacement between the fixture halves, caused by the compressive force from the testing machine, induces shear stress in the notched section of the specimen, allowing the shear properties of the material to be evaluated accurately. Finally, each test was stopped when a visible failure occurred either visually or was observed through the live load-displacement graph produced by LabVIEW Software.

4.3.5.3 Data Collection and Processing

The data was collected through the LabVIEW software as in the other tests. The NIDAQ was also used to record the strain readings from the gauges. The frequency of data collected was the same as the other tests mentioned previously.

The collected data from the experiment was then processed, and Equation 4-15 was used to calculate the shear strain.

$$\gamma_n = |\varepsilon_{+45}| + |\varepsilon_{-45}| \qquad \textit{Equation 4-15}$$

where γ_n is the engineering shear strain at nth data point, ε_{+45} and ε_{-45} are the normal strain at ith data point of each gauge. The ultimate engineering shear strain, γ^a, is taken either at the ultimate load or at 5% of the total strain if the material exhibits non-linear

behavior and deform without shear failure, whichever comes first. This value is taken mainly to avoid irregularities in the experimental data that can happen when the fibers reorient after shear failure, allowing the fibers to carry a major portion of the load.

Equation 4-16 is used to calculate the shear modulus.

$$G^{chord} = \Delta\tau/\Delta\gamma \qquad \textit{Equation 4-16}$$

in which G^{chord} is the shear chord modulus of elasticity in MPa, $\Delta\tau$ and $\Delta\gamma$ are the stress increment, and the corresponding strain increment is taken in the linear elastic portion of the shear stress-shear strain curve.

4.3.6 **Izod Impact Test**

An impact test evaluates a material's resistance to failure when subjected to a suddenly applied force, such as a collision, falling object, or instantaneous blow. This test measures the impact energy, or the energy absorbed before the material fractures. Various methods are used to assess the impact resistance of plastics. The notched Izod impact test is the most commonly used method among these. This test is essential for comparing the relative impact resistance of different materials under controlled laboratory conditions.

By providing critical data on a material's toughness by using Izod Impact test, engineers can predict how materials will perform in real-world conditions where they are subjected to dynamic or suddenly applied loads. The Izod impact test also helps identify potential material weaknesses, which later helps improve material formulations and processing techniques.

4.3.6.1 Test Fixture and Specimen Preparation

The Izod impact test is conducted using a Tinius Olsen Model 66 Plastic Impact Tester, which complies with the ASTM D256-23, "Standard Test Methods for Determining the Izod Pendulum Impact Resistance of Plastics (Polymers)" [145]. The device for this test consists of a pendulum-type hammer released from a fixed height to strike a notched specimen, which is mounted vertically in a vice. The hammer's swing and impact on the specimen apply 22.6 Joules (200 in-lbs) of energy to the specimen at a consistent

velocity, and the test's gauge records the energy absorbed by the specimen during the impact.

Specimen preparation for the Izod impact test involved precise cutting and notching of the specimens to ensure consistency in the results. Specimens with dimensions of 63.5 mm in length, 12.7 mm in width, and a thickness of around 6.5 mm were extracted from the panels. The waterjet cutter was fed with the specimen's shape and dimensions through a G-code generated using Autodesk Fusion 360 KMotion software.

According to the ASTM D256-23 standard [145], the test specimens must have a specific notch geometry to create a stress concentration that promotes a brittle fracture. The standard specimen includes a notch angle of 90 degrees made at a distance of 31.8 mm from one end of the specimen length (see Figure 4-9b). The notch has a radius of 0.25 mm and a depth of 2.54 mm. The specimen notch was precisely positioned in the device's grip, as shown in Figure 4-9*c*.

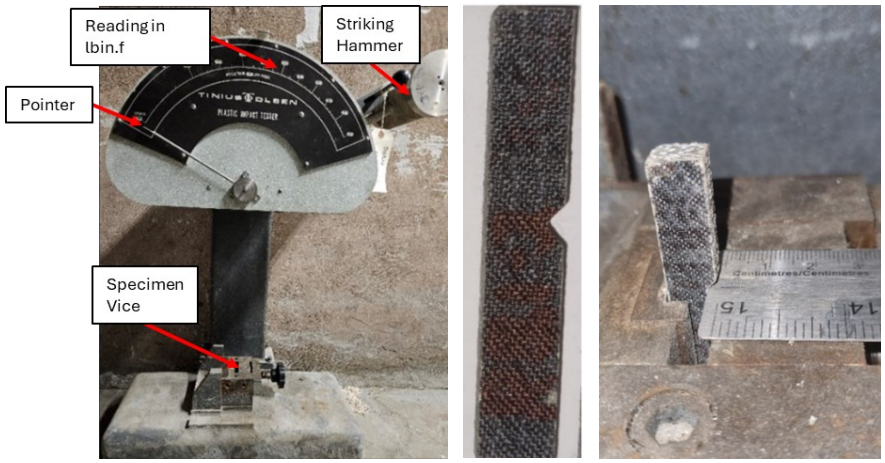

Figure 4-9: (a) Izod coupon, (b) Tinius Olsen Impact Tester and (c) aligning the coupon in the vice.

4.3.6.2 Data Collection and Processing

Before testing the specimens, the hammer was operated to assess the friction in the bearing of the hammer and the friction due to the hammer's travel through the air. The total energy consumed by these factors was estimated to be approximately 1 in-lbf.

Subsequently, each specimen was tested, and the energy absorbed by the specimen and the failure mode were recorded. A total of five specimens were tested.
The net Izod energy was found by Equation 4-17:

$$Net\ Izod\ Energy = BE_1 - TE_1 \qquad \textit{Equation 4-17}$$

where BE_1 is the initial break energy corrected for friction and windage and TE_1 is the toss energy.

4.3.7 **Micromechanics Analyses**

Several micromechanical models were used to determine the physical properties of the heterogenous composites, including the Rule of Mixture (RoM). RoM is a basic model derived based on the constituents' volume fraction to predict composites' elastic properties. The RoM assumes that the fiber and the matrix are fully bonded and thus would have equal strains under an applied load. The RoM is used to estimate the strength of the unidirectional fiber composites by considering the volume fractions of the fiber and matrix components [151]. The RoM is also utilized to find other elastic properties as well like Poisson's ratio and shear modulus of the constituent fibers and matrices. The following equation determines the longitudinal elastic modulus (along the fibers):

$$E_1 = E_f.V_f + E_m.V_m \qquad \textit{Equation 4-18}$$

where E_f and E_m are the modulus of elasticity of the fiber and matrix, respectively, and V_f and V_m are the volume fraction of the fiber and matrix, respectively.

The Halpin-Tsai model [145] was also utilized to find the other mechanical properties. The model considers the geometric characteristics and the orientation of the fiber filler. The desired properties can be obtained by using the following Equation 4-19:

$$M = \left(\frac{1 + \xi\eta V_f}{1 - \eta V_f}\right) M_m \qquad \textit{Equation 4-19}$$

in which, the coefficient η is given by Equation 4-20

$$\eta = \frac{\frac{M_f}{M_m} - 1}{\frac{M_f}{M_m} + \xi} \qquad \textit{Equation 4-20}$$

In the above equations, M is the desired property (i.e., E_1, E_2, ν_{12}, G_{12}), M_f and M_m are the corresponding fiber and matrix parameters, respectively, and V_f is the fiber volume fraction.

The parameter "ξ" is called the reinforcing factor, and it depends on the fiber cross-sectional geometry, fiber packing geometry and the loading conditions. For this research, ξ was determined to have a value of two (2) when calculating the transverse elastic modulus of elasticity of the composite.

Another indirect approach to determining the tensile and compressive strength of a unidirectional (UD) composite is done by incorporating the Back-Out Factor (BoF). BoF is a factor determined multiplied by the experimental values obtained from tensile and compressive tests on cross-ply laminate. It is the ratio of the axial stiffness of the cross-ply laminate to that of the unidirectional plies. This factor is a simplified estimation based on the laminated plate theory. Thus, this simplified theory is only applicable in homogenous composites with $[0/90]_{ns}$ (cross-ply laminates with an equal number of 0° and 90° plies (i.e., symmetric plies)) or angle ply composites with similar provisions [152–154]. The general formula for balanced and symmetric cross-ply lamina is:

$$BoF = \frac{Q_{11}^0 A_{22} - Q_{12}^0 A_{12} t}{A_{11} A_{22} - A_{12}} \qquad \textit{Equation 4-21}$$

where Q_{ij}^0 are the ij elements of the reduced stiffness matrix for a unidirectional ply and A_{ij} represent the axial stiffness terms of a unidirectional laminate in a plane stress configuration.

The above equation can be simplified for laminates with the configuration $[0/90]_{ns}$, resulting in Equation 4-22:

$$BoF = \frac{\frac{1}{2} E_{11}(E_{11} + E_{12}) - (v_{12}E_{12})^2}{\frac{1}{4}(E_{11} + E_{22})^2 - (v_{12}E_{22})^2} \qquad \textit{Equation 4-22}$$

where E_1 and E_2 are the modulus of elasticity in the axial and transverse directions of a unidirectional ply, respectively, E_{12} is the shear modulus (i.e., = G_{12}) and v_{12} = the major Poisson's ratio.

However, further simplification was required in this research for the evaluation of the compressive unidirectional properties using the backing-out factor due to the unavailability of the transverse modulus of the UD composites. Hart-Smith [154] presented a generalized equation based on the simplified rule of mixture in conjunction with the thin plate theory. This method assumes the composite to be a thin plate, and hence, Poisson's ratio effect can be overlooked, which he claimed to work for determining both the tensile and compressive strengths test from cross-ply tests. The Hart-Smith equation is as follows:

$$\sigma_{11} = \frac{\sigma_x}{V_{f_0} + (1 - V_{f_0})\,\frac{E_2}{E_1}} \qquad \textit{Equation 4-23}$$

where V_{f_0} is the fiber volume fraction of 0° fiber in the cross-ply composite, σ_x is the tensile strength of the cross-ply composite and σ_{11} is the tensile strength of the UD composite.

Moreover, the Military Handbook, MIL-17-F [155] considers the transverse modulus (E_2) effect insignificant; hence, it can be ignored. All the methods described assume linear stress-strain behaviour to failure. For the composite. If E_2 is unavailable, this method involves measuring only the modulus from a unidirectional specimen and modulus, E_x from the cross-ply laminate being tested, with the assumption that the laminate fails by the same mechanism and at the same strain as the plies in a unidirectional specimen and that it does not fail prematurely, allowing for the calculation of lamina strength in the axial direction to be:

$$\sigma_1 = \frac{E_1}{E_x} \times \sigma_x \qquad \textit{Equation 4-24}$$

In the above equation, σ_x is the tensile/compressive strength of the cross-ply laminate and σ_1 is the strength of its UD laminate.

Additionally, in order to calculate (shear modulus) G_{12} and compare it with the experimental results obtained from the shear test, the equation based on the theory of elasticity [156] was employed. The results were then verified against those obtained from Halpin-Tsai's model for calculating G_{12}. The elasticity equation is as follows:

$$G_{12} = G_m \left[\frac{G_f + (1 + V_f) + G_m(1 - V_f)}{G_f + (1 - V_f) + G_m(1 + V_f)}\right] \quad \textit{Equation 4-25}$$

where V_f and G_f are the fiber volume fraction and modulus of the fiber, respectively, and G_m is the shear modulus of the matrix used for the composite. Other models, such as Hahn's model, were also considered to verify the results obtained experimentally and analytically.

Lastly, a compression test of uniaxial basalt fiber composites (achieved by burning off the biaxial fibers) was conducted to determine the accuracy of the tests carried out and to verify the back-out factor. More details on the specimen preparation are provided in section 5.7.

This test was conducted in accordance with ASTM D6641M [150], the standard for Compressive Properties of Polymer Matrix Composite Materials, using a Combined Loading Compression (CLC) fixture. The specimens were carefully tabbed with fiberglass to prevent Euler buckling and ensure the load would be concentrated in the gage section. A laser extensometer was used to measure the strain during the tests. The preparation of the specimens involved aligning and securing the fibers with fiberglass tabs to prevent premature failure due to buckling. This method allowed for a detailed analysis of the compressive strength and modulus of the uniaxial fibers.

Figure 4-10 shows (a) the tabbed specimen and (b) the specimen during the test.

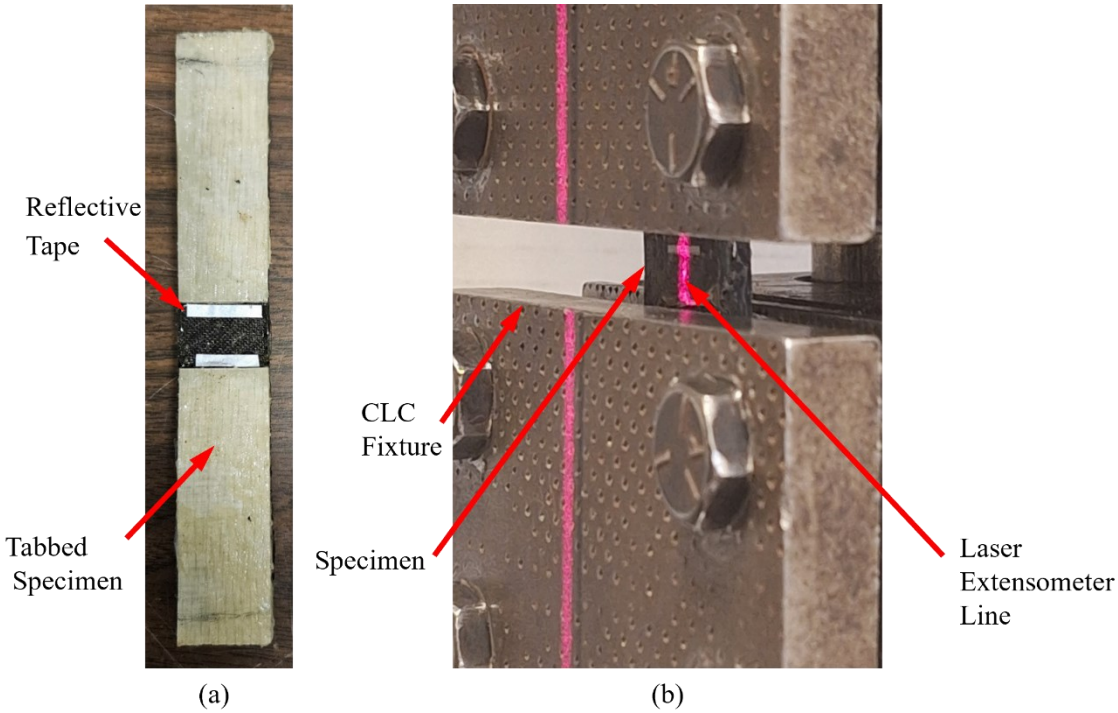

Figure 4-10: (a) tabbed specimen and (b) specimen with the test set-up.

These analyses were conducted to enhance understanding of the material's micromechanics, compare the analyses with similar research found in the literature, and assess the validity of the Back-out Factor and other micromechanics approaches.

In addition to the specific test measurements and the analyses mentioned above, other essential calculations were performed to analyze the data comprehensively across all experiments. These calculations included determining the average values of the results and calculating the standard deviation, which measures the dispersion or spread of the data points around the mean. Furthermore, the coefficient of variation (CV), the ratio of the standard deviation to the mean expressed as a percentage, was also calculated for each test category. Lastly, all these calculations were processed using Microsoft Excel, and the results are presented in table form.

4.3.8 **SEM and Digital Microscopic Analyses**

The Scanning Electron Microscopy (SEM) analysis was conducted on re[presentative test specimens to ascertain the composites' microstructural characteristics and failure mechanisms. SEM provides high-resolution images of the specimen's surface, allowing

for detailed examination of the fiber-matrix interface, fracture surfaces, and microstructural defects. The Electron Hitachi S-4700 FE Scanning Electron Microscope was used for this analysis. This advanced equipment offers magnifications up to approximately 500,000x. It can form images using secondary and back-scattered electrons—the digital image acquisition capability of the microscope, along with the coating units for gold and carbon.

For the impacted specimens, the analysis focused on the regions around the fracture zone. Samples were carefully prepared by cutting small sections from the impacted areas and mounting them on SEM stubs. These sections were then coated with a thin layer of gold to enhance conductivity and improve image quality. The SEM images revealed the nature of the fiber breakage, matrix cracking, and fiber pull-out. Detailed observations highlighted the extent of damage, including any voids or delamination, which are critical in understanding the composite's impact resistance and failure modes. Also, the SEM images provided insights into fiber buckling, shear-out, matrix crushing, and the interaction between fibers and the matrix. Additionally, the images were used to assess the uniformity of fiber distribution and the bonding quality between the fibers and the matrix.

Moreover, complementing SEM, Digital Microscopic Analysis provided a broader overview of surface morphology at lower magnifications. This method was mainly helpful in identifying larger-scale features such as cracks, delamination, buckling and other surface irregularities that SEM might miss due to its higher magnification focus. In addition to that, all the experiment coupons were observed under the digital microscope to understand the type of failure.

CHAPTER 5 RESULTS AND DISCUSSION

This chapter presents a comprehensive discussion of the results obtained from the tests conducted, aiding a better understanding of the performance of the composite panels. Moreover, this chapter presented only the average of combined test results; the individual specimen test result graph is included in Appendix A.

Stress-strain curves generated from the tensile tests offer a deep understanding of the material's behaviour under tension, compression, shear, flexural and impact loading states, allowing us to determine the ultimate strengths, yield strengths, and modulus of elasticity. The load-deflection curves resulting from flexural tests yield valuable information about the composite's bending behaviour, allowing for the calculation of flexural strength and modulus, which, in most practical cases, would better represent the expected performance for a given material.

Furthermore, the impact energy values obtained from the Izod impact tests are also evaluated and discussed, shedding light on the composite's resilience to a suddenly applied load. Additionally, micromechanical analyses were performed to verify the results and provide a deeper understanding of the composite behaviour.

SEM and Digital Microscopic analyses are also presented, discussing the microstructural aspects of the fractured surfaces, which helps to identify the failure mechanisms and assess the quality of the fiber-matrix interface. Lastly, a thorough comparison is carried out between the mechanical properties of the composite panels manufactured using basalt fiber with the two resin systems.

5.1 FIBER VOLUME AND VOID CONTENT EVALUATION

The void content of basalt Recyclamine and basalt epoxy composites was evaluated. Using the burn-off test, as mentioned in 4.3.1, the weight percentages of the fibers and resins were determined. Finally, the void content of the tested composites was established. The results are presented in Table 5-1.

Table 5-1: Average fiber and resin volume fraction and weight % of the tested composites.

Material	Average Fiber Weight %	Average Resin Weight %	Average Fiber Volume Fraction	Average Resin Volume Fraction
Basalt-epoxy	66.2	33.8	52.9	42.7
Basalt-Recyclamine	70.2	29.3	56.0	39.1

These results were then used to obtain the void content of the basalt composites. All void contents fell below 5% of the total volume of the composites, with basalt-Recyclamine having a slightly higher void content as shown in Table 5-2. The slightly lower void content could be partially due to the lesser viscosity of the Recyclamine system, which could have created air pockets due to the speed of the resin travel. The composites are manufactured with an approximately 1.2:1 resin-to-fibre weight ratio to account for resin loss during all experiments. As seen in the table, basalt fiber occupies most of the volume of a composite because it has a higher density than resins. Also, the density of basalt-Recyclamine is relatively lower than that of basalt-epoxy.

Table 5-2: Density of basalt and its composites and their void content.

Material	Average Density (g/ml)	Theoretical Density (g/ml)	Void Content (%)
Basalt fiber	-	2.3	-
Basalt-epoxy	1.6	1.8	4.4
Basalt-Recyclamine	1.5	1.6	4.9

5.1.1 Causes of Excessive Void Content and its Influence on Mechanical Properties

Void contents as low as 1%, or 2.5 to 5 % volume in certain circumstances, are usually considered acceptable for structural components [157]. Void content in composite laminates plays a critical role in determining their mechanical properties, with a significant drop in performance observed when void content exceeds 1-2% [158].

During the resin infusion process, higher flow rates (pressure) often lead to the formation of micro-voids in the initial stages as the resin quickly permeates the fiber network, trapping small amounts of air in the process, while macro-voids emerge later as the flow moves away from the inlet in the latter half of the laminate and the resin flow may not be sufficient to displace all the trapped air, especially over longer distance [158,159]. This low pressure could also lead to resin evaporation which has a potential to generate voids [138]. Moreover, air bubbles and absorbed moisture can volatilize and expand during heating stage or curing, causing the formation of voids. All defects present at resin consolidation remain trapped inside laminate [157].

The presence of voids, particularly in amounts greater than 2%, can severely impact mechanical properties such as interlaminar shear strength (ILSS) and short-beam shear (SBS) strength and compressive strength. Landro et al. [160] conducted tests on carbon-epoxy. A notable decrease in interlaminar shear strength is observed as void content increases; for example, a void content of 6.6% leads to an estimated reduction in SBS of about 25%. This illustrates the sensitivity of interlaminar properties to void presence. Tensile strength is a fiber-dominated property which is less affected by voids, with laminates containing 4-6% voids exhibiting only a slight reduction in tensile failure load by about 4%.

However, voids are more adversely affected by compressive strength, with a reduction of approximately 10% in the load-carrying capacity observed when the void content reaches around 4%. This reduction in compressive strength is primarily due to fiber buckling, which is more evident under compressive loading conditions, particularly in laminates where fiber misalignment is present. This effect is also reported by Harper et al. [161], the authors conclude that matrix-dominated moduli E_{22} and G_{12} are significantly affected by void content, with these properties decreasing as void content increases. In contrast, the fiber-dominated properties E_{11} and ν_{12} exhibit little dependence on void content. Similar phenomenon can also be observed in the compressive test conducted in this research (see section 5.3). Thus, while tensile properties are somewhat resilient to voids, interlaminar and compressive properties show a significant decrease as void content increases.

Another study [162] examined how the presence of voids in carbon-epoxy laminates affects their mechanical strength. The research involved creating laminates with different levels of void content and testing them using methods that measure their ability to resist shear forces and bending. The results showed a clear connection between the amount of voids and the strength of the material. Specifically, for every 1% increase in void content, the interlaminar shear strength decreased by 9.7%, the flexural strength dropped by 10.3%, and the flexural modulus declined by 5.3%. If the void content increases by 2%, the material's strength could decrease by about 20%, and its stiffness could drop by around 10%. This shows the significance of striving for lower void content due to its impact on composite materials' overall performance.

5.2 TENSILE TEST RESULTS

The basalt-Recyclamine composite had a smooth surface, while the basalt-epoxy composite had a relatively rougher one, which, again, could be attributed to the low viscosity of the Recyclamine, which makes it flow more easily and evenly over the surface of the composite material during the manufacturing process. Table 5-3 reports the average value of the tensile properties of both composites, and Figure 5-1 and Figure 5-2 show the stress-strain curves and images of the tested specimens, respectively.

Table 5-3: Average tensile strength and modulus of elasticity of the two composite specimens.

Material	Tensile Property	Avg. Value	Standard Deviation	Coeff. Var.
Basalt - epoxy	Strength (MPa)	464	25.9	5.6
	Strain (mm/mm)	0.024	0.0038	15.7
	Modulus (GPa)	22.0	2.0	8.7
Basalt – Recyclamine	Strength (MPa)	390.9	30.7	7.9
	Strain (mm/mm)	0.019	0.0037	19.9
	Modulus (GPa)	20.2	0.8	4.1

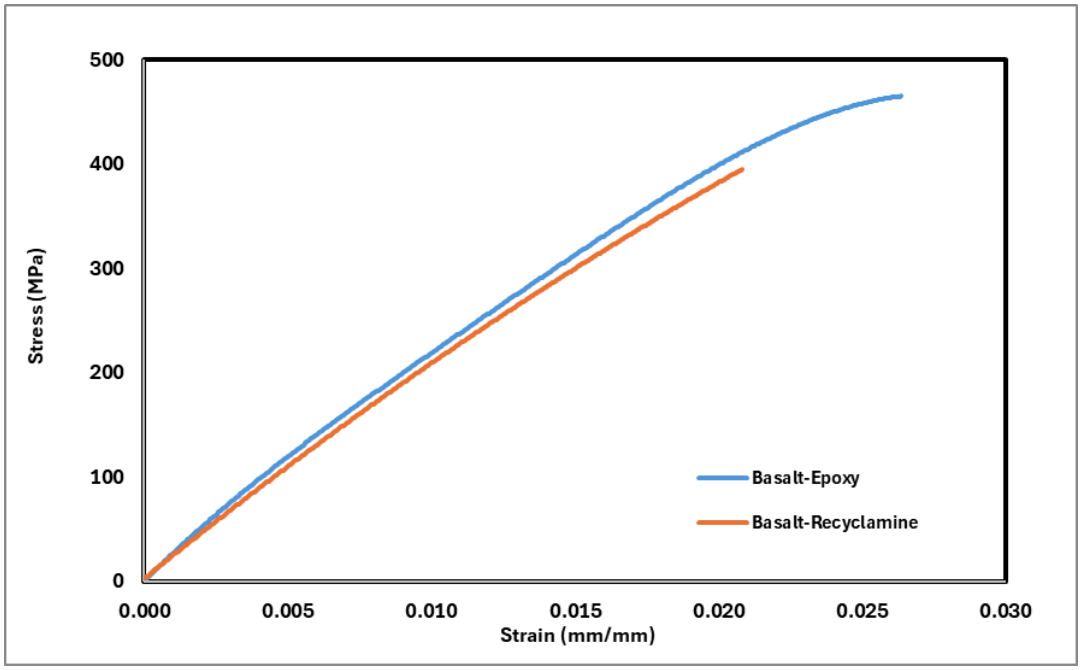

Figure 5-1: Average tensile stress-strain curve of basalt-epoxy and basalt-Recyclamine specimens.

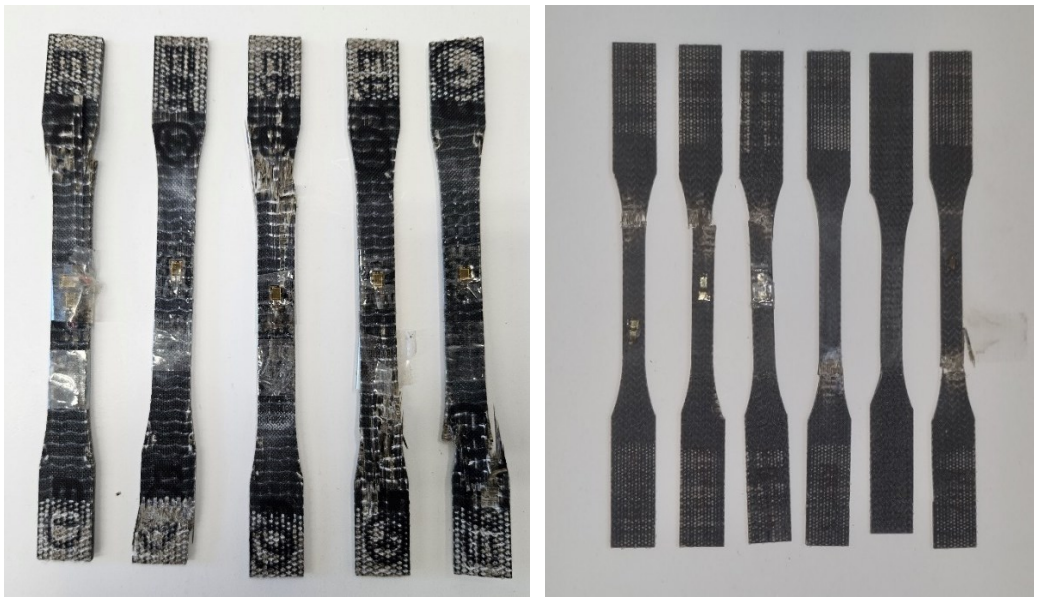

(a) (b)

Figure 5-2: Post-failure tensile test specimens (a) basalt-epoxy, (b) basalt-Recyclamine.

As seen in Figure 5-2, the majority of the failure occurred near the grip, as opposed to the middle of the specimen's gage length, as speculated; this is largely due to stress concentration near the grip. However, this failure mode is acceptable according to the standard followed.

The basalt-epoxy composite exhibited an average tensile strength of 464 MPa, whereas the basalt-Recyclamine composite showed a lower average tensile strength of 390.9 MPa. The basalt-epoxy composite demonstrated an average failure/ultimate strain of 2.4%. In contrast, the basalt-Recyclamine composite had a slightly lower average ultimate strain of 1.9%. The tensile modulus provides insight into the stiffness of the composites. The basalt-epoxy composite had an average tensile modulus of 22.0 GPa, whereas the basalt-Recyclamine composite displayed a slightly lower modulus of 20.2 GPa. This suggests that the basalt-epoxy composite is slightly stiffer, which can be beneficial for applications needing high rigidity and dimensional stability. Conversely, the somewhat lower modulus of the basalt-Recyclamine composite indicates a more flexible or ductile material that can better withstand dynamic and impact loads without catastrophic failure.

5.3 Compression Test Results

As previously mentioned, the compression tests were conducted following ASTM D3410. Each specimen was secured using a combined loading compression (CLC) fixture, and five specimens were tested for both composites.

Table 5-4 reports the value of the compressive characteristics of both the materials and Figure 5-3 and Figure 5-4 show the graphs and post-failure images of basalt-epoxy and basalt-Recyclamine, respectively.

Table 5-4: Average compressive strength and modulus of the two composites.

Material	Compressive Property	Avg. Value	Standard Deviation	Coeff. Var.
Basalt - epoxy	Strength (MPa)	233.9	16	6.9
	Strain (mm/mm)	0.011	0.001	8.6
	Modulus (GPa)	24.0	0.6	2.5
Basalt – Recyclamine	Strength (MPa)	237.7	15.1	6.3
	Strain (mm/mm)	0.039	0.011	29.2
	Modulus (GPa)	27.5	1.5	5.6

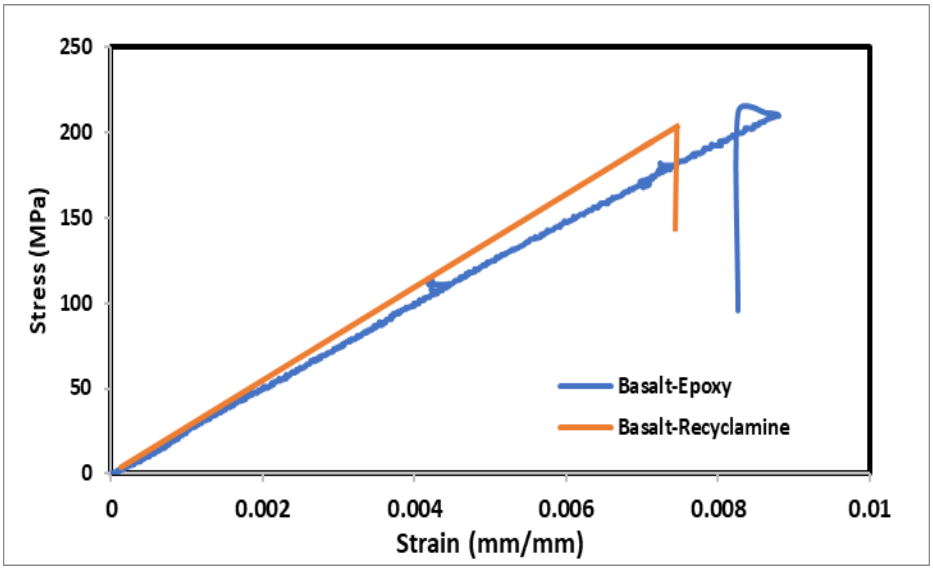

Figure 5-3: Average compressive stress-strain curves of basalt-epoxy and basalt-Recyclamine specimens.

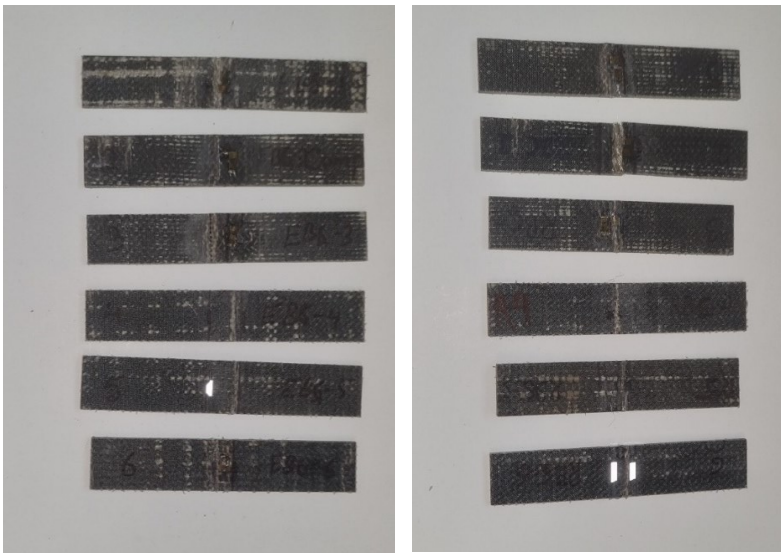

(a) (b)

Figure 5-4: Post-compression failure test specimens (a) basalt-epoxy, (b) basalt-Recyclamine.

Due to the nature of compression tests and their shorter gauge length compared to tensile tests, the compressive loads induced Saint-Venant's stress, causing a mismatch in strain [163], affecting the accuracy of the strain data. The void content in a composite also affects its mechanical properties since these voids interfere with the effective transfer of load among the fibers and generate microcracks. This effect becomes more prominent in compression loading because the interaction of fibers and matrix material plays a more pronounced role in bearing the load than tension tests as described in section 5.1.1. These behaviours are evident based on the materials' lower compressive strength and modulus compared to those evaluated under tensile loading. However, basalt-epoxy specimens 4 and 5 exhibited non-linear behaviour, where changes in the strain occur as voids collapse and the transverse fibers crumple onto each other. The basalt-Recyclamine also indicates a higher strain of 3.9%, re-asserting its ductile nature.

The Recyclamine-based composite showed a higher ultimate compressive strength, with an average compressive strength of 237.7 MPa, compared to 233.9 MPa for basalt-epoxy. This difference can be explained by the failure modes observed during compression loading, resulting in micro-buckling and shear crimping, which were seen in epoxy-based composite specimens. However, A relatively more brittle matrix like epoxy helps maintain the fiber alignment, leading to a slightly more effective load bearing. On the

other hand, Recyclamine, being somewhat more ductile than epoxy, tolerates greater fiber deformation and transfers the load among the fiber more effectively due to its better bond adhesion to the fibers. The stated hypothesis can be supported by the higher compressive modulus of elasticity of 27.5 GPa of the Recyclamine composite, while the basalt-epoxy composite exhibited an average compressive modulus of 24 GPa.

5.4 FLEXURAL TEST RESULTS

As previously mentioned, the flexural tests were conducted following ASTM D7264 [143], the standard test method for flexural properties of polymer matrix composite materials. This test provided a deeper understanding of the composites under bending loads.

Table 5-5 presents the flexural mechanical properties of both composites, and Figure 5-5 and Figure 5-6 shows the stress-strain curves post-flexural failure test images of basalt-epoxy and basalt-Recyclamine, respectively.

Table 5-5: Average flexural strength and modulus of the composites.

Material	Flexural Property	Avg. Value	Standard Deviation	Coeff. Var.
Basalt - epoxy	Strength (MPa)	441.4	20.8	4.7
	Modulus (GPa)	21.9	0.57	2.6
Basalt – Recyclamine	Strength (MPa)	372.1	14.8	4.0
	Modulus (GPa)	23	0.7	3.1

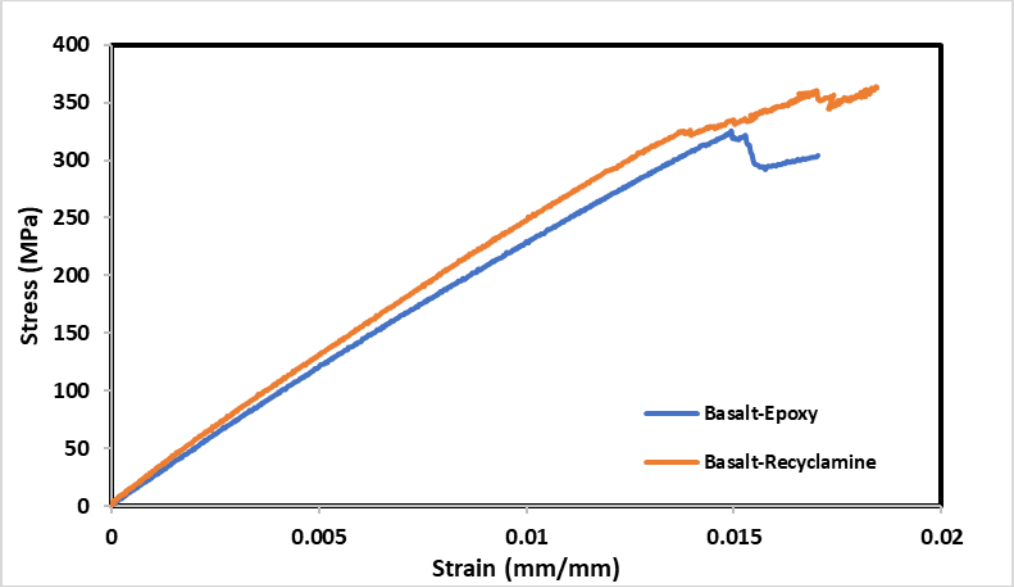

Figure 5-5: Average flexural stress-strain curves of basalt-epoxy specimens.

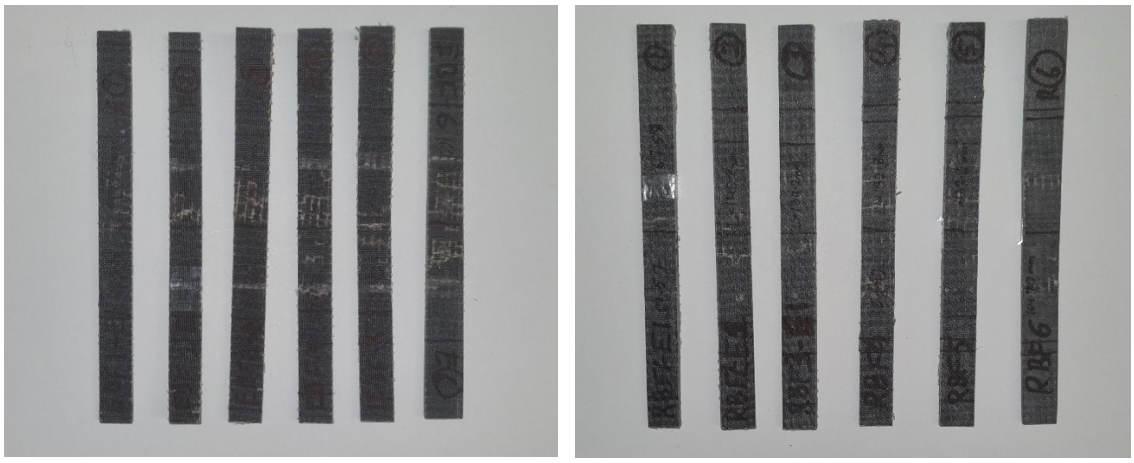

(a) (b)

Figure 5-6: Post-flexural failure test specimens (a) basalt-epoxy, (b) basalt-Recyclamine.

As evident from the tabulated values, the basalt-epoxy composite demonstrated an average flexural strength of 441.4 MPa, while the basalt-Recyclamine composite showed a lower average flexural strength of 372.1 MPa.

Regarding the flexural modulus, the basalt-epoxy composite had an average value of 21.9 GPa. Interestingly, the basalt-Recyclamine composite exhibited a higher average flexural modulus of 23 GPa. The higher modulus in the basalt-Recyclamine composite means it had a stiffer response to bending loads despite its lower flexural strength.

5.5 Shear Test Results

As previously mentioned, the shear tests were performed following ASTM D5379M [144], which involves using the V-notched beam method to determine the shear properties of composite materials. Table 5-6 reports the shear properties of both composites, and Figure 5-7 and Figure 5-8 show the graphs and post-failure images of the two composites.

Table 5-6: Average shear strength and modulus of the composites.

Material	Shear Property	Avg. Value	Standard Deviation	Coeff. Var.
Basalt - epoxy	Strength (MPa)	42.6	2.5	5.8
	Modulus (GPa)	2.6	0.3	10.5
Basalt – Recyclamine	Strength (MPa)	52.8	1.8	3.4
	Modulus (GPa)	2.9	0.4	13.0

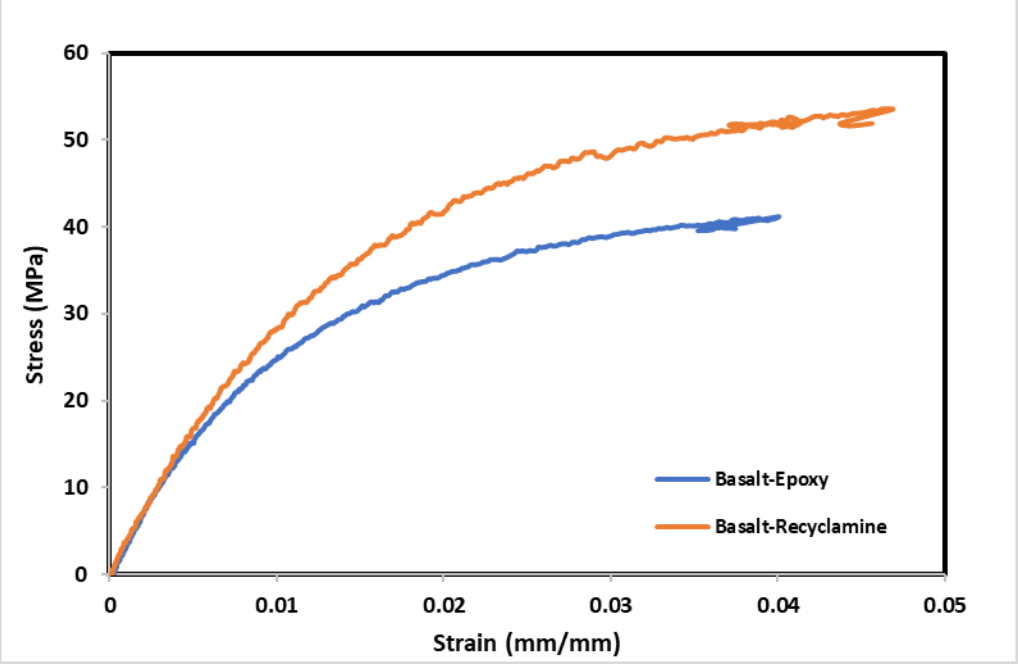

Figure 5-7: Average shear stress-strain curves of basalt-epoxy specimens.

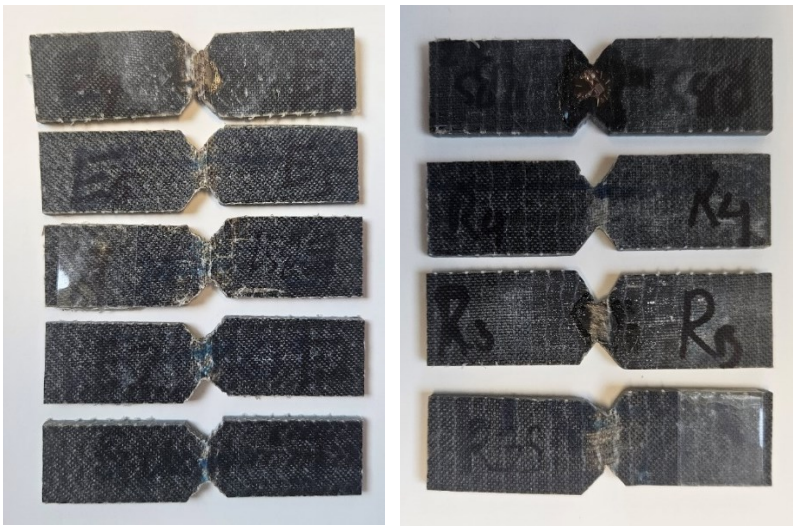

(a) (b)

Figure 5-8: Post-failure shear test specimens (a) basalt-epoxy, (b) basalt-Recyclamine.

Compared to the previously reported mechanical property values, the difference in the shear responses of the composites was greater. The basalt-epoxy composite withheld an average maximum shear stress of 42.59 MPa, while the basalt-Recyclamine composite had a higher average maximum shear stress of 52.78 MPa.

Regarding the shear modulus, the basalt-epoxy composite displayed an average value of 2,620 MPa, whereas the basalt-Recyclamine composite exhibited a higher average shear modulus of 2,950 MPa. The higher shear modulus in the basalt-Recyclamine composite indicates a noticeably stiffer response under pure shear loading load.

5.6 IZOD IMPACT TEST RESULTS

The Izod impact tests were conducted following ASTM D256-23, the standard test method for determining the impact resistance of plastics and composite materials using the Izod pendulum apparatus. This test measures the material's ability to absorb energy and resist fracture when subjected to a sudden impact. Table 5-7 reports the results of the Izod tests.

Table 5-7: Average impact resistance of the test specimens.

Material	Avg. Impact Resistance (J/m)	Standard Deviation	Coeff. var.
Basalt – epoxy	1639	73	4
Basalt – Recyclamine	1595	51	3

As seen in the table, the basalt-epoxy has a greater resistivity to impact with average impact resistance of 1639 J/m, whereas Recyclamine has an average of 1595 J/m. The difference is attributed to the fact that both resin systems have good toughness and energy absorption capabilities under sudden impact loading. The slight reduction in average impact resistance compared to basalt-epoxy could be due to the Recyclamine's ability to deform more under impact, leading to a gradual absorption of energy rather than a sharp fracture. However, basalt-epoxy has a little more brittle failure as seen in Figure 5-9(a) since the specimens have lesser fiber pull out, therefore, require higher initial energy for breaking [164].

(a) (b)

Figure 5-9: Post-impact test specimens (a) basalt-epoxy, (b) basalt-Recyclamine.

5.7 MICROMECHANICS ANALYSES

A few micromechanical approaches, as outlined in the literature review, were used to verify and compare the results. The micromechanical approaches used in this research are the Rule of Mixtures (RoM), Halpin-Tsai models, the equation based on the theory of elasticity, Hahn's model and the Back-Out Factor (BoF) to determine the tensile and compressive moduli and strengths, respectively (see section 4.3.7).

For basalt-epoxy, the longitudinal elastic modulus (E_1) calculated using RoM was found to be 43.8 GPa, and the transverse elastic modulus (E_2) computed using the Halpin-Tsai model was 11.9 GPa. These values match closely to the reported values in the literature for other basalt-epoxy systems [113], where the longitudinal and transverse elastic moduli have been reported as 44.3 ± 2.3 GPa and 11.9 ± 1.2 GPa, respectively.

The tensile strength ($\sigma_{1,\,tens.}$) calculated using the BoF approach is 703.1 MPa, while using the RoM and simplified Classic Lamination Plate Theory (CLPT) approaches yielded a higher value of 1002.2 MPa. The Military Handbook alternative approach provided a tensile strength of 923.8 MPa, with the theoretical models generally predicting conservative strengths than those observed experimentally (1310 ± 34 MPa).

It is worth noting that it is a well-accepted fact that the theoretical models produce reasonably accurate results for predicting the elastic modulus of composites of aerospace-grade composites. In contrast, they fall short of producing accurate results for predicting the strength of composites. It should be noted that a majority of these models were developed mainly commissioned by the aerospace industry.

Additionally, their integrities were verified through experimental results obtained using aerospace-grade (autoclaved) composites. Such composites are mainly fabricated using prepreg, where fibers are uniformly distributed and precisely aligned, with minimal voids in their host matrices due to the application of continuous uniform pressure and vacuum used by Plappert et al. [113]. They used BFRP prepregs in that investigation, and the panels were fabricated using an autoclave (i.e., resin cured at high temperature, under vacuum and highly consolidated conditions). Therefore, due to precise fiber alignment

and lack of any voids and optimal consolation condition, the panel generated produces optimal mechanical properties compared to the panels fabricated by resin infusion technique, using dry fabric and a room-cured resin. However, the fibers in hand-laid composites are not as uniformly and precisely distributed in the matrix. Moreover, minimizing void content would be impossible in such a fabrication method. These factors cause predictions with lower accuracies in comparison to the aerospace-grade composites.

The compressive properties of the basalt-epoxy composite were also evaluated using the RoM, BoF, and CLPT methods. The compressive strength ($\sigma_{1,\,Compress.}$) calculated using BoF was 354.2 MPa, while the RoM and CLPT - Simplified method provided a higher value of 504.9 MPa. The Military Handbook alternative approach yielded a compressive strength of 427.1 MPa. Plappert et al. [113] reported an experimentally evaluated compressive strength of 776 ± 25 MPa. These values indicate a difference between the theoretical and experimental values, suggesting that the calculated methods may underestimate the compressive performance; hence, they are safe to use for the preliminary prediction of material properties.

Moreover, additional compressive experiments were performed on basalt-epoxy composite. Coupons were fabricated with unidirectional fibers to further probe the results obtained through theoretical models and literature review. The experimentally evaluated compressive modulus was found to be 39.1 GPa, which closely aligns with the calculated values and those reported in the literature. However, the compressive strength was observed to be 215.2 MPa, significantly lower than anticipated. This discrepancy is believed to be due to several factors. Due to the unavailability of uniaxial basalt fabric, the transverse fibers of the cross-ply fabric were painstakingly removed to generate the uniaxial test specimens, which were constructed using 18 plies.

Naturally, the fibers in the resulting uniaxial fabric were not uniformly distributed due to the fact that the stitched threads holding the cross-ply fabric had to be removed. This process left a fabric that was partially disturbed despite our uttermost effort. In addition, the resulting uniaxial fabric was somewhat wavy due to the removal of the transverse

fibers. These factors resulted in specimens with a lower fiber volume fraction, imprecise fiber alignment and nonuniform fiber distribution. In addition, the numerous fabric titches had to be removed by burning them with a butane torch. The flame could also have affected the fibre sizing, reducing the fiber/matrix interfacial strength and thereby affecting the composite's strength.

The author deduces that the method used by Halpin-Tsai overestimates the shear modulus by more than 300 %, resulting in a value of 9.3 GPa for the in-plane shear, whereas Hahn's model somewhat overestimates the modulus, yielding a value of 3.9 GPa. It should be noted that all the models noted in this thesis have been tested against aerospace-grade composites. The Hahn's model value is very close to the experimentally obtained value of 3.73 ± 0.29 GPa reported by Plappert et al. [113]. As stated earlier, they used prepreg and autoclave processing technique, producing highly consolidated and consistent composite. On the other hand, the shear modulus value of 2.2 GPa, obtained using the model derived based on the theory of elasticity, better agrees with our experimentally obtained value of 2.6 GPa (see section 5.5).

Table 5-8 compares the analytically calculated and experimentally evaluated values for the basalt-epoxy. Figure 5-10 and Figure 5-11 show the visual plots of the unidirectional compression tests and the post-failure images of the coupons, respectively.

Table 5-8: Comparison of basalt-epoxy composite's experimental and analytically calculated tensile and compressive properties.

Back-Out Factor (BoF) =	1.5						
Type	**Elastic Moduli (E_1)**		**Strength (σ)**				**Shear Modulus (G)**
Tensile	**$E_{1, Calc. - RoM}$** (GPa)	**$E_{2, Calc. - H-Tsai}$** (GPa)	-	**$\sigma_{1, Calc. - BoF}$** (MPa)	**$\sigma_{1, Calc. - Simplified RoM and CLPT}$** (MPa)	**$\sigma_{1, Calc. - Mil Alter.}$** (MPa)	**$G_{12, Calc, Elastic Soln.n}$** (GPa)
	43.8	11.9	-	703.1	1002.2	923.9	2.2
Compressive	**$E_{1, Exp.}$** (GPa)	**$E_{1, Calc. – BoF}$** (GPa)	**$\sigma_{1, Exp.}$** (MPa)	**$\sigma_{1, Calc. - BoF}$** (MPa)	**$\sigma_{1, Calc. - Simplified RoM and CLPT}$** (MPa)	**$\sigma_{1, Calc. - Mil Alter.}$** (MPa)	$G_{12, Experimental}$ (GPa)
	39.1	43.2	174.8	354.5	504.9	427.1	2.6

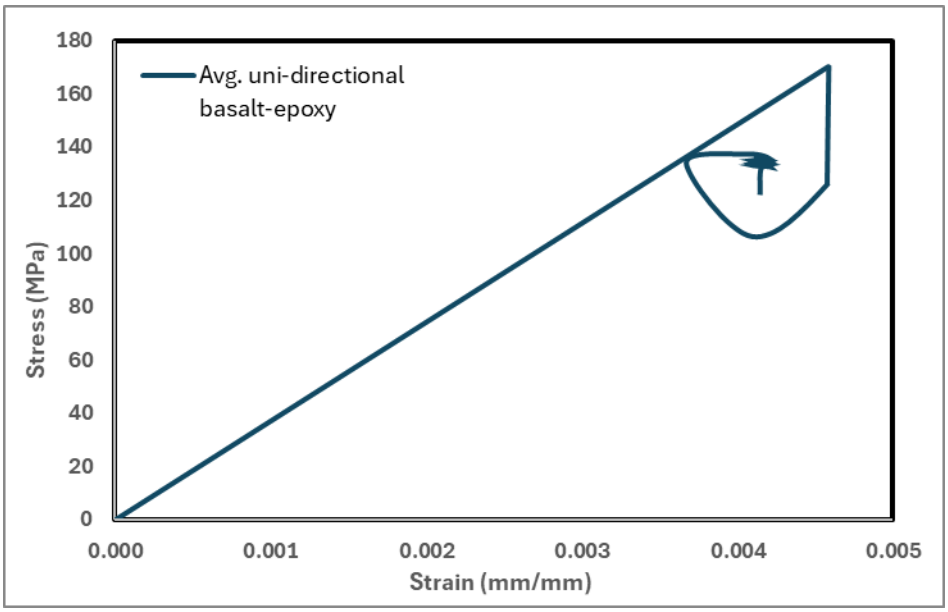

Figure 5-10: Avg. compressive stress-strain curve of unidirectional basalt-epoxy composite.

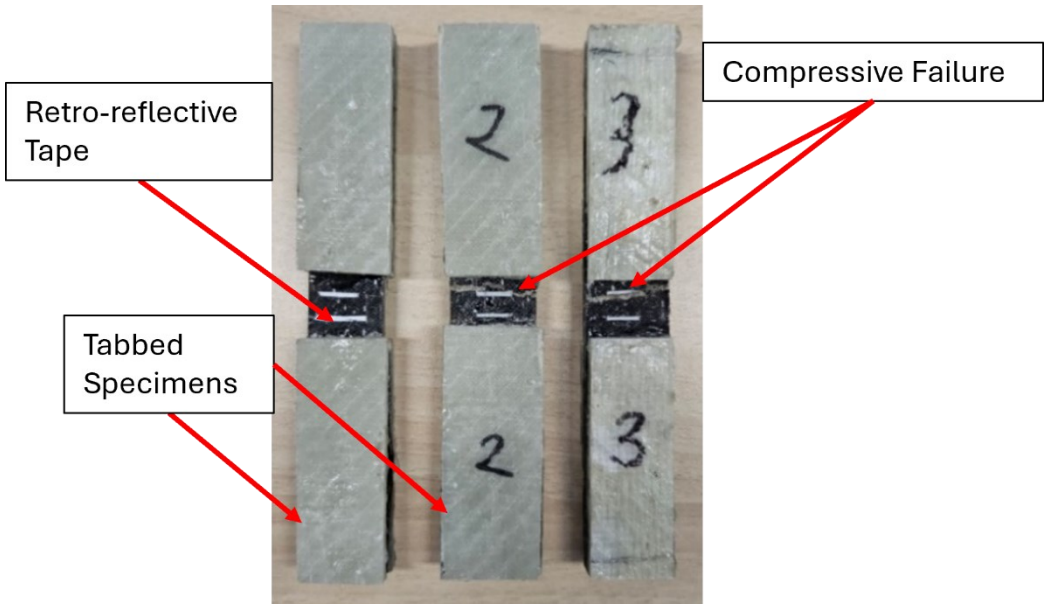

Figure 5-11: Post-compression failure images of the unidirectional basalt-epoxy composite specimens.

A similar analysis was conducted for basalt-Recyclamine. The longitudinal elastic modulus (E_1) calculated using the Rule of Mixtures (RoM) was 41.4 GPa. The transverse elastic modulus (E_2) computed using the Halpin-Tsai model was 12.2 GPa. The tensile strength calculated using the Back-out Factor (BoF) was 575.3 MPa. Additionally, using the Simplified RoM and Classic Lamination Plate Theory (CLPT), the tensile strength was calculated to be 813.1 MPa, and the Military Alternative Approach yielded a value of

798.7 MPa. These theoretical models predict conservative tensile strengths compared to the experimental results of epoxy-based basalt fiber.

The compressive properties of the basalt-Recyclamine composite were also evaluated through experimental and theoretical approaches. The compressive modulus calculated using the BoF method was 48.3 GPa, slightly higher than the experimental values reported by Plappert et al. [113]. The compressive strength calculated using the BoF was 349.8 MPa, while the Simplified RoM and CLPT methods provided a value of 494.5 MPa. The Military Alternative Approach yielded a compressive strength of 357.4 MPa. Similar to the tensile properties, the calculated compressive strengths are generally lower than the experimental values. Lastly the analysis of shear modulus was similar to that of basalt-epoxy and was found to be 2.4 GPa using the elastic solution and the experimental result is 2.6 GPa. Table 5-9 shows a summary of the basalt-Recyclamine analytical and experimental values for ease of comparison.

Table 5-9: Comparison of the experimental and analytically calculated tensile and compressive properties of basalt-Recyclamine composite.

Back-Out Factor (BoF) = 1.5						
Type	**Elastic Moduli (E)**		**Strength (σ)**			**Shear Modulus (G)**
Tensile	**$E_{1, Calc. - RoM}$** (GPa)	**$E_{2, Calc., - H-Tsai}$** (GPa)	**$\sigma_{1, Calc. - BoF}$** (MPa)	**$\sigma_{1, Calc. - Simplified RoM and CLPT}$** (MPa)	**$\sigma_{1, Calc. - Mil Alter.}$** (MPa)	**$G_{12, Calc, Elastic Soln.n}$** (GPa)
	41.4	12.2	575.3	813.1	798.7	2.4
Compressive	**$E_{1, Calc. - BoF}$** (GPa)	-	**$\sigma_{1, Calc. - BoF}$** (MPa)	**$\sigma_{1, Calc. - Simplified RoM and CLPT}$** (MPa)	**$\sigma_{1, Calc. - Mil Alter.}$** (MPa)	$G_{12, Experimental}$ (GPa)
	48.3	-	349.8	494.5	357.4	2.6

The experimental and analytical values validated the applicability of the back-out factor approach and its simplification using micromechanics; these two yielded good results in finding the modulus and strength of the composites, giving conservative values in both cases.

5.8 SEM AND DIGITAL MICROSCOPE ANALYSIS

The resin system's SEM was analyzed in terms of their resin matrices and fiber reinforcement to understand the fiber–resin interaction. Figure 5-12 and Figure 5-13 show the images generated by the SEM of impacted specimens of both epoxy and Recyclamine composites, respectively, with a magnification of 65 times.

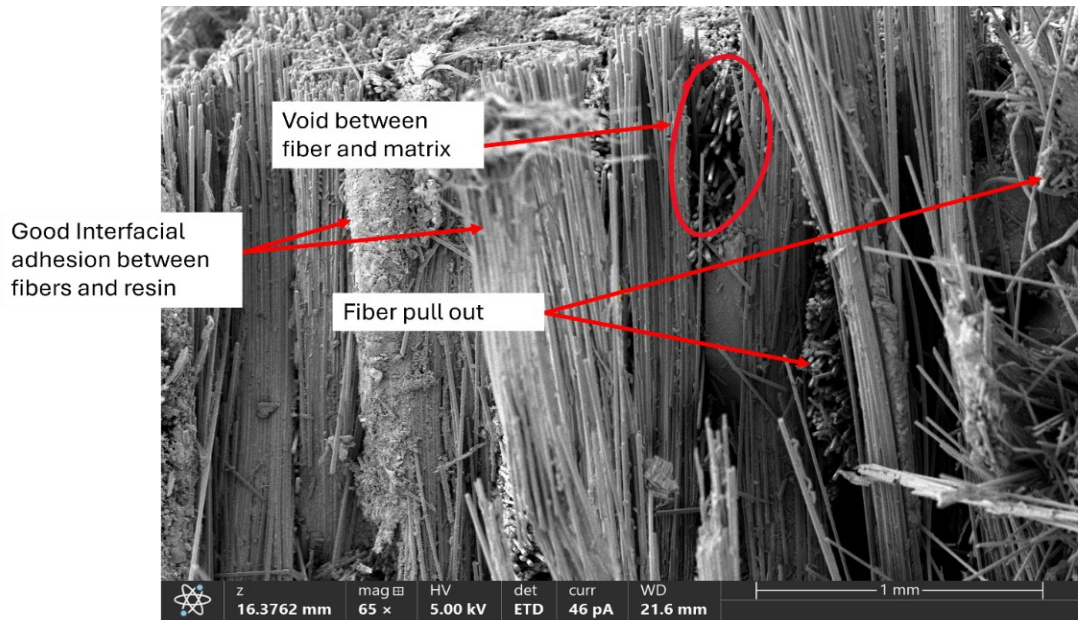

Figure 5-12: SEM image of fractured basalt-epoxy specimen (×65).

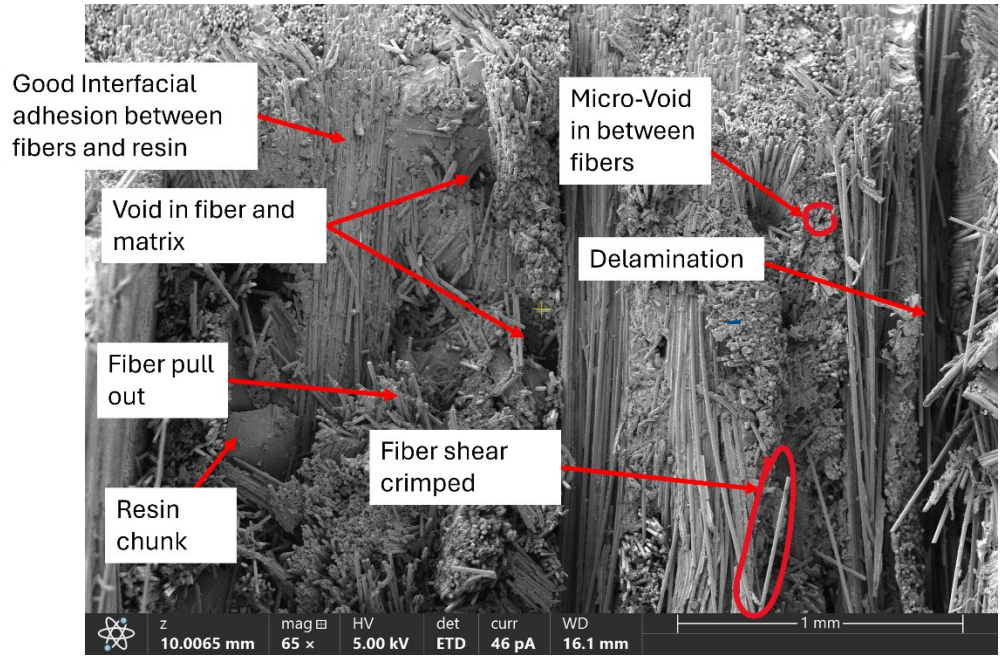

Figure 5-13: SEM image of fractured basalt-Recyclamine specimen (×65).

The SEM images reveal important details about the microstructures of basalt-epoxy and basalt-Recyclamine composites. The good interfacial adhesion between the fibers and resin is evident in both specimens, facilitating effective load transfer. However, there are a noticeable number of voids in the specimen, which can act as stress concentrators and potentially lead to cracks. The image also shows fiber pull-out, where fibers are extracted from the matrix under stress, a common failure mode in composites.

A similar trend is also seen in basalt-Recyclamine specimens. The voids indicate areas where the resin did not fully penetrate, weakening the composite structure. Additionally, the presence of resin chunks suggests incomplete resin flow or curing during fabrication.

The basalt-epoxy composite shows somewhat better interfacial adhesion but suffers from voids and fiber pull-out. In contrast, the basalt-Recyclamine composite has issues with voids, fiber misalignment, and resin chunks. These defects can significantly impact the mechanical properties of the composites.

Figure 5-14 illustrates the microscopic images of the failure mechanisms of the two composites under various loading states. As shown in Figure 5-14(a), the prominent failure mode is by fiber breakage in the two composites under a tensile loading state. Additionally, fiber pull-out is visible in both composites but is more prominent in the basalt-Recyclamine specimen, indicating that fiber-matrix debonding was a factor for the Recyclamine composite.

Under compressive loading, the basalt-epoxy composite shows micro-buckling and less fiber pull-out, indicating a stronger fiber-matrix bond but leading to a more brittle failure as evident in Figure 5-14(b). In contrast, the basalt-Recyclamine composite exhibits fiber pull-out, suggesting a weaker fiber-matrix bond but allowing for a more ductile failure with greater energy absorption. Moreover, the basalt-epoxy showed an interesting surface morphology. The analysis reveals fiber buckling at the skin, fiber shearing, delamination in the mid-plane, and fiber crushing/pull-out near the surface. These failures indicate localized compressive stress, matrix-fiber interface failure, and continued load-bearing by some fibers.

As seen in Figure 5-14(c), under bending, the basalt-epoxy composite displayed failure in the bottom surface, which was subjected to compressive stress, including delamination and matrix cracking. Likewise, the basalt-Recyclamine composite also shows compression failure with delamination and matrix cracking and ultimately fails on the compression side, accompanied by fiber shearing.

Figure 5-14(d) shows the failure modes under pure shear. Matrix shear cracking, delamination, and fiber breakage is evident in the basalt-epoxy specimen. In contrast, in the basalt-Recyclamine composite, fiber pull-out mode replaces fiber breakage mode seen in its counterpart, suggesting a weak fiber-matrix bond and greater energy absorption before failure.

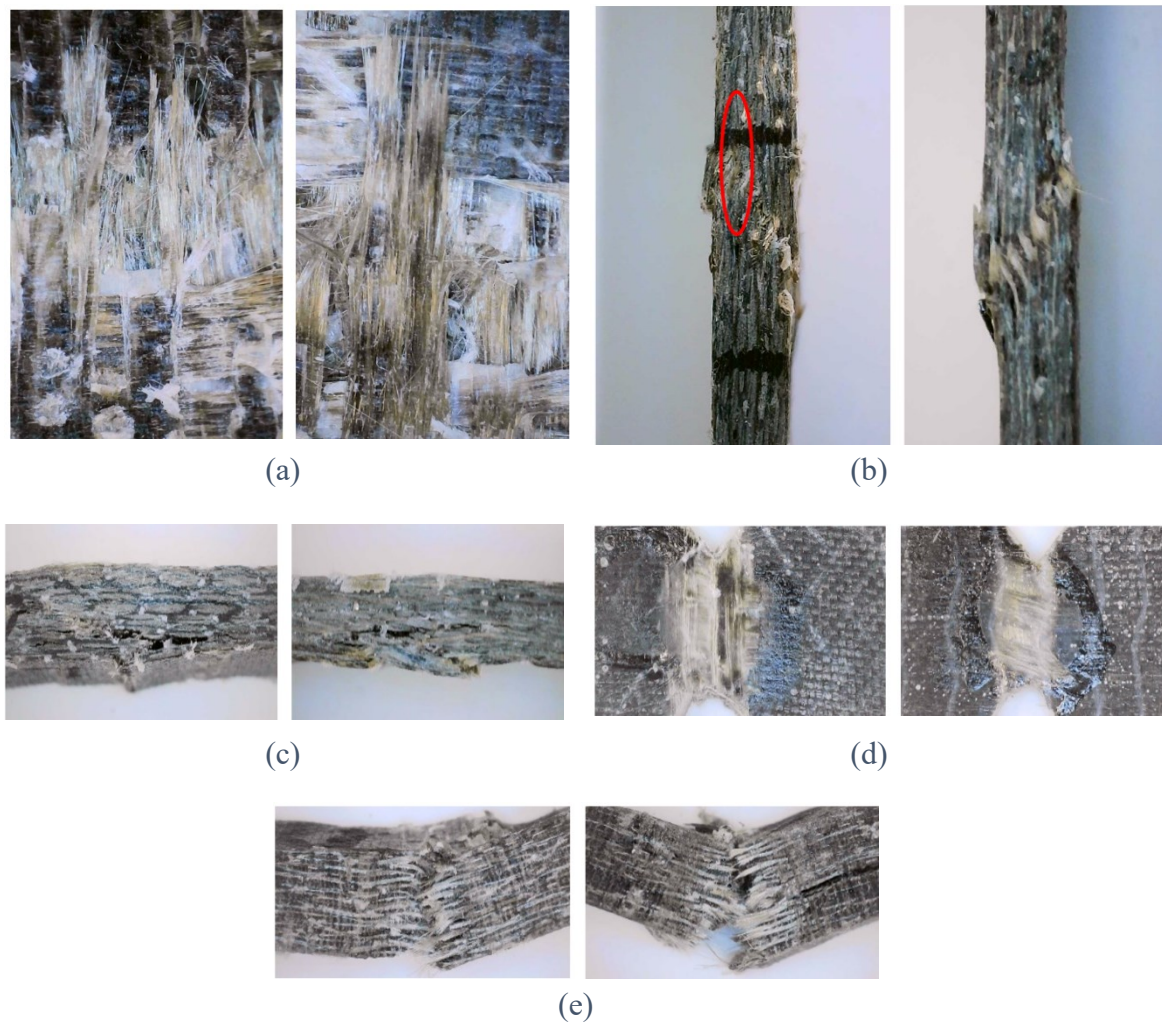

Figure 5-14: Microscopic images failure modes of basalt-epoxy (left) and basalt-Recyclamine (right) subjected to (a) tensile, (b) compression, (c) flexural, (d) shear, and (e) impact.

The failure mode under impact loading in basalt-epoxy composite was a combination of fiber breakage, matrix cracking, and some delamination, indicating a strong but brittle failure (see Figure 5-14(e)). In contrast, the basalt-Recyclamine composite exhibits fiber pull-out, matrix cracking, and delamination, suggesting a weaker bond but greater energy absorption and a more ductile failure mode.

5.9 Applicability of Basalt-Recyclamine Composites in Automotive Industry

Basalt-Recyclamine presents significant potential for industrial applications, especially within the automotive industry. For instance, Basfiber is a leading company in the production of basalt composites in various industrial applications. It claims that basalt has substantial advantages over traditional glass fibers, such as 20-25% higher tensile strength, 10-15% higher tensile modulus, and a 150°C higher melting point. Additionally, basalt fibers exhibit superior resistance to acids, corrosion, and alkalis, far exceeding the performance of glass fibers and offering a significant advantage over metals typically used in automotive applications. This corrosion resistance also eliminates the need for additional protective coatings or treatments reducing costs in the life cycle of composites [165].

In the automotive industry, basalt fiber composites are increasingly used to manufacture many car parts. These include external components such as bumpers, underbodies, hoods, fairings, spoilers, and interior elements like decorative panels and body protection parts. Basalt fibers are also used in thermal and sound insulation materials for vehicle interiors, engines, and exhaust silencers, improving passenger comfort and vehicle performance. Moreover, basalt fiber composites are employed in special applications like brake pads, friction discs, engine gaskets, and exhaust catalysts, where their high strength, thermal stability, and wear resistance provide significant benefits [166].

Several automotive components currently made from traditional materials could potentially be replaced with basalt-Recyclamine composites. These include body parts, engine gaskets, brake pads, friction discs, and exhaust catalysts. The manufacturing methods suitable for these replacements include vacuum molding for large structural

components, injection molding for precision parts, filament winding for cylinders for automotive use and wet lay-up for custom shapes and designs. The integration of Recyclamine® technology allows these components to maintain high performance standards while offering the added benefit of recyclability, contributing to a more sustainable and environmentally friendly automotive industry [167].

The manufacturing of basalt fiber-based automotive parts involves several advanced techniques. For example, BCF (Basalt Continuous Fiber) chopped strand mats and basalt fabrics impregnated with binders are used in vacuum molding to mass-produce complex-shaped composite parts such as bumpers and car bodies. This method, along with others such as injection molding, cold stamping, spraying, drawing and hand lay-up processes, allows for the efficient production of durable, high-performance components [168]. The incorporation of Recyclamine® technology in these processes can significantly enhance the performance of the composites and ensure that the final products are fully recyclable, aligning with the automotive industry's increasing focus on sustainability and environmental responsibility. Figure 5-15 showcases a car in Germany Engineering Bureau entirely made of entirely basalt fiber composite to show the potential of basalt fiber in the automotive industry.

Figure 5-15: Car body entirely made of basalt-composite fiber [167].

5.10 COST ANALYSIS

The cost analysis comparing basalt fiber and E-glass shows the potential for basalt to be more widely adopted as a reinforcement material in structural composites. Basalt fibers

are recognized for their performance, such as high tensile strength, good thermal stability, enhanced chemical resistance and offer significant advantages over E-glass. Although the manufacturing process for basalt fibers is generally more efficient, requiring less energy and no secondary additives, the prime cost to manufacture E-glass is 1.0-1.4 USD/kg and basalt is 0.8-1.2 USD/kg [167]. The commercial price of basalt fibers remains slightly higher due to current production scales and market dynamics where the cost of E-glass is 1.2-2.0 USD/kg and basalt is 2-3 USD/kg. The commercial price of E-glass makes their composites the most cost-effective option currently available. When combined with epoxy resin, which typically costs around $49.35 USD per kilogram, the overall cost for basalt epoxy composites is higher than E-glass composites but justified by basalt's superior mechanical properties and resistance to high temperatures and corrosive environments where these performance attributes are critical. As production scales up and becomes more efficient, the cost of basalt composites is expected to decrease, potentially making them competitive with E-glass in more markets [169].

The introduction of Recyclamine enables full recyclability of composites. The exact price of Recyclamine resin is not specified, but it is expected to be similar to or slightly higher than the epoxy used in basalt composites. However, long-term savings and environmental benefits offset this increase, such as reduced disposal costs and material recovery at the end of the product’s lifecycle. The cost of basalt-Recyclamine composites is expected to be similar to or slightly higher than traditional basalt epoxy composites, but the sustainable advantages make it a compelling choice for industries focusing on reducing environmental impact and meeting sustainable development goals (SDG).

Moreover, the cost of basalt fiber composites will likely decrease as larger production facilities are established, and new manufacturing techniques are adopted [170]. These advancements could make basalt composites more cost-competitive with E-glass, particularly when considering their superior performance and sustainability. The convergence in manufacturing costs between basalt and E-glass suggests that basalt fiber could soon become a potential alternative for a broader range of applications, especially in industries that prioritize durability, performance, and environmental responsibility.

CHAPTER 6 CONCLUSION AND RECOMMENDATIONS FOR FUTURE RESEARCH

Numerous research studies have established that basalt-epoxy-based composite performs similarly or even better than E-glass-epoxy [99,113,113,171–173]. However, the recent advancement in resin chemistry has created fully recyclable epoxy resins. One such resin is Recyclamine. To the author's knowledge, no investigation has been conducted to characterize the performance of basalt, a mineral-based fiber with abundant base resources embedded in Recyclamine. Therefore, the main goal of this research was to characterize the mechanical performance of basalt-reinforced Recyclamine and compare its performance against the widely used E-glass epoxy, which is also considered the most cost-effective composite. The research focused on characterizing the composites' tensile, compression, flexural, shear and impact properties. This study aimed to enhance the limited mechanical response database available for Recyclamine-based composites with basalt fiber reinforcements. As stated, basalt is an eco-friendly fiber that, when combined with Recyclamine, a recyclable thermoset resin, offers a cost-effective and environmentally friendly composite material with excellent mechanical properties suitable for structural applications. The composites were fabricated using (Vacuum Assisted Resin Infusion Moulding (VARIM) and according to ASTM standards.

Additionally, various micromechanical approaches were incorporated to determine their applicability in predicting the basic mechanical properties of such composites.

6.1 CONCLUSIONS

The following conclusions are drawn based on the results obtained in the investigation:

- Tensile Properties: Basalt-epoxy composites exhibited a higher average maximum tensile stress of 464 MPa compared to 390.9 MPa for basalt-Recyclamine composites. The higher tensile strength of the basalt-epoxy composite can be attributed to the rigidity of the epoxy matrix, which provides higher stiffness and better load-bearing capacity. However, the ductile nature of the Recyclamine matrix in basalt-

Recyclamine composites allows for better energy absorption and distribution under stress, contributing to a different mechanical performance profile.

- Compression Properties: Basalt-Recyclamine composites demonstrated superior performance in compression tests, with an average maximum compressive stress of 237.7 MPa and a compressive modulus of 27.5 GPa. This improved performance is due to the ductile nature of the Recyclamine matrix, which enhances load distribution and energy absorption, preventing premature failure. Basalt-epoxy composites had an average maximum compressive stress of 233.9 MPa and a compressive modulus of 24.0 GPa. The rigidity of the epoxy matrix aids in maintaining fiber alignment under compressive loads, but its brittle nature can lead to less effective energy absorption than the Recyclamine matrix.
- Flexural Properties: Basalt-epoxy composites showed higher flexural strength, with an average maximum flexural stress of 441.4 MPa and a flexural modulus of 21.9 GPa. The stiffness of the epoxy matrix supports the fibers effectively under bending loads. Basalt-Recyclamine composites, while exhibiting a lower average maximum flexural stress of 372.1 MPa, demonstrated a higher flexural modulus of 23.4 GPa due to the Recyclamine matrix's ductile nature, allowing for more uniform stress distribution.
- Shear Properties: Basalt-Recyclamine composites outperformed basalt-epoxy composites regarding shear strength and modulus, with an average maximum shear stress of 52.78 MPa and a shear modulus of 2.9 GPa. The superior interfacial bonding and ductility of the Recyclamine matrix contribute to better load transfer and resistance to shear forces. Basalt-epoxy composites exhibited an average maximum shear stress of 42.59 MPa and a shear modulus of 2.6 GPa.
- Impact Resistance: While basalt-epoxy composites showed a slightly higher average impact resistance of 1,639 J/m compared to 1,595 J/m for basalt-Recyclamine composites, the latter demonstrated more consistent performance under impact conditions. The ductile nature of Recyclamine aids in absorbing and distributing impact energy more uniformly, reducing the likelihood of catastrophic failure.
- Micromechanics Analyses: The micromechanics analysis of basalt-epoxy and basalt-Recyclamine composites utilized approaches like the Rule of Mixtures (RoM),

Halpin-Tsai models, and the Back-Out Factor (BoF) to verify the tensile and compressive moduli and strengths. The longitudinal and transverse elastic moduli for basalt-epoxy matched literature values, with calculated moduli of 43.8 GPa (E_1) and 11.9 MPa (E_2). Tensile strengths varied in different approaches. Compressive strengths were similarly calculated and validated. For basalt-Recyclamine, RoM calculated a longitudinal modulus of 41.4 GPa and a transverse modulus of 12.2 MPa. Tensile and compressive strengths were also calculated and compared.

- SEM Analysis: The SEM analysis provided insights into the microstructural characteristics of the composites. Basalt-epoxy showed good interfacial adhesion but had voids and fiber pull-out issues. In contrast, basalt-Recyclamine exhibited micro-voids, fiber strand misalignment, and resin chunks, which could impact mechanical performance. These microstructural differences explain the variations in mechanical properties observed during testing. The digital microscope analyses provided detailed insights into the microstructural behaviour of the composites. The analyses revealed that basalt-epoxy composites exhibited a more uniform fiber distribution with fewer voids, contributing to their higher tensile strength. In contrast, the basalt-Recyclamine composites displayed better fibre-matrix adhesion and less micro-cracking, which enhances their compressive strength and ductility. Digital microscope images also showed that the basalt-Recyclamine composites had smoother fracture surfaces, indicating better energy absorption and distribution capabilities.

6.2 FUTURE RECOMMENDATIONS

Using basalt fibers with Recyclamine resin shows great promise for creating sustainable, high-performance and cost-effective composites; however, more research is needed to realize their potential fully. One key area is environmental testing. Future studies should evaluate how these composites perform under extreme temperatures and varying humidity levels, which is crucial for aerospace, automotive, and marine applications. Additionally, the combined effects of moisture and temperature on the mechanical properties of Recyclamine composites need to be studied, including evaluating their performance under fluctuating environmental conditions.

Long-term durability is another important focus. Research should investigate the aging and degradation of basalt-Recyclamine composites, especially their resistance to ultraviolet radiation and environmental wear. Additionally, it is believed that only three studies have considered the incorporation of recycled Recyclamine resin. More studies are needed to understand how multiple recycling processes affect the material's properties and performance.

Exploring different fiber orientations and stacking sequences can optimize the composite design for specific applications. While this study used a [0/90] stacking sequence, future research should look into other configurations like quasi-isotropic layups. This could improve performance in shear and impact tests, offering better-tailored solutions for various engineering challenges.

Fatigue testing is crucial to understand how these composites perform under cyclic loading conditions. This is particularly relevant for transportation and infrastructure applications where materials are continually stressed. Research should focus on the fracture and fatigue behaviour of basalt-Recyclamine composites to design more durable and reliable materials.

In addition to the abovementioned recommendation, further research into the composites' joints is essential. Bolted joints are important in engineering applications due to their load-bearing capacity and ease of assembly. Studies on carbon/basalt hybrid composites have shown that incorporating basalt layers can enhance mechanical performance and cost efficiency in bolted joints [174]. Similarly, investigating the performance of basalt-Recyclamine composites under bolted conditions could provide valuable insights into their structural applications, ensuring they meet the demands of industries requiring durable and reliable mechanical connections.

By addressing these areas, future research can unlock the full potential of basalt-Recyclamine composites, enhancing their applicability in diverse industries.

BIBLIOGRAPHY

[1] A. Wazeer, A. Das, C. Abeykoon, A. Sinha, A. Karmakar, Composites for electric vehicles and automotive sector: A review, Green Energy and Intelligent Transportation 2 (2023) 100043. https://doi.org/10.1016/j.geits.2022.100043.

[2] A. Zaman, S.A. Gutub, M.A. Wafa, A review on FRP composites applications and durability concerns in the construction sector, Journal of Reinforced Plastics and Composites 32 (2013) 1966–1988. https://doi.org/10.1177/0731684413492868.

[3] C.E. Bakis, L.C. Bank, V.L. Brown, E. Cosenza, J.F. Davalos, J.J. Lesko, A. Machida, S.H. Rizkalla, T.C. Triantafillou, Fiber-Reinforced Polymer Composites for Construction—State-of-the-Art Review, J. Compos. Constr. 6 (2002) 73–87. https://doi.org/10.1061/(ASCE)1090-0268(2002)6:2(73).

[4] D.K. Rajak, D.D. Pagar, P.L. Menezes, E. Linul, Fiber-Reinforced Polymer Composites: Manufacturing, Properties, and Applications, Polymers (Basel) 11 (2019) 1667. https://doi.org/10.3390/polym11101667.

[5] S. Halliwell, FRPs — The Environmental Agenda, Advances in Structural Engineering 13 (2010) 783–791. https://doi.org/10.1260/1369-4332.13.5.783.

[6] D.S. Bajwa, S. Bhattacharjee, Current Progress, Trends and Challenges in the Application of Biofiber Composites by Automotive Industry, Journal of Natural Fibers 13 (2016) 660–669. https://doi.org/10.1080/15440478.2015.1102790.

[7] C. Baley, A. Bourmaud, P. Davies, Eighty years of composites reinforced by flax fibres: A historical review, Composites Part A: Applied Science and Manufacturing 144 (2021) 106333. https://doi.org/10.1016/j.compositesa.2021.106333.

[8] F.M. AL-Oqla, S.M. Sapuan, M. Jawaid, Integrated Mechanical-Economic–Environmental Quality of Performance for Natural Fibers for Polymeric-Based Composite Materials, Journal of Natural Fibers 13 (2016) 651–659. https://doi.org/10.1080/15440478.2015.1102789.

[9] J. Liu, S. Wang, Y. Peng, J. Zhu, W. Zhao, X. Liu, Advances in sustainable thermosetting resins: From renewable feedstock to high performance and recyclability, Progress in Polymer Science 113 (2021) 101353. https://doi.org/10.1016/j.progpolymsci.2020.101353.

[10] R. Brooks, S.M. Shanmuga Ramanan, S. Arun, Composites in Automotive Applications: Design, in: Reference Module in Materials Science and Materials Engineering, Elsevier, 2017. https://doi.org/10.1016/B978-0-12-803581-8.03961-8.

[11] 2014-volkswagen-xl1-carbon-fiber-body-parts.jpg (1500×938), (n.d.). https://belauto.com.my/wp-content/uploads/2014/12/2014-volkswagen-xl1-carbon-fiber-body-parts.jpg (accessed April 21, 2024).

[12] K. Bielefeldt, J. Walkowiak, W. Papacz, Composites and Reinforced Plastics in the Automotive Industry, Applied Mechanics and Materials 611 (2014) 352–357. https://doi.org/10.4028/www.scientific.net/AMM.611.352.

[13] H. Adam, Carbon fibre in automotive applications, Materials & Design 18 (1997) 349–355. https://doi.org/10.1016/S0261-3069(97)00076-9.

[14] D.K. Rajak, P.H. Wagh, E. Linul, A Review on Synthetic Fibers for Polymer Matrix Composites: Performance, Failure Modes and Applications, Materials 15 (2022) 4790. https://doi.org/10.3390/ma15144790.

[15] T. Sathishkumar, J. Naveen, S. Satheeshkumar, Hybrid fiber reinforced polymer composites – a review, Journal of Reinforced Plastics and Composites 33 (2014) 454–471. https://doi.org/10.1177/0731684413516393.

[16] FRPs — The Environmental Agenda, (n.d.). https://journals-sagepub-com.ezproxy.library.dal.ca/doi/epdf/10.1260/1369-4332.13.5.783 (accessed February 7, 2024).

[17] A. Ragothaman, W. Anderson, Air Quality Impacts of Petroleum Refining and Petrochemical Industries, in: Environments, 2017: p. 66. https://doi.org/10.3390/environments4030066.

[18] R. Hao, S. Xue, H. Sun, T. Yang, H. Wang, Emission Characteristics and the Environmental Impact of VOCs from Typical FRP Manufacture Industry, Atmosphere 13 (2022) 1274. https://doi.org/10.3390/atmos13081274.

[19] S. RameshKumar, P. Shaiju, K.E. O'Connor, R.B. P, Bio-based and biodegradable polymers - State-of-the-art, challenges and emerging trends, Current Opinion in Green and Sustainable Chemistry 21 (2020) 75–81. https://doi.org/10.1016/j.cogsc.2019.12.005.

[20] volatile-organic-compounds.pdf, (n.d.). https://www.canada.ca/content/dam/hc-sc/documents/services/air-quality/indoor-air-contaminants/volatile-organic-compounds/volatile-organic-compounds.pdf (accessed March 26, 2024).

[21] Contact us via LiveChat!, (n.d.). https://secure.livechatinc.com/ (accessed August 27, 2024).

[22] V. Kočí, E. Picková, Life Cycle Perspective of Liquid Epoxy ResinUse in the Automotive Industry, Pol. J. Environ. Stud. 29 (2019) 653–667. https://doi.org/10.15244/pjoes/100495.

[23] The looming 840,000 ton waste problem that isn't single-use plastics, ScienceDaily (n.d.). https://www.sciencedaily.com/releases/2023/07/230703133034.htm (accessed March 26, 2024).

[24] M. Rovinaru, A. Rus, The Economic and Ecological Impacts of Dismantling End-of-Life Vehicles in Romania, Sustainability 11 (2019) 6446. https://doi.org/10.3390/su11226446.

[25] V. Lebrun, A. Kheffi, M. Gohy, R. Fafchamps, C. Collart, C. Maquinay, LANDFILL GAS (LFG) FUGITIVE EMISSIONS ON LANDFILL SURFACE - COMPARATIVE TEST OF ON SITE ANALYSIS DEVICES, (2007).

[26] Waste Law - an overview | ScienceDirect Topics, (n.d.). https://www.sciencedirect.com/topics/social-sciences/waste-law (accessed March 26, 2024).

[27] A.E. Krauklis, C.W. Karl, A.I. Gagani, J.K. Jørgensen, Composite Material Recycling Technology—State-of-the-Art and Sustainable Development for the 2020s, Journal of Composites Science 5 (2021) 28. https://doi.org/10.3390/jcs5010028.

[28] J. Li, K. Yu, P. Gao, Recycling and pollution control of the End of Life Vehicles in China, J Mater Cycles Waste Manag 16 (2014) 31–38. https://doi.org/10.1007/s10163-013-0226-6.

[29] Waste Framework Directive - European Commission, (n.d.). https://environment.ec.europa.eu/topics/waste-and-recycling/waste-framework-directive_en (accessed March 26, 2024).

[30] Commission Directive (EU) 2017/2096 of 15 November 2017 amending Annex II to Directive 2000/53/EC of the European Parliament and of the Council on end-of life vehicles (Text with EEA relevance.), 2017. http://data.europa.eu/eli/dir/2017/2096/oj/eng (accessed March 26, 2024).

[31] A. uz Zaman, S.A. Gutub, M.F. Soliman, M.A. Wafa, Sustainability and human health issues pertinent to fibre reinforced polymer composites usage: A review, Journal of Reinforced Plastics and Composites 33 (2014) 1069–1084. https://doi.org/10.1177/0731684414521087.

[32] S. Sakai, H. Yoshida, J. Hiratsuka, C. Vandecasteele, R. Kohlmeyer, V.S. Rotter, F. Passarini, A. Santini, M. Peeler, J. Li, G.-J. Oh, N.K. Chi, L. Bastian, S. Moore, N. Kajiwara, H. Takigami, T. Itai, S. Takahashi, S. Tanabe, K. Tomoda, T. Hirakawa, Y. Hirai, M. Asari, J. Yano, An international comparative study of end-of-life vehicle (ELV) recycling systems, J Mater Cycles Waste Manag 16 (2014) 1–20. https://doi.org/10.1007/s10163-013-0173-2.

[33] Tushar Sonar, S. Patil, V. Deshmukh, R. Acharya, Natural Fiber Reinforced Polymer Composite Material-A Review, (2015).

[34] P.P. Bijlwan, L. Prasad, A. Sharma, Recent advancement in the fabrication and characterization of natural fiber reinforced composite: A review, Materials Today: Proceedings 44 (2021) 1718–1722.

[35] M.J. Mochane, T.C. Mokhena, T.H. Mokhothu, A. Mtibe, E.R. Sadiku, S.S. Ray, I.D. Ibrahim, O.O. Daramola, Recent progress on natural fiber hybrid composites for advanced applications: A review, Express Polymer Letters 13 (2019) 159–198.

[36] D. Saber, A.H. Abdelnaby, Recent Developments in Natural Fiber as Reinforcement in Polymeric Composites: A Review, Asian Journal of Applied Science and Technology 06 (2022) 56–75.

[37] K.N. Keya, N.A. Kona, F.A. Koly, K.M. Maraz, Md.N. Islam, R.A. Khan, Natural fiber reinforced polymer composites: history, types, advantages, and applications, Materials Engineering Research 1 (2019) 69–87.

[38] S. Abuthakeer, R. Vasudaa, A. Nizamudeen, Application of Natural Fiber Composites in Engineering Industries: A Comparative Study, Applied Mechanics and Materials 854 (2016) 59–64. https://doi.org/10.4028/www.scientific.net/AMM.854.59.

[39] L. Mohammed, M.N.M. Ansari, G. Pua, M. Jawaid, M.S. Islam, A Review on Natural Fiber Reinforced Polymer Composite and Its Applications, International Journal of Polymer Science 2015 (2015) e243947. https://doi.org/10.1155/2015/243947.

[40] O. Faruk, A.K. Bledzki, H.-P. Fink, M. Sain, Progress Report on Natural Fiber Reinforced Composites, Macromolecular Materials and Engineering 299 (2014) 9–26. https://doi.org/10.1002/mame.201300008.

[41] R. Vinayagamoorthy, A review on the polymeric laminates reinforced with natural fibers, Journal of Reinforced Plastics and Composites 36 (2017) 1577–1589. https://doi.org/10.1177/0731684417718385.

[42] Plastic Market Size, Share, Trends & Growth Report, 2030, (n.d.). https://www.grandviewresearch.com/industry-analysis/global-plastics-market (accessed April 9, 2024).

[43] M. Cagrı Uyanik, A. Tamer Erturk, Recent Developments of Natural Fibres: Natural Fibre Biocomposites, Treatments, and Characterizations, J. Phys.: Conf. Ser. 2549 (2023) 012001. https://doi.org/10.1088/1742-6596/2549/1/012001.

[44] P. Gañán, D. Marín, D.H. Builes, 11 - Potential of natural fiber in unsaturated polyester biocomposite application, in: S. Thomas, C.J. Chirayil (Eds.),

Applications of Unsaturated Polyester Resins, Elsevier, 2023: pp. 169–203. https://doi.org/10.1016/B978-0-323-99466-8.00013-7.

[45] M. Pervaiz, M.M. Sain, Carbon storage potential in natural fiber composites, Resources, Conservation and Recycling 39 (2003) 325–340. https://doi.org/10.1016/S0921-3449(02)00173-8.

[46] L. Jino, V. Dev Prasad, M. Ajay Eswar, E. Manoj, A. Jacob, S. Arockia Suthan, A. Jayaganthan, A. Anderson, Review on natural fibre composites reinforced with nanoparticles, Materials Today: Proceedings (2023). https://doi.org/10.1016/j.matpr.2023.01.126.

[47] L. Prabhu, V. Krishnaraj, S. Sathish, S. Gokulkumar, N. Karthi, L. Rajeshkumar, D. Balaji, N. Vigneshkumar, K.S. Elango, J. Karpagam, V.J. Vijayalakshmi, E.R. Gowarthan, H. Jayakumar, Experimental investigation on mechanical properties of flax/banana/ industrial waste tea leaf fiber reinforced hybrid polymer composites, Materials Today: Proceedings 45 (2021) 8136–8143. https://doi.org/10.1016/j.matpr.2021.02.111.

[48] A. Golieskardi, M.E. Hoque, M. Golieskardi, 1 - Introduction to green biocomposites, in: M.E. Hoque, A. Sharif, M. Jawaid (Eds.), Green Biocomposites for Biomedical Engineering, Woodhead Publishing, 2021: pp. 3–18. https://doi.org/10.1016/B978-0-12-821553-1.00002-8.

[49] N. Chand, M. Fahim, 1 - Natural fibers and their composites, in: N. Chand, M. Fahim (Eds.), Tribology of Natural Fiber Polymer Composites (Second Edition), Woodhead Publishing, 2021: pp. 1–59. https://doi.org/10.1016/B978-0-12-818983-2.00001-3.

[50] R. Kumar, M.I. Ul Haq, A. Raina, A. Anand, Industrial applications of natural fibre-reinforced polymer composites – challenges and opportunities, International Journal of Sustainable Engineering 12 (2019) 212–220. https://doi.org/10.1080/19397038.2018.1538267.

[51] Oinam Roselyn Devi, New Sustainable Fibres and their application in Textiles: A Review, IJMTST 06 (2020) 136–141. https://doi.org/10.46501/IJMTST0609S22.

[52] S.K. Verma, A. Gupta, V.K. Patel, B. Gangil, L. Ranikoti, The Potential of Natural Fibers for Automotive Sector, in: J.K. Katiyar, S. Bhattacharya, V.K. Patel, V. Kumar (Eds.), Automotive Tribology, Springer, Singapore, 2019: pp. 31–49. https://doi.org/10.1007/978-981-15-0434-1_3.

[53] I. Kong, 3 - Properties of bio-based fibers, in: S.M. Rangappa, M. Puttegowda, J. Parameswaranpillai, S. Siengchin, S. Gorbatyuk (Eds.), Advances in Bio-Based Fiber, Woodhead Publishing, 2022: pp. 33–64. https://doi.org/10.1016/B978-0-12-824543-9.00027-X.

[54] W. Shahri, I. Tahir, B. Ahad, Abaca Fiber: A Renewable Bio-resource for Industrial Uses and Other Applications, in: K.R. Hakeem, M. Jawaid, U. Rashid (Eds.), Biomass and Bioenergy: Processing and Properties, Springer International Publishing, Cham, 2014: pp. 47–61. https://doi.org/10.1007/978-3-319-07641-6_3.

[55] I. Elfaleh, F. Abbassi, M. Habibi, F. Ahmad, M. Guedri, M. Nasri, C. Garnier, A comprehensive review of natural fibers and their composites: An eco-friendly alternative to conventional materials, Results in Engineering 19 (2023) 101271. https://doi.org/10.1016/j.rineng.2023.101271.

[56] Noor S. Sadeq, Zaid G. Mohammadsalih, Dr.M.Mubarak Ali2, Natural fibers and their applications: A review, Jornual of AL-Farabi for Engineering Sciences 1 (2022) 13–13. https://doi.org/10.59746/jfes.v1i1.13.

[57] Y. Fan, Study on Preparation and Application of Banana Fiber-Based Composites, J. Phys.: Conf. Ser. 2539 (2023) 012093. https://doi.org/10.1088/1742-6596/2539/1/012093.

[58] Plant fibers, their composites, and applications, Elsevier, Cambridge, MA, 2022.

[59] T. Sen, H.N.J. Reddy, Various Industrial Applications of Hemp, Kinaf, Flax and Ramie Natural Fibres, International Journal of Innovation 2 (2011).

[60] S. Shinoj, R. Visvanathan, S. Panigrahi, M. Kochubabu, Oil palm fiber (OPF) and its composites: A review, Industrial Crops and Products 33 (2011) 7–22. https://doi.org/10.1016/j.indcrop.2010.09.009.

[61] W. Ghori, N. Saba, M. Jawaid, M. Asim, A review on date palm (*phoenix dactylifera*) fibers and its polymer composites, IOP Conf. Ser.: Mater. Sci. Eng. 368 (2018) 012009. https://doi.org/10.1088/1757-899X/368/1/012009.

[62] M.A. Mahmud, F.R. Anannya, Sugarcane bagasse - A source of cellulosic fiber for diverse applications, Heliyon 7 (2021). https://doi.org/10.1016/j.heliyon.2021.e07771.

[63] R.A. Kurien, A. Biju, K.A. Raj, A. Chacko, B. Joseph, C.P. Koshy, Chicken feather fiber reinforced composites for sustainable applications, Materials Today: Proceedings 58 (2022) 862–866. https://doi.org/10.1016/j.matpr.2021.10.400.

[64] B. Bakhshandeh, S.S. Nateghi, M.M. Gazani, Z. Dehghani, F. Mohammadzadeh, A review on advances in the applications of spider silk in biomedical issues, International Journal of Biological Macromolecules 192 (2021) 258–271. https://doi.org/10.1016/j.ijbiomac.2021.09.201.

[65] P. Jagadeesh, V.S.H. Ningappa, M. Puttegowda, Y.G.T. Girijappa, S.M. Rangappa, M.R. Khan, I. Khan, S. Siengchin, Pongamia pinnata shell powder filled sisal/kevlar hybrid composites: Physicomechanical and morphological

characteristics, Polymer Composites 42 (2021) 4434–4447. https://doi.org/10.1002/pc.26160.

[66] Full article: Physico-Chemical Properties of Fiber Extracted from the Flower of Celosia Argentea Plant, (n.d.). https://www.tandfonline.com/doi/full/10.1080/15440478.2019.1629149 (accessed April 21, 2024).

[67] M.A. Masuelli, Introduction of Fibre-Reinforced Polymers − Polymers and Composites: Concepts, Properties and Processes, in: Fiber Reinforced Polymers - The Technology Applied for Concrete Repair, IntechOpen, 2013. https://doi.org/10.5772/54629.

[68] Lignocellulose-based Hybrid Bilayer Laminate Composite: Part I - Studies on Tensile and Impact Behavior of Oil Palm Fiber-Glass Fiber-reinforced Epoxy Resin, (n.d.). https://doi.org/10.1177/0021998305047267.

[69] Thermoplastics - an overview | ScienceDirect Topics, (n.d.). https://www.sciencedirect.com/topics/agricultural-and-biological-sciences/thermoplastics (accessed April 21, 2024).

[70] max.zm, Thermoplastics vs. Thermosets, VEM Tooling (2022). https://www.vem-tooling.com/thermoplastics-vs-thermosets/ (accessed April 21, 2024).

[71] A.K. Singh, B.P. Panda, S. Mohanty, S.K. Nayak, M.K. Gupta, Recent Developments on Epoxy-Based Thermally Conductive Adhesives (TCA): A Review, Polymer-Plastics Technology and Engineering 57 (2018) 903–934. https://doi.org/10.1080/03602559.2017.1354253.

[72] Thermoplastic vs Thermoset Plastics, (2023). https://resources.pcb.cadence.com/blog/2023-thermoplastic-vs-thermoset-plastics (accessed April 22, 2024).

[73] N. Saba, M. Jawaid, O.Y. Alothman, M. Paridah, A. Hassan, Recent advances in epoxy resin, natural fiber-reinforced epoxy composites and their applications, Journal of Reinforced Plastics and Composites 35 (2016) 447–470. https://doi.org/10.1177/0731684415618459.

[74] Y. Jiang, J. Li, D. Li, Y. Ma, S. Zhou, Y. Wang, D. Zhang, Bio-based hyperbranched epoxy resins: synthesis and recycling, Chem. Soc. Rev. 53 (2024) 624–655. https://doi.org/10.1039/D3CS00713H.

[75] Tips to reduce BPA exposure, Mayo Clinic (n.d.). https://www.mayoclinic.org/healthy-lifestyle/nutrition-and-healthy-eating/expert-answers/bpa/faq-20058331 (accessed April 23, 2024).

[76] E. Ramon, C. Sguazzo, P. Moreira, A Review of Recent Research on Bio-Based Epoxy Systems for Engineering Applications and Potentialities in the Aviation Sector, Aerospace 5 (2018) 110. https://doi.org/10.3390/aerospace5040110.

[77] X. Liu, X. Yi, J. Zhu, Bio-based epoxies and composites as environmentally friendly alternative materials, in: Elsevier, 2018: pp. 621–637. https://doi.org/10.1016/B978-0-08-101021-1.00019-8.

[78] S. Kumar, S.K. Samal, S. Mohanty, S.K. Nayak, Recent Development of Biobased Epoxy Resins: A Review, Polymer-Plastics Technology and Engineering 57 (2018) 133–155. https://doi.org/10.1080/03602559.2016.1253742.

[79] X. Tao, M. Wei, X. Hu, Y. Tang, W. Wei, J. Liu, X. Li, Novel resveratrol-based hyperbranched epoxy resin suitable for comprehensive modification of epoxy resins, Polymer (2024) 127093. https://doi.org/10.1016/j.polymer.2024.127093.

[80] F.I. Chowdhury, 4 - Sustainable resin systems for polymer composites, in: Md.R. Rahman (Ed.), Advances in Sustainable Polymer Composites, Woodhead Publishing, 2021: pp. 89–108. https://doi.org/10.1016/B978-0-12-820338-5.00004-7.

[81] N.R. Kondekar, Epoxy Resins – A High Performance Material for Industrial, Decorative and Protective Applications., Paintindia Exhi-Bition (2002) 123–131.

[82] L.Z. Linganiso, R.D. Anandjiwala, 4 - Fibre-reinforced laminates in aerospace engineering, in: S. Rana, R. Fangueiro (Eds.), Advanced Composite Materials for Aerospace Engineering, Woodhead Publishing, 2016: pp. 101–127. https://doi.org/10.1016/B978-0-08-100037-3.00004-3.

[83] G. Jogur, A. Nawaz Khan, A. Das, P. Mahajan, R. Alagirusamy, Impact properties of thermoplastic composites, Textile Progress 50 (2018) 109–183. https://doi.org/10.1080/00405167.2018.1563369.

[84] Thermoset and Thermoplastic Resins, (n.d.). https://www.tencom.com/blog/thermoset-and-thermoplastic-resins (accessed April 22, 2024).

[85] N.A. Nordin, F.M. Yussof, S. Kasolang, Z. Salleh, M.A. Ahmad, Wear Rate of Natural Fibre: Long Kenaf Composite, Procedia Engineering 68 (2013) 145–151. https://doi.org/10.1016/j.proeng.2013.12.160.

[86] Y. Nishida, Fabrication Processes for Composites, in: Y. Nishida (Ed.), Introduction to Metal Matrix Composites: Fabrication and Recycling, Springer Japan, Tokyo, 2013: pp. 27–52. https://doi.org/10.1007/978-4-431-54237-7_2.

[87] [PDF] Present State of the Art of Composite Fabric Forming: Geometrical and Mechanical Approaches | Semantic Scholar, (n.d.).

https://www.semanticscholar.org/reader/c5c912b9166919e9f1fb2b7e781acbb1b6a6e33e (accessed April 23, 2024).

[88] A review on the polymeric laminates reinforced with natural fibers, (n.d.). https://doi.org/10.1177/0731684417718385.

[89] B. Denkena, C. Schmidt, P. Weber, Automated Fiber Placement Head for Manufacturing of Innovative Aerospace Stiffening Structures, Procedia Manufacturing 6 (2016) 96–104. https://doi.org/10.1016/j.promfg.2016.11.013.

[90] A.S. Herrmann, J. Nickel, U. Riedel, Construction materials based upon biologically renewable resources—from components to finished parts, Polymer Degradation and Stability 59 (1998) 251–261. https://doi.org/10.1016/S0141-3910(97)00169-9.

[91] S. Rassmann, R.G. Reid, R. Paskaramoorthy, Effects of processing conditions on the mechanical and water absorption properties of resin transfer moulded kenaf fibre reinforced polyester composite laminates, Composites Part A: Applied Science and Manufacturing 41 (2010) 1612–1619. https://doi.org/10.1016/j.compositesa.2010.07.009.

[92] M. Gascons, N. Blanco, K. Matthys, Evolution of manufacturing processes for fiber-reinforced thermoset tanks, vessels, and silos: a review, IIE Transactions 44 (2012) 476–489. https://doi.org/10.1080/0740817X.2011.590177.

[93] Manufacturing of Natural Fibre Reinforced Polymer Composites, n.d. https://link.springer.com/book/10.1007/978-3-319-07944-8 (accessed April 23, 2024).

[94] Natural fiber–reinforced composites: A review on material, manufacturing, and machinability, (n.d.). https://doi.org/10.1177/0892705719844546.

[95] K. Oksman, A.P. Mathew, R. Långström, B. Nyström, K. Joseph, The influence of fibre microstructure on fibre breakage and mechanical properties of natural fibre reinforced polypropylene, Composites Science and Technology 69 (2009) 1847–1853. https://doi.org/10.1016/j.compscitech.2009.03.020.

[96] V. Fiore, T. Scalici, G. Di Bella, A. Valenza, A review on basalt fibre and its composites, Composites Part B Engineering 74 (2015) 74–94. https://doi.org/10.1016/j.compositesb.2014.12.034.

[97] H. Yaghoobi, F. Taheri, Mechanical performance of a novel environmentally friendly basalt-elium® thermoplastic composite and its stainless steel-based fiber metal laminate, Polymer Composites 42 (2021) 4660–4672. https://doi.org/10.1002/pc.26176.

[98] A. Chilali, W. Zouari, M. Assarar, H. Kebir, R. Ayad, Effect of water ageing on the load-unload cyclic behaviour of flax fibre-reinforced thermoplastic and

thermosetting composites, Composite Structures 183 (2018) 309–319. https://doi.org/10.1016/j.compstruct.2017.03.077.

[99] J.J. Llanos, K. Wang, F. Taheri, Characterization of Low- and High-Velocity Responses of Basalt–Epoxy and Basalt–Elium Composites, Polymers 16 (2024) 926. https://doi.org/10.3390/polym16070926.

[100] D. Amit, D. Pradip, M. Satish, Recyclamine® - Novel Amine Building Blocks for a Sustainable World, in: SAMPE neXus 2021, NA SAMPE, 2021. https://doi.org/10.33599/nasampe/s.21.0632.

[101] S. Pastine, Can epoxy composites be made 100% recyclable?, Reinforced Plastics 56 (2012) 26–28. https://doi.org/10.1016/S0034-3617(12)70109-1.

[102] P.K. Dubey, S.K. Mahanth, A. Dixit, S. Changmongkol, Recyclable epoxy systems for rotor blades, IOP Conf. Ser.: Mater. Sci. Eng. 942 (2020) 012014. https://doi.org/10.1088/1757-899X/942/1/012014.

[103] The 2022 winners of JEC Composites Innovation Awards unveiled - JEC, Https://Www.Jeccomposites.Com/ (n.d.). https://www.jeccomposites.com/news/spotted-by-jec/the-2022-winners-of-jec-composites-innovation-awards-unveiled/ (accessed August 28, 2024).

[104] Home, (n.d.). https://www.siemens-energy.com/global/en/home.html, https://www.siemensgamesa.com/global/en/home.html (accessed August 28, 2024).

[105] C. Kish, Niche Snowboards Interview — The World's First Recyclable Snowboard, STOKE (2017). https://www.stokecertified.com/niche-snowboards-interview-worlds-first-recyclable-snowboard/ (accessed August 28, 2024).

[106] Recyclamine, (n.d.). https://www.recyclamine.com/changing-industries-for-better (accessed August 28, 2024).

[107] E. Muñoz, J.A. García-Manrique, Water Absorption Behaviour and Its Effect on the Mechanical Properties of Flax Fibre Reinforced Bioepoxy Composites, International Journal of Polymer Science 2015 (2015) e390275. https://doi.org/10.1155/2015/390275.

[108] A. Moudood, A. Rahman, A. Öchsner, M. Islam, G. Francucci, Flax fiber and its composites: An overview of water and moisture absorption impact on their performance, Journal of Reinforced Plastics and Composites 38 (2019) 323–339. https://doi.org/10.1177/0731684418818893.

[109] E.A. Esleman, G. ÖNAL, Effect of saltwater on the mechanical properties of basalt/carbon/glass-epoxy hybrid composites, Journal of Composite Materials 56 (2022) 3783–3799. https://doi.org/10.1177/00219983221122926.

[110] S. Dattilo, G. Cicala, P.M. Riccobene, C. Puglisi, L. Saitta, Full Recycling and Re-Use of Bio-Based Epoxy Thermosets: Chemical and Thermomechanical Characterization of the Recycled Matrices, Polymers 14 (2022) 4828. https://doi.org/10.3390/polym14224828.

[111] A.D. La Rosa, D.R. Banatao, S.J. Pastine, A. Latteri, G. Cicala, Recycling treatment of carbon fibre/epoxy composites: Materials recovery and characterization and environmental impacts through life cycle assessment, Composites Part B: Engineering 104 (2016) 17–25. https://doi.org/10.1016/j.compositesb.2016.08.015.

[112] F. Ferrari, C. Esposito Corcione, R. Striani, L. Saitta, G. Cicala, A. Greco, Fully Recyclable Bio-Based Epoxy Formulations Using Epoxidized Precursors from Waste Flour: Thermal and Mechanical Characterization, Polymers 13 (2021) 2768. https://doi.org/10.3390/polym13162768.

[113] D. Plappert, G.C. Ganzenmüller, M. May, S. Beisel, Mechanical Properties of a Unidirectional Basalt-Fiber/Epoxy Composite, Journal of Composites Science 4 (2020) 101. https://doi.org/10.3390/jcs4030101.

[114] M. Kulpa, A. Wiater, M. Rajchel, T. Siwowski, Comparison of Material Properties of Multilayered Laminates Determined by Testing and Micromechanics, Materials 14 (2021) 761. https://doi.org/10.3390/ma14040761.

[115] S.A. Yasmeen, U.T.S. Kumar, M.V.S. Teja, V. Viswarachandu, Evaluation of Mechanical Properties of Basalt based Composite Structures, 07 (2020).

[116] C. Li, H. Wang, X. Zhao, Y. Fu, X. He, Y. Song, Investigation of Mechanical Properties for Basalt Fiber/Epoxy Resin Composites Modified with La, Coatings 11 (2021) 666. https://doi.org/10.3390/coatings11060666.

[117] V. Manikandan, J.T. Winowlin Jappes, S.M. Suresh Kumar, P. Amuthakkannan, Investigation of the effect of surface modifications on the mechanical properties of basalt fibre reinforced polymer composites, Composites Part B: Engineering 43 (2012) 812–818. https://doi.org/10.1016/j.compositesb.2011.11.009.

[118] K. Karthik, D. Rajamani, E.P. Venkatesan, M.I. Shajahan, A.A. Rajhi, A. Aabid, M. Baig, B. Saleh, Experimental Investigation of the Mechanical Properties of Carbon/Basalt/SiC Nanoparticle/Polyester Hybrid Composite Materials, Crystals 13 (2023) 415. https://doi.org/10.3390/cryst13030415.

[119] P. Amuthakkannan, V. Manikandan, J.T.W. Jappes, M. Uthayakumar, Hybridization effect on mechanical properties of short basalt/jute fiber-reinforced polyester composites, Science and Engineering of Composite Materials 20 (2013) 343–350. https://doi.org/10.1515/secm-2012-0144.

[120] A. Lotfi, H. Li, D.V. Dao, G. Prusty, Natural fiber–reinforced composites: A review on material, manufacturing, and machinability, Journal of Thermoplastic

Composite Materials 34 (2021) 238–284. https://doi.org/10.1177/0892705719844546.

[121] D.U. Shah, P.J. Schubel, P. Licence, M.J. Clifford, Determining the minimum, critical and maximum fibre content for twisted yarn reinforced plant fibre composites, Composites Science and Technology 72 (2012) 1909–1917. https://doi.org/10.1016/j.compscitech.2012.08.005.

[122] Basalt Continuous Fiber, (2011). https://web.archive.org/web/20110707103310/http://www.albarrie.com/techfabrics/continuousfiber.aspx (accessed May 14, 2024).

[123] C. Ralph, P. Lemoine, A. Boyd, E. Archer, A. McIlhagger, The effect of fibre sizing on the modification of basalt fibre surface in preparation for bonding to polypropylene, Applied Surface Science 475 (2019) 435–445. https://doi.org/10.1016/j.apsusc.2019.01.001.

[124] BA-650-13-0.90-127 Bi-Axial Basalt Fabric, Basalt Samples Online Store (n.d.). https://www.basalt.guru/shop/product/ba-650-13-0-90-127-bi-axial-basalt-fabric/ (accessed May 15, 2024).

[125] SBS MSDS.pdf, (n.d.).

[126] BA-650-13-0.90-127_SBS.pdf, (n.d.).

[127] H. Liu, Y. Yu, M. Zhang, H. Yu, L. Li, Y. Liu, H. Yang, Z. Tian, Effect of sizing agent on properties of basalt fiber/blended resin matrix composites, J Mater Sci 58 (2023) 5642–5657. https://doi.org/10.1007/s10853-023-08373-y.

[128] Fabrics - Basalt Fiber Tech Products, (n.d.). https://www.basaltft.com/products/fab.htm (accessed May 14, 2024).

[129] K.L. Pickering, M.G.A. Efendy, T.M. Le, A review of recent developments in natural fibre composites and their mechanical performance, Composites Part A: Applied Science and Manufacturing 83 (2016) 98–112. https://doi.org/10.1016/j.compositesa.2015.08.038.

[130] Mohite - AE-681 Composite Materials.pdf, (n.d.). https://home.iitk.ac.in/~mohite/Composite_introduction.pdf (accessed May 15, 2024).

[131] TDS Recyclamine R101 Rev 01.pdf, (n.d.).

[132] Recyclamine Brochure - Briozen Brochure_Digital_V2_Recyclable_May2022.pdf, (n.d.).

[133] TDS - Briozen YDL5557 - THR9357_8_Rev.03.pdf, (n.d.).

[134] 105-206-Epoxy-Resin-1.pdf, (n.d.).

[135] 105 System | WEST SYSTEM Epoxy, (n.d.). https://www.westsystem.com/products/105-system/ (accessed May 15, 2024).

[136] K.-T. Hsiao, D. Heider, 10 - Vacuum assisted resin transfer molding (VARTM) in polymer matrix composites, in: S.G. Advani, K.-T. Hsiao (Eds.), Manufacturing Techniques for Polymer Matrix Composites (PMCs), Woodhead Publishing, 2012: pp. 310–347. https://doi.org/10.1533/9780857096258.3.310.

[137] S. Prabhakaran, V. Krishnaraj, M.S. kumar, R. Zitoune, Sound and Vibration Damping Properties of Flax Fiber Reinforced Composites, Procedia Engineering 97 (2014) 573–581. https://doi.org/10.1016/j.proeng.2014.12.285.

[138] D. Chen, K. Arakawa, C. Xu, Reduction of void content of vacuum-assisted resin transfer molded composites by infusion pressure control, Polymer Composites 36 (2015) 1629–1637. https://doi.org/10.1002/pc.23071.

[139] (PDF) Flow rate control during vacuum-assisted resin transfer molding (VARTM) processing, (n.d.). https://www.researchgate.net/publication/248407417_Flow_rate_control_during_vacuum-assisted_resin_transfer_molding_VARTM_processing (accessed May 17, 2024).

[140] D30 Committee, Test Methods for Constituent Content of Composite Materials, (n.d.). https://doi.org/10.1520/D3171-22.

[141] D30 Committee, Test Method for Tensile Properties of Polymer Matrix Composite Materials, (n.d.). https://doi.org/10.1520/D3039_D3039M-17.

[142] D30 Committee, Test Method for Compressive Properties of Polymer Matrix Composite Materials Using a Combined Loading Compression (CLC) Test Fixture, (n.d.). https://doi.org/10.1520/D6641_D6641M-16E02.

[143] D30 Committee, Test Method for Flexural Properties of Polymer Matrix Composite Materials, (n.d.). https://doi.org/10.1520/D7264_D7264M-07.

[144] D30 Committee, Test Method for Shear Properties of Composite Materials by the V-Notched Beam Method, (n.d.). https://doi.org/10.1520/D5379_D5379M-19E01.

[145] D20 Committee, Test Methods for Determining the Izod Pendulum Impact Resistance of Plastics, (n.d.). https://doi.org/10.1520/D0256-23E01.

[146] Tensile-Dog Bone D638-22.pdf, (n.d.).

[147] WaterJet_User_Manual.pdf, (n.d.).

[148] Specific GravityD792-20.pdf, (n.d.).

[149] E. Komurlu, F. Cihangir, A. Kesimal, S. Demir, Effect of Adhesive Type on the Measurement of Modulus of Elasticity Using Electrical Resistance Strain Gauges, Arab J Sci Eng 41 (2016) 433–441. https://doi.org/10.1007/s13369-015-1837-0.

[150] D30 Committee, Test Method for Compressive Properties of Polymer Matrix Composite Materials with Unsupported Gage Section by Shear Loading, (n.d.). https://doi.org/10.1520/D3410_D3410M-16E01.

[151] S. Zhao, Z. Zhao, Z. Yang, L. Ke, S. Kitipornchai, J. Yang, Functionally graded graphene reinforced composite structures: A review, Engineering Structures 210 (2020) 110339. https://doi.org/10.1016/j.engstruct.2020.110339.

[152] J.S. Welsh, D.F. Adams, Testing of angle-ply laminates to obtain unidirectional composite compression strengths, Composites Part A: Applied Science and Manufacturing 28 (1997) 387–396. https://doi.org/10.1016/S1359-835X(96)00138-8.

[153] M. Scafè, M. Labanti, A. Coglitore, G. Raiteri, R. Dlacic, E. Troiani, E. Besseghini, M.P. Falaschetti, Experimental determination of compressive strength of an unidirectional composite lamina: indirect estimate by Using Back-out Factor (BF), (2013).

[154] L.J. Hart-Smith, E. Troiani, 7.7 Backing-Out Composite Lamina Strengths from Cross-Ply Testing, in: Comprehensive Composite Materials II, Elsevier, 2018: pp. 119–130. https://doi.org/10.1016/B978-0-12-803581-8.03922-9.

[155] MIL-HDBK-17-1F.pdf, (n.d.).

[156] A.K. Kaw, Mechanics of composite materials, 2. ed, CRC Taylor & Francis, Boca Raton, FL, 2006.

[157] J. Kastner, B. Plank, D. Salaberger, J. Sekelja, Defect and Porosity Determination of Fibre Reinforced Polymers by X-ray Computed Tomography, (n.d.).

[158] X. Liu, F. Chen, A review of void formation and its effects on the mechanical performance of carbon fiber reinforced plastic, Engineering Transactions 64 (2016) 33. https://et.ippt.gov.pl/index.php/et/article/view/280 (accessed August 27, 2024).

[159] M.W. Brandley, Void Modeling in Resin Infusion, (n.d.).

[160] L. Di Landro, A. Montalto, P. Bettini, S. Guerra, F. Montagnoli, M. Rigamonti, Detection of Voids in Carbon/Epoxy Laminates and Their Influence on Mechanical Properties, Polymers and Polymer Composites 25 (2017) 371–380. https://doi.org/10.1177/096739111702500506.

[161] A Note on the Effects of Voids Upon the Hygral and Mechanical Properties of AS4/3502 Graphite/Epoxy, (n.d.). https://doi.org/10.1177/002199838702100306.

[162] S. Ghiorse, Effect of void content on the mechanical properties of carbon/epoxy laminates, in: 1993. https://www.semanticscholar.org/paper/Effect-of-void-content-on-the-mechanical-properties-Ghiorse/adccf7e8c29ebf532874ffee0ca77b3535204025 (accessed August 27, 2024).

[163] Stress Singularities - FEA-Solutions (UK) Ltd - Finite Element Analysis For Your Product Design, (2021). https://fea-solutions.co.uk/stress-singularities/ (accessed August 7, 2024).

[164] H.M. Yoo, M.S. Kim, B.S. Kim, D.J. Kwon, S.W. Choi, Impact and shear properties of carbon fabric/ poly-dicyclopentadiene composites manufactured by vacuum-assisted resin transfer molding, E-Polymers 19 (2019) 437–443. https://doi.org/10.1515/epoly-2019-0045.

[165] Basalt_fiber_for_automotive_industry_SI.pdf, (n.d.). https://basfiber.com/system/storage/download/Basalt_fiber_for_automotive_industry_SI.pdf (accessed August 28, 2024).

[166] Automotive industry, (n.d.). https://lavaintel.com/automotive_en (accessed August 28, 2024).

[167] JEC Composites Magazine - N°148 - november 2022, (n.d.). https://digital-magazine.jeccomposites.com/reader/657efaac-a1ef-4709-b90a-42f4ae1bcbbf?origin=%2Fjec-composites-magazine%2Fjec-composites-magazine%2Fn148-2022 (accessed August 28, 2024).

[168] Microsoft Word - 04.Ćwiek.pdf, (n.d.).

[169] D. Zhu, Y. Tang, M.Z. Rahman, 12 - Basalt fiber: composites and applications, in: S.M. Rangappa, V. Ayyappan, G. Manik, S. Siengchin (Eds.), Synthetic and Mineral Fibers, Their Composites and Applications, Woodhead Publishing, 2024: pp. 337–361. https://doi.org/10.1016/B978-0-443-13623-8.00012-5.

[170] I.R. Chowdhury, R. Pemberton, J. Summerscales, Developments and Industrial Applications of Basalt Fibre Reinforced Composite Materials, Journal of Composites Science 6 (2022) 367. https://doi.org/10.3390/jcs6120367.

[171] A. Dorigato, A. Pegoretti, Fatigue resistance of basalt fibers-reinforced laminates, Journal of Composite Materials 46 (2012) 1773–1785. https://doi.org/10.1177/0021998311425620.

[172] V. Lopresto, C. Leone, I. De Iorio, Mechanical characterisation of basalt fibre reinforced plastic, Composites Part B: Engineering 42 (2011) 717–723. https://doi.org/10.1016/j.compositesb.2011.01.030.

[173] Y. Yao, D. Zhu, H. Zhang, G. Li, B. Mobasher, Tensile Behaviors of Basalt, Carbon, Glass, and Aramid Fabrics under Various Strain Rates, Journal of

Materials in Civil Engineering 28 (2016) 04016081. https://doi.org/10.1061/(ASCE)MT.1943-5533.0001587.

[174] Z. Sajid, S. Karuppanan, K.E. Kee, N. Sallih, S.Z.H. Shah, Carbon/basalt hybrid composite bolted joint for improved bearing performance and cost efficiency, Composite Structures 275 (2021) 114427. https://doi.org/10.1016/j.compstruct.2021.114427.

APPENDIX A SUMMARY OF TEST DATA

TENSILE TEST RESULTS

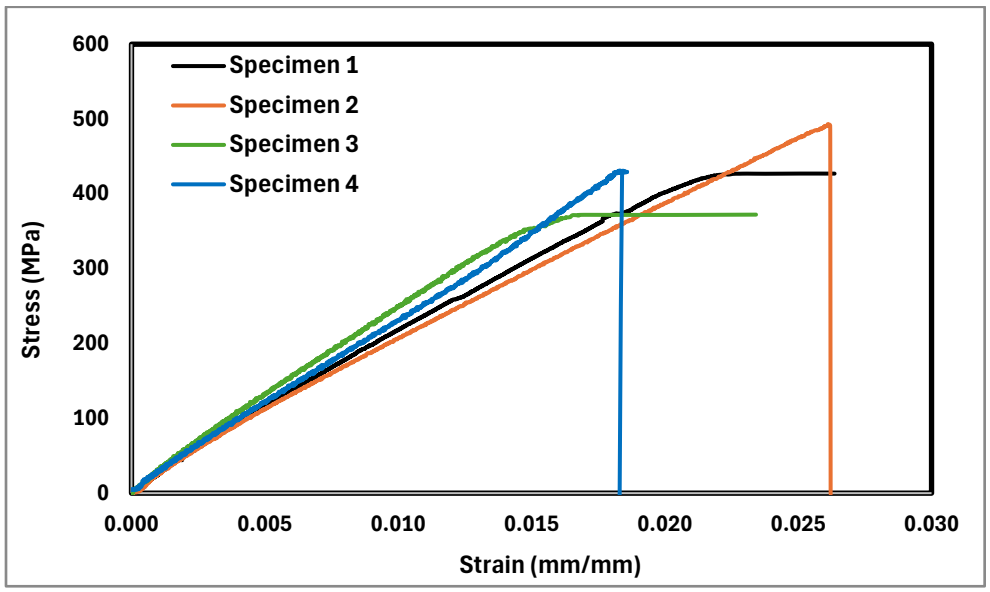

Figure A- 1: Tensile stress-strain curve of basalt-epoxy specimens.

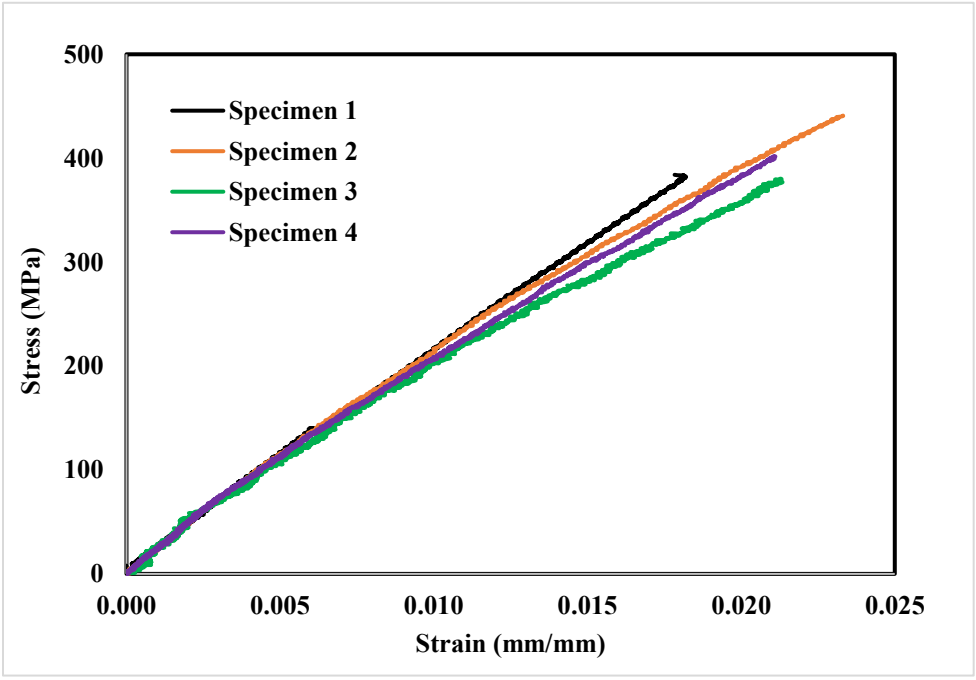

Figure A- 2: Tensile stress-strain curve of basalt-Recyclamine specimens.

COMPRESSION TEST RESULTS

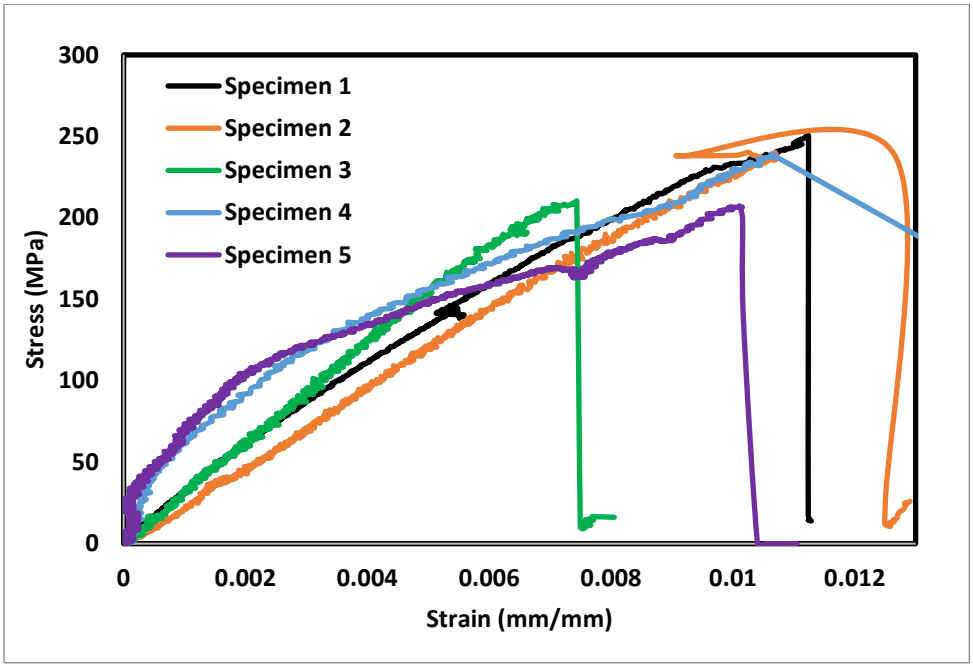

Figure A- 3: Compressive stress-strain curve of basalt-epoxy specimens.

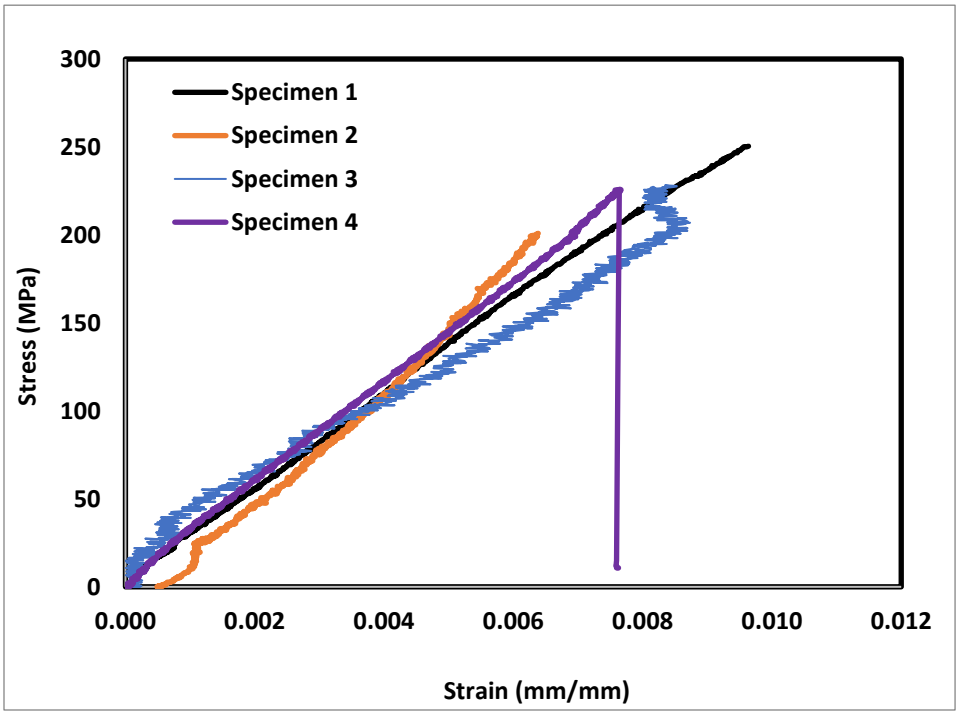

Figure A- 4: Compressive stress-strain curve of basalt-Recyclamine specimens.

FLEXURAL TEST RESULTS

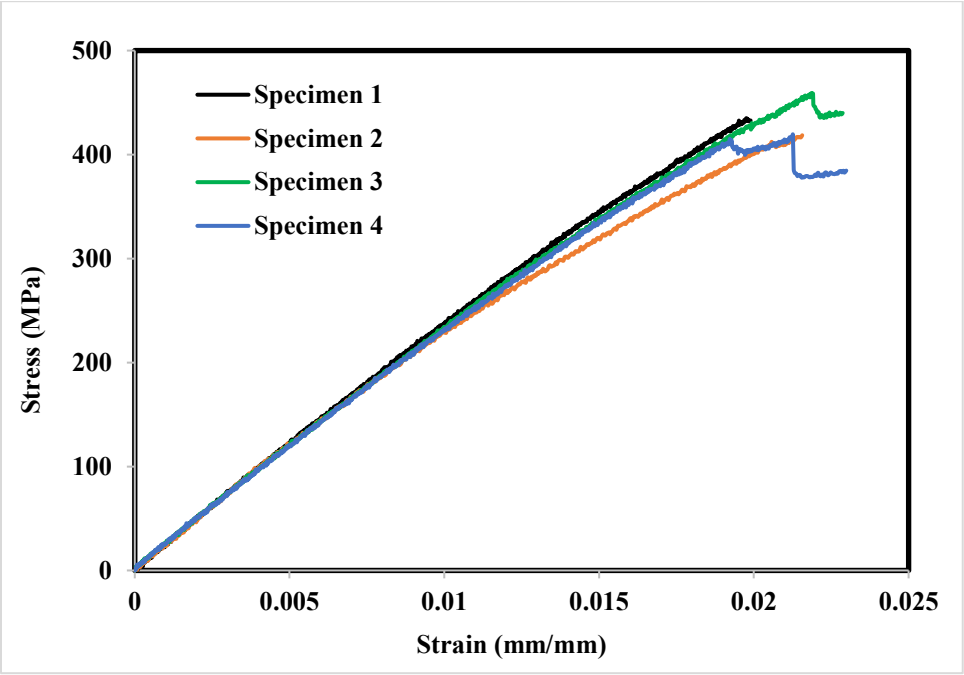

Figure A- 5: Flexural stress-strain curve of basalt-epoxy specimens.

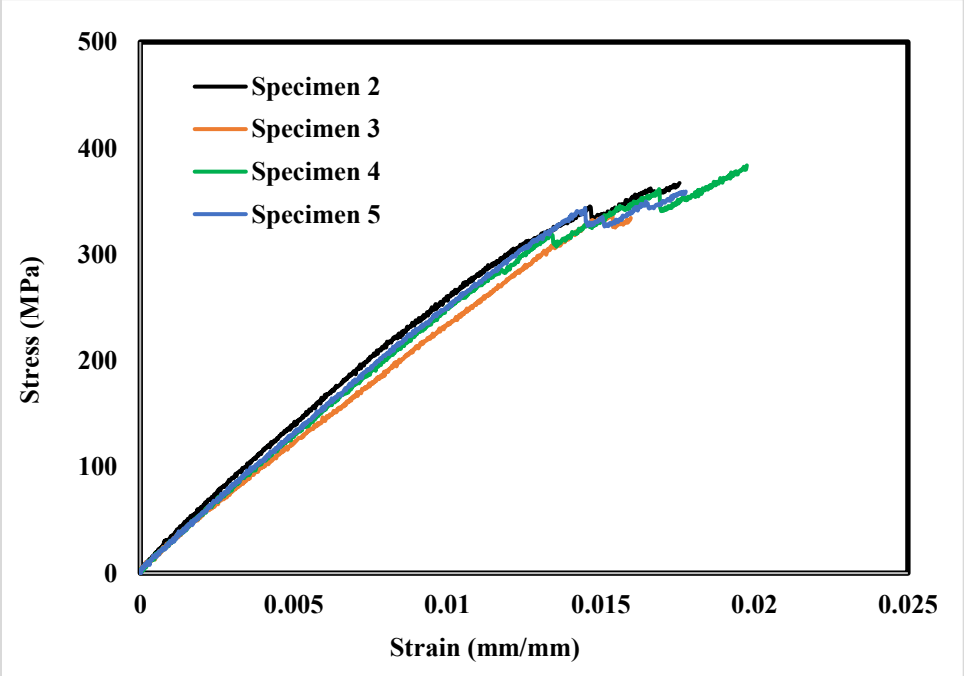

Figure A- 6: Flexural stress-strain curve of basalt-Recyclamine specimens.

SHEAR TEST RESULTS

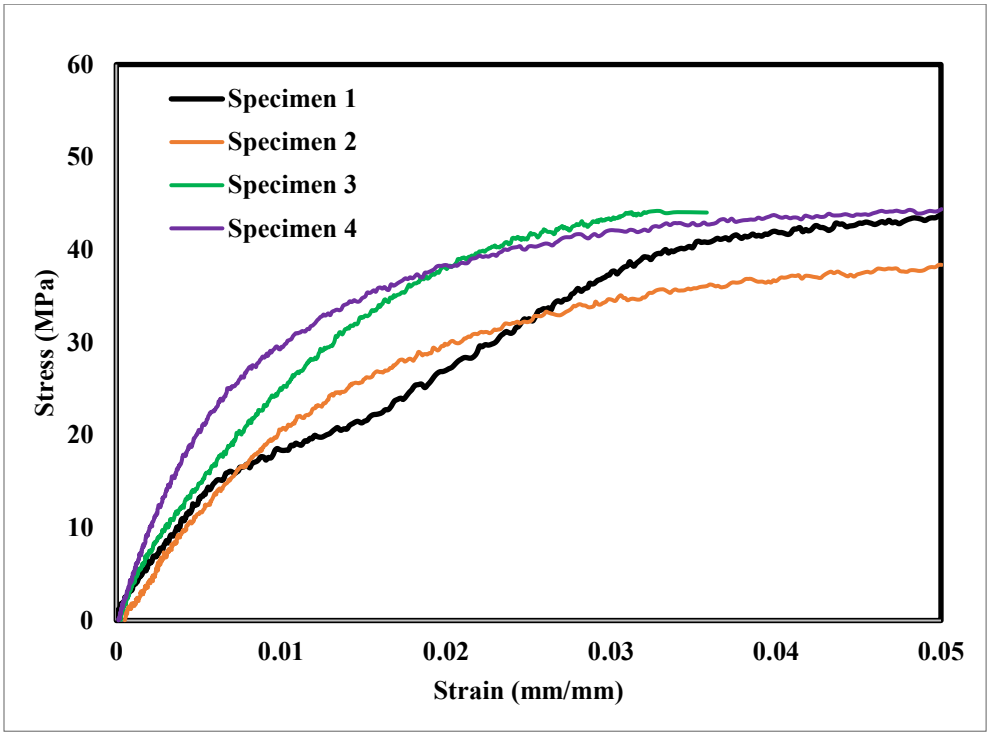

Figure A- 7: Shear stress-strain curve of basalt-epoxy specimens.

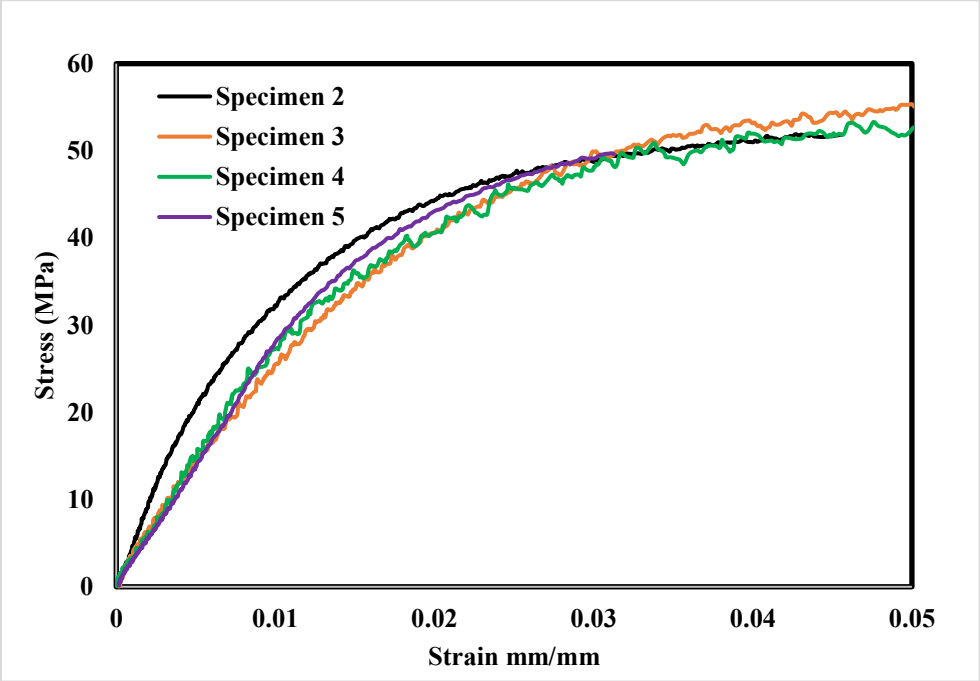

Figure A- 8: Shear stress-strain curve of basalt-Recyclamine specimens.

UNIDIRECTIONAL COMPRESSION TEST RESULTS

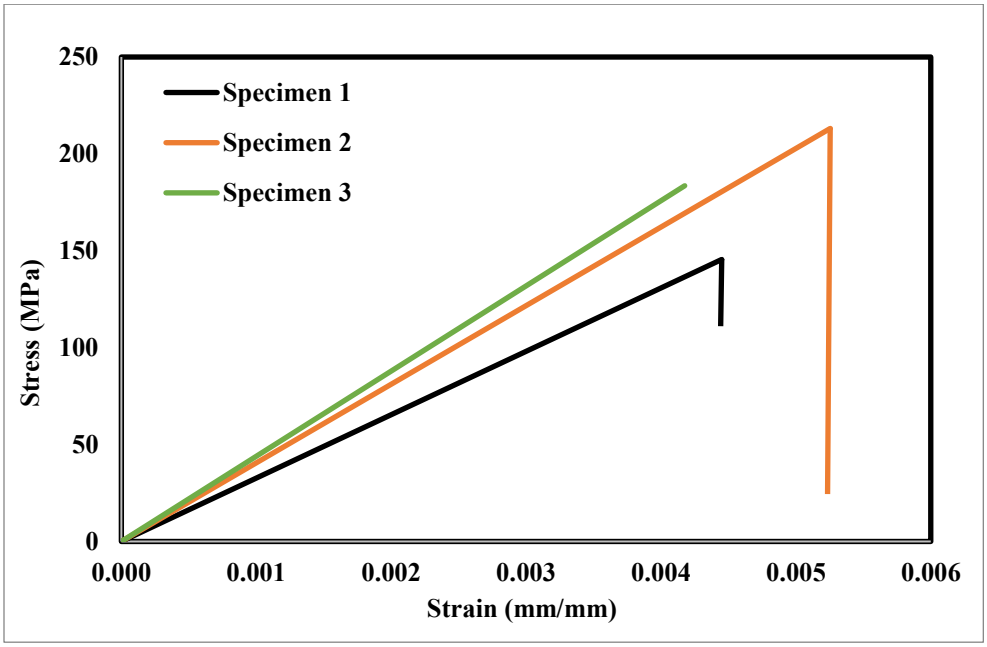

Figure A- 9: Compressive stress-strain curve of unidirectional basalt-epoxy specimens.